November 12, 2018

Revised manuscript

Dear Dr. Michel Van Roozendael,

we would like to take the opportunity to thank you for your efforts and that you accepted the editorship of our manuscript "BOREAS - a new MAX-DOAS profile retrieval algorithm for aerosols and trace gases".

Please find enclosed a revised version of our manuscript where we implemented comments by the referees. We revised the original manuscript according to their suggestions and provided also additional information as requested by the referees. We would like to mention that we also changed the data shown in the correlation plots of Figures 13, 14, 17 and 18 because we accidentally included the 12th of September. This day was initially removed from the plots. The new correlation plots correspond to the depicted time series now.

Below, the author comments are provided that have already been uploaded to the AMT web page on 05 November 2018. We also attached a new version of the revised manuscript in which changes in comparison to the initial version are highlighted. We hope that with the submission of the author comments and the revision of the manuscript, our article will be accepted for publication in AMT.

Yours sincerely,
Tim Bösch (on behalf of the co-authors)

List of Attachments

- Author comments to Referee #1
- Author comments to Referee #2
- Revised manuscript with highlighted changes
- Revised manuscript

Author reply to Referee #2

Tim Bösch et al.

November 5, 2018

We thank Referee #1 for carefully reading our manuscript and for the helpful comments which will improve the quality of our manuscript. We will reply to the comments point by point.

> Legend:
> - referee comments
> - author comments
> - old text from the manuscript
> - **changed text in the manuscript**

This paper reports a new MAX-DOAS profiling algorithm detailedly. The algorithm is based on a scientific reasonable method. The results have good correlation with the results from the other instruments.

Thank you very much for the positive comment.

However, from the paper, it appears that the algorithm is similar to the other profiling algorithms based on the optimal estimation method. The title of this paper is about a NEW algorithm, so you should highlight what is really NEW and innovative in your algorithm, and what are the advantages comparing to the other MAX-DOAS profiling algorithms. These points should also be included in the Abstracts.

To the authors knowledge, the approach of the aerosol retrieval is completely new. The trace gas retrieval, presented in this manuscript, is based on the optimal estimation (OE) method and is similar to retrievals used in other studies. However, the applied approach on improving the regularization ratio empirically as well as the a priori pre-scaling option are new and might help the community to reduce oscillations and wrongly weighted a priori constraints.

We will follow the suggestion of the reviewer by adding the following lines to the abstract:

The aerosol profile retrieval is based on a novel approach in which the absorption depth of O_4 is directly used in order to retrieve extinction coefficient profiles instead of the commonly used perturbation theory method. The retrieval of trace gases is done with the frequently used optimal estimation method but significant improvements on how to deal with wrongly weighted a priori constraints and for scenarios in which the a priori profile is inaccurate are presented.

Furthermore, the latter point will be also mentioned in the Introduction:

In order to improve the standard OE method for trace gases, a simple way of changing the weighting between a priori and measurement constraints is introduced by varying a regularization factor so that oscillations are minimized. Additionally, the usage of a priori pre-scaling will be highlighted as one way of improving results when the a priori profile is far away from the real atmosphere.

In Figure 4, readers cannot easily distinguish between the curves corresponding to E2 and E3. Different line styles should be used for the curves of different episodes (also in the other similar figures). In the right-hand chart, the pre-scaled a priori profiles ought to be depicted.

As suggested, the linestyles were changed and the pre-scaled a priori profiles were included. The following four figures were adapted for this purpose and will be added to the new manuscript.
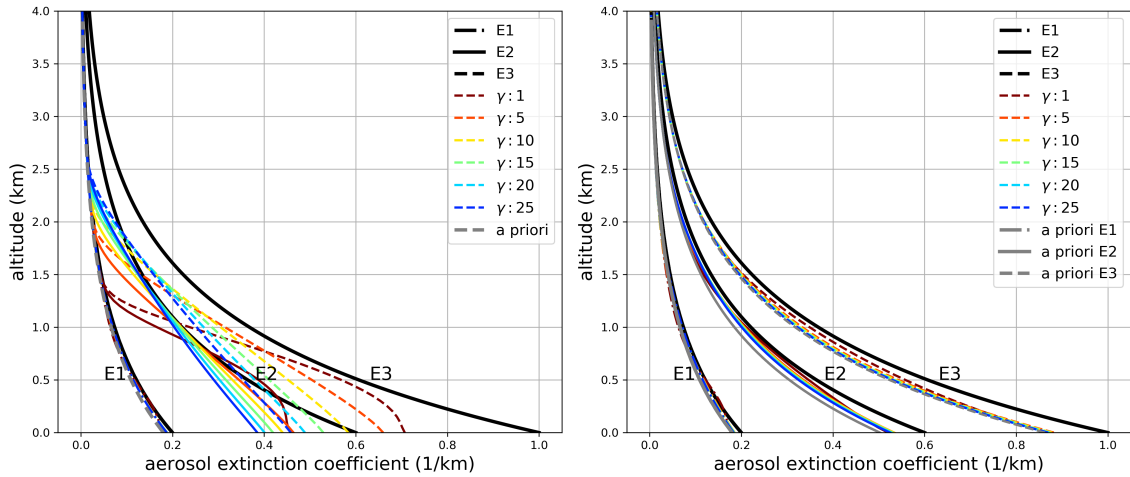

Figure 1: **(Changed version of manuscript Figure 4)** Retrieval results with a fixed (left) and a pre-scaled a priori profile (right) with varying Tikhonov parameters γ for SNR = 3000. Small γ values mean less smoothing of the resulting profiles.
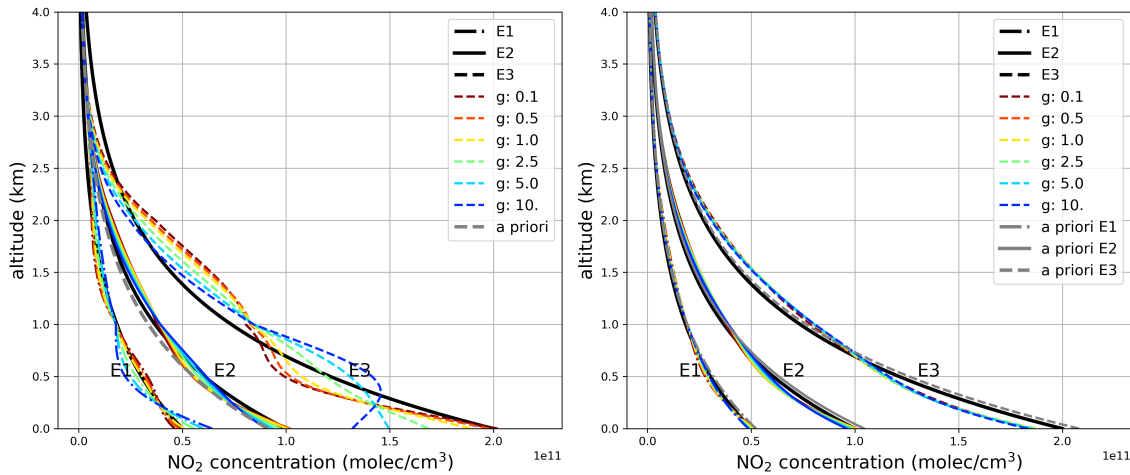

Figure 2: **(Changed version of manuscript Figure 7)** Retrieval results with a fix (left) and a pre-scaled a priori profile (right) with g factors. Small g values mean less measurement weighting for the resulting profiles.
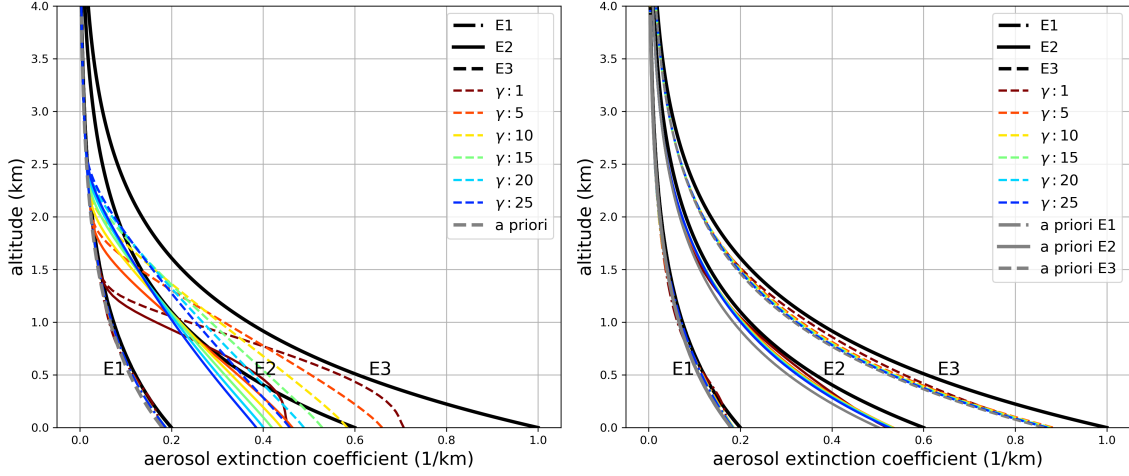
Figure 3: **(Changed version of manuscript Figure A2)** Retrieval results with a fix (left) and a pre-scaled a priori profile (right) with varying Tikhonov parameters γ for SNR = 3000. Small γ values mean less smoothing of the resulting profiles.
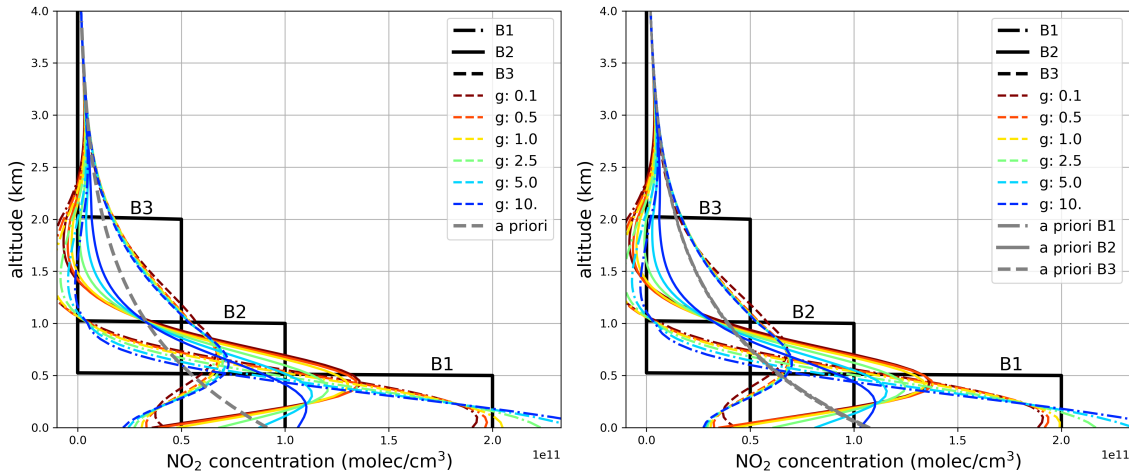

Figure 4: **(Changed version of manuscript Figure A9)** Retrieval results with a fix (left) and a pre-scaled a priori profile (right) with g factors. Small g values mean less measurement weighting for the resulting profiles.

Moreover, I cannot understand about how are the a priori profiles pre-scaled.

For both, the aerosol and the trace gas retrieval, the corresponding a priori profiles are scaled so that the AOT and VCD of the new a priori profiles match the values found from an initial calculation with a "zero"-profile and from the 30° dSCD measurement for aerosols and trace gases, respectively.

In order to clarify this approach, the aerosol pre-scaling description will be extended by the following lines in Section 4.1.1:

In Equation 15, the a priori profile x_0 is set to 0 but the remaining terms stay unchanged in order to retrieve a reliable AOT value without limiting the solution by a certain profile shape.

3

The AOT from this pre-calculation is used to scale the a priori profile for the true run.

The AOT from this pre-calculation is used to scale the a priori profile for the main run by calculating a scaling factor from the initial a priori AOT and the new value which is applied to all initial extinction coefficients before the main inversion.

In Section 4.1.2, the following lines will be changed in the trace gas pre-scaling description:

This vertical column density V is used as a pre-scaling values for the a priori profile.

The new a priori profile is scaled to match this vertical column density V by calculating a scaling factor from the initial and the retrieved V which is applied to all initial concentration values before the main inversion.

In the chapter about CINDI-2 campaign (4.3), the results are compared with the results from other instruments. However, it is also important to compare with the MAX-DOAS result from the same instrument but retrieved with the other algorithms.

We fully agree with the reviewers suggestion. However, the BOREAS algorithm participated in a comparison study for synthetic data and real data which will pe published by Frieß et al. (2018) and Tirpitz et al. (2018), respectively. In both studies, several community algorithms are presented and compared to each other so that we decided to focus only on a validation study with ancillary measurements instead of repeating comparisons shown in the other two papers.

Some well-known and fundamental introductions can be simplified. For example, it is unnecessary to explain the definition of single scattering albedo in detail and show the equation.

We follow the reviewers suggestion by removing the definition of single scattering albedo and slant column density from the manuscript.

In the description of the algorithm, it is better to use the symbols that are commonly used in the related papers. For example, in Equation (3), it is better to use "AMF" instead of "M", "SCD" instead of "S", and "VCD" instead of "V". In Equation (5), you can just use "BAMF" instead of the curlicue M.

The authors believe that one letter variable symbols make the understanding of longer equations easier. Furthermore, these variables are also used in the literature (cf. Platt, 1994) and in other publications (cf. e.g. Marquard et al., 2000). One exception is M for the air mass factor which was chosen because A is additionally used for the averaging kernels.

Minor corrections:

Page 1, Line 4: "in a second part" $\rightarrow$ "in the second part".

Will be changed as suggested.

Page 9, Line 5: If Δy is a vector, then it should be described as "has N·M elements" instead of "has the dimension N·M×1"; otherwise it should be described as a matrix.

Will be changed as suggested.

Similarly, Line 10, the state vector Δx should have "L elements". Line 11, "N·M×L" $\rightarrow$ "(N·M)×L".

Will be changed as suggested.

Page 20, Line 14: "CINDI2" → "CINDI-2".

Will be changed as suggested.

References

Marquard, L. C., T. Wagner, and U. Platt (Jan. 20, 2000). "Improved Air Mass Factor Concepts for Scattered Radiation Differential Optical Absorption Spectroscopy of Atmospheric Species". In: *Journal of Geophysical Research: Atmospheres* 105.D1, pp. 1315–1327. ISSN: 2156-2202. DOI: 10.1029/1999JD900340.

Platt, Ulrich (1994). "Differential Optical Absorption Spectroscopy (DOAS)". In: *Air Monitoring by Spectroscopic Techniques*. 127. New York: John Wiley & Sons, pp. 27–84. ISBN: 0-471-55875-3.

Author reply to Referee #3

Tim Bösch et al.

November 5, 2018

We thank Referee #3 for carefully reading our manuscript and for the helpful comments which will improve the quality of our manuscript. We will reply to the comments point by point.

Legend:
- referee comments
- author comments
- old text from the manuscript
- **changed text in the manuscript**

In this paper, Tim Bösch et al. presented a new MAX-DOAS profile inversion algorithm, named as BOREAS. As the author noted, the algorithm could be the first one which retrieve profiles based on optical depths of absorbers. The algorithm is well verified through sensitivity tests with synthetic data and comparisons with various collocated independent data during the CINDI-2 campaign. In general the scientific topic is meaningful.

Thank you very much for the positive comment.

However I think the authors should clarify two major points before publication:

1) The unique feature of the BOREAS algorithm is doing inversion based on optical depths of absorbers. The approach allows including DSOT at different wavelengths in a profile inversion. However the authors do not discuss the improvement of doing inversion with optical depths compared to with slant column densities. If there is no a considerable improvement, innovativeness of the algorithm is doubtable.

The authors would like to clarify that inversion with optical depths is only applied to the aerosol retrieval. In order to make this clear, the following lines will be added to the abstract:
The aerosol profile retrieval is based on a novel approach in which the absorption depth of O_4 is directly used in order to retrieve extinction coefficient profiles instead of the commonly used perturbation theory method. The retrieval of trace gases is done with the frequently used optimal estimation method but significant improvements on how to deal with wrongly weighted a priori constraints and for scenarios in which the a priori profile is inaccurate are presented.
The aerosol approach was chosen in order to avoid the standard perturbation theory method. We believe that the perturbation of an a priori profile, the calculation of the weighting function matrix, the comparison of model and measured dSCD as well as the subsequent perturbation of the next layer, are time consuming and maybe complex steps which can be avoided when utilizing the optical depths. However, it should be noted that for simple atmospheric conditions, larger differences of the profiling results to other community algorithms are not expected. The generally good agreement of algorithms will be presented in the upcoming papers of Frieß et al. (2018) and Tirpitz et al. (2018).

2) In section 4, the author demonstrates that profile inversion can be improved if a priori shape is used to scale a pre-calculated AOT and VCD. However the improvement only works when a priori profile is similar with the true atmospheric profile. How do we know whether or not the a-priori shape is close to the real atmospheric profile for real measurements? If a wrong priori shape is assumed, does the method

The knowledge of the true atmospheric profiles is not necessary in order to apply a priori pre-scaling. If the true profile is similarly shaped as the a priori profile, a clear improvement is achieved. When the true profile has a different shape, the pre-scaling does not deteriorate the results. This can be seen in Figure A2 on the example of box profiles for aerosols and in Figure A9 for NO_2. Especially the B3 scenario shape is not even close to an exponential profile. Even though no clear improvement can be observed, no deterioration can be seen either. Additionally, the number of iterations for the aerosol retrieval is reduced when using an a priori profile closer to the true atmospheric conditions.
In order to clarify this, the following lines will be adapted in Section 4.1.1 in the manuscript:

However, no improvement is found when the shape of the a priori profile deviates strongly from the true atmospheric condition (see box profiles in appendix A).
However, no improvement is found when the shape of the a priori profile deviates strongly from the true atmospheric condition but no deterioration either (see box profiles in appendix A).

Specific Comments:

1) In section 3, the authors do not clarify that how the algorithm deals with negative values which could be retrieved.

The aerosol profile retrieval works in the logarithmic space and thus no negative values can be retrieved. The optimal estimation based trace gas retrieval works in the linear space. Here, negative values are possible, especially when the regularization ratio is wrongly weighted. However, a priori pre scaling leads to a better weighting of a priori constrains in addition to the usage of a regularization parameter $g \neq 1$. Negative values are still possible but rare. While negative values are meaningless from a chemical/physical perspective they can be understood as a representation of uncertainties in the respective altitude region from a mathematical point of view.
The following line will be added to Section 3.1 in the manuscript:

Equation 15 is solved in the logarithmic space in order to avoid negative values.

Additionally, Section 3.2 will be adapted:

Equation 18 is solved in the linear space. Negative values are possible but can be avoided by applying appropriate a priori constraints.

2) Line 10 on page 11: aerosols can impact the sensitivities of MAX-DOAS measurements to trace gas profiles, especially at high altitudes. The optimal settings of inversion parameters could depend on aerosols. Therefore sensitivity tests should also be done under typical aerosol conditions, especially a heavy aerosol load.

We fully agree with the reviewers suggestion. However, the BOREAS algorithm participated in a comparison study for synthetic data and real data which will pe published by Frieß et al. (2018) and Tirpitz et al. (2018), respectively. Especially in the first study, various combinations of aerosol and trace gas profiles (also with a heavy aerosol load) are investigated in order to answer this question. Therefore, we would like to avoid repeating similar investigations on this matter in this manuscript.

3) Figure 4 (left): It is hard to identify which color curves are corresponding to individual true profiles. Please try to mark them.

As suggested, the linestyles were changed and the pre-scaled a priori profiles were included (as asked by

reviewer #2). The following four figures were adapted for this purpose and will be added to the revised manuscript.
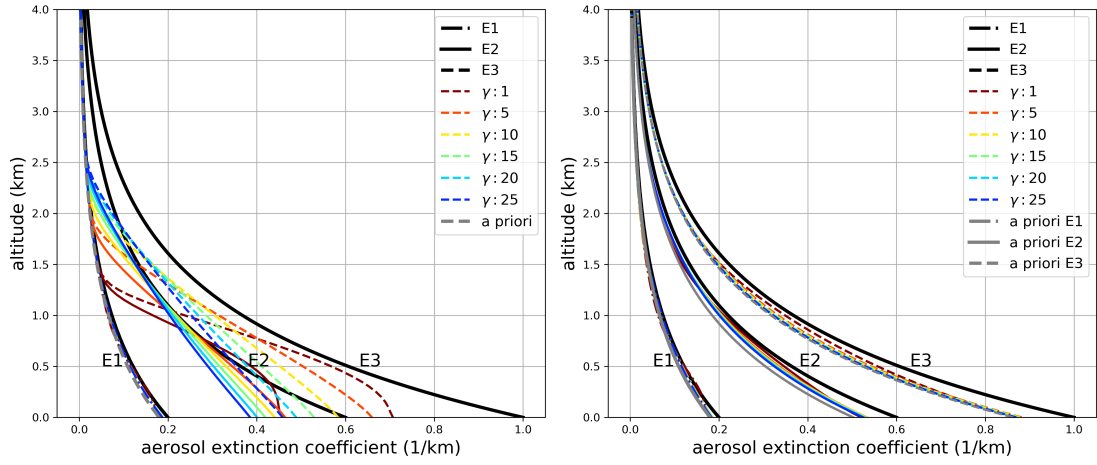

Figure 1: **(Changed version of manuscript Figure 4)** Retrieval results with a fixed (left) and a pre-scaled a priori profile (right) with varying Tikhonov parameters γ for SNR = 3000. Small γ values mean less smoothing of the resulting profiles.
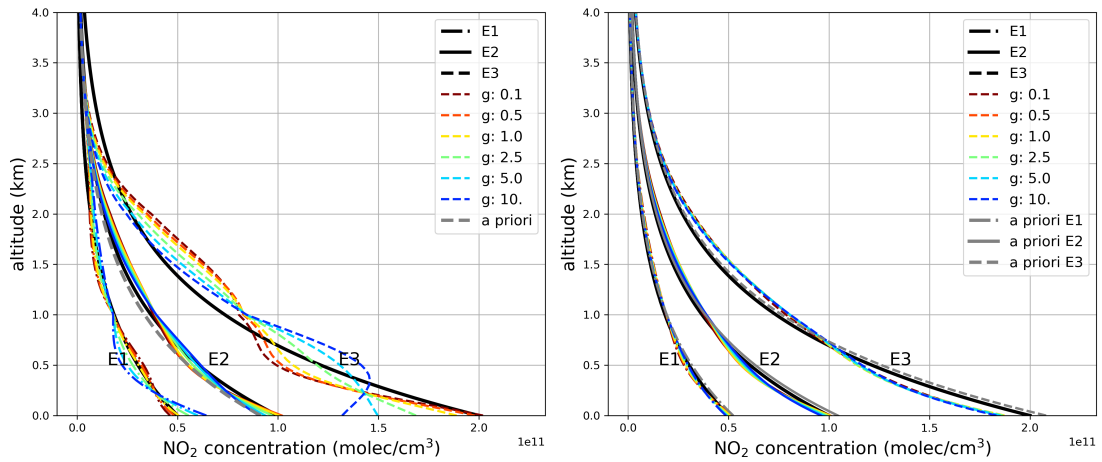

Figure 2: **(Changed version of manuscript Figure 7)** Retrieval results with a fix (left) and a pre-scaled a priori profile (right) with g factors. Small g values mean less measurement weighting for the resulting profiles.
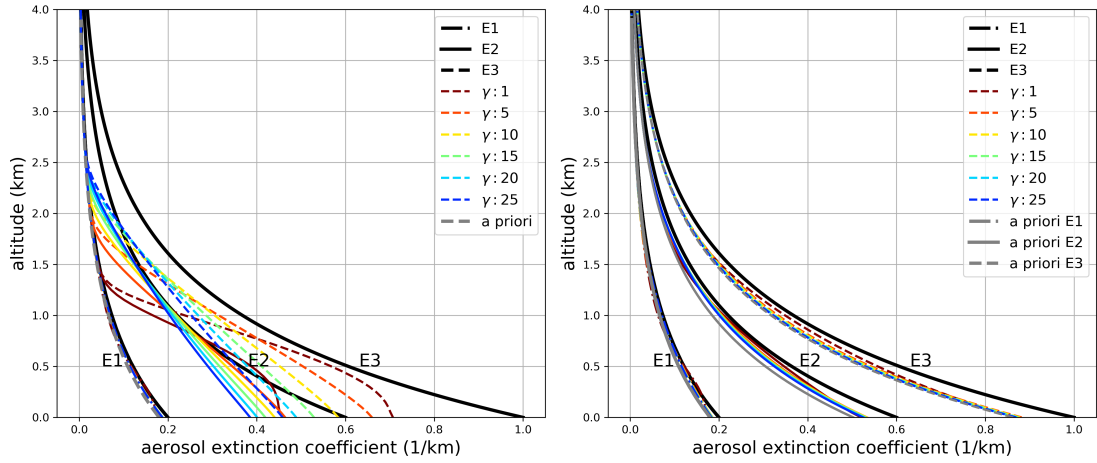
Figure 3: **(Changed version of manuscript Figure A2)** Retrieval results with a fix (left) and a pre-scaled a priori profile (right) with varying Tikhonov parameters γ for SNR = 3000. Small γ values mean less smoothing of the resulting profiles.
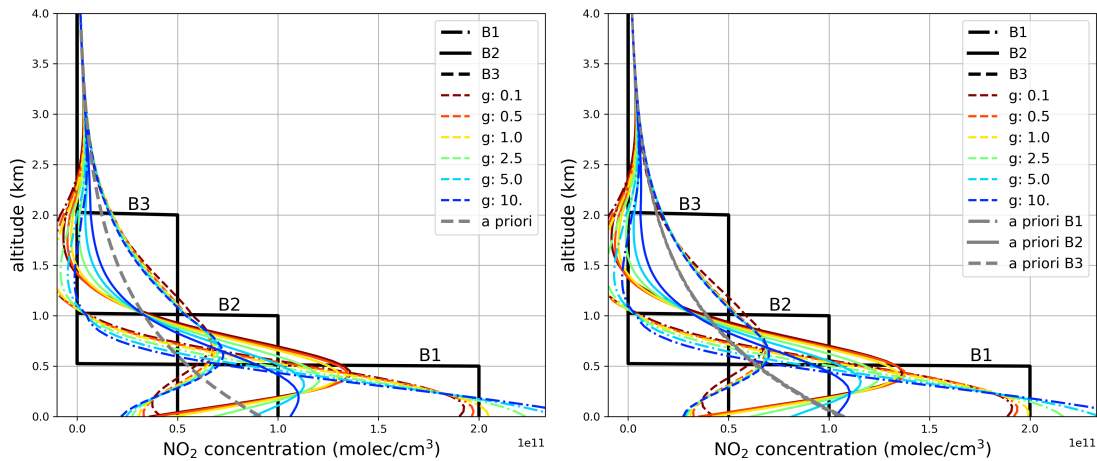

Figure 4: **(Changed version of manuscript Figure A9)** Retrieval results with a fix (left) and a pre-scaled a priori profile (right) with g factors. Small g values mean less measurement weighting for the resulting profiles.

4) Section 4.2: The author claim that total error of aerosol and trace gas profile inversion contains the three parts. However the level of converge, namely differences of modelled and measured SOT, could also contribute some errors. The converge level also depends on the maximum number of iterations.

The RMS between measured and simulated dSOT or dSCD differences for the aerosol or trace gas retrieval, respectively, is a complicated quantity as it does not say a lot about the quality of the retrieved profiles. If constraints on the measurement are chosen too weak, very good agreement can be achieved between measured and modelled slant columns but the resulting profiles often show strong oscillation because of the ill-posed problem of profile inversion. Local minima in the respective RMS quantities exist but their analysis is, especially for aerosols, time consuming and the interpretation depends strongly on the actual atmospheric conditions. Due to this issue, we do not suggest the usage of these quantities for an error analysis with respect to the quality of the retrieved profiles.

For the retrieval of aerosol profiles, higher altitude a priori variances were set to smaller values in order to reduce issues near the grid boundary where the sensitivity is lowest but small instabilities might lead to strong oscillations. The small errors should not be misinterpreted as lower uncertainties in the specific altitudes but are deliberately suppressed.

The following lines will be added to Section 4.2 in the manuscript to explain this issue:

Note that the errors are nearly zero for higher altitudes because of the height depending variances which were chosen in order to reduce possible retrieval instabilities in altitude regimes where the sensitivity is lowest.

6) Line 5 on page 22: The definition of a-priori variance actually increase constraint of a-priori in the inversion at high altitudes. Do you follow the same definition in the synthetic test? The definition could impact the conclusions of discussions on the optimal settings of Tikhonov, a-priori shape scaling.

For the depicted synthetic scenarios a similar definition was chosen. We agree that this is an additional constraint but the optimal Tikhonov parameter is generally not strongly affected by this choice as the variances are only of minor importance when changing the Tikhonov parameter drastically. The a priori pre-scaling is not negatively affected by this choice. Also a constant variance would yield in a clear improvement under the assumptions discussed in the corresponding sections (4.1.1, 4.1.2).

In addition the definition could also cause that the inversion can not retrieve lifted layers of aerosols and trace gases well. Actually the problem can be seen in Fig. 16 and Fig. 19.

We agree partially. The definition reduces the sensitivity in higher altitudes as we force the result stronger into the direction of the a priori profile. With the assumption of an exponentially shaped a priori, we further assumed the main load/concentration to be close to the surface. While the aerosol retrieval is still able to retrieve elevated layers due to the applied iterations, the trace gas retrieval will fail in retrieving the proper maximum value and altitude. However, in theses cases, the profiling results will still show elevated features as can be seen in Figure 16 but not in Figure 19. Unfortunately, both Figures show two difficulties. Figure 16 depicts elevated layers (08:00 and 10:00 UTC) in altitudes where the chance of a successful retrieval is low, which is independent from the a priori variance. Only the change to another a priori profile would result in a clearly better retrieval response. On the other hand, Figure 19 shows elevated layers with such a small vertical extent that the vertical resolution of MAX-DOAS profiling is simply not sufficient.

The following lines will be added to the manuscript (Section 4.3) in order to clarify that the choice of a height depending variance is of minor importance for the results:

The a priori variance was decreasing with altitude from 1.5 at the surface to 0.01 at 4 km.

The a priori variance was decreasing with altitude from 1.5 at the surface to 0.01 at 4 km. This definition was chosen to improve the profiling results for lower altitudes where the main aerosol load/concentration can be expected and in order to suppress instabilities at the upper grid boundary where the sensitivity is lowest.

BOREAS - a new MAX-DOAS profile retrieval algorithm for aerosols and trace gases

Tim Bösch[1], Vladimir Rozanov[1], Andreas Richter[1], Enno Peters[1,a], Alexei Rozanov[1],
Folkard Wittrock[1], Alexis Merlaud[4], Johannes Lampel[3,9], Stefan Schmitt[3], Marijn de Haij[2],
Stijn Berkhout[6], Bas Henzing[5], Arnoud Apituley[2], Mirjam den Hoed[2], Jan Vonk[6],
Martin Tiefengraber[7,8], Moritz Müller[7,8], and John Philip Burrows[1]

[1]Institute of Environmental Physics, University of Bremen, Bremen, Germany
[2]Royal Netherlands Meteorological Institute (KNMI), De Bilt, the Netherlands
[3]Institute of Environmental Physics, University of Heidelberg, Heidelberg, Germany
[4]Royal Belgian Institute for Space Aeronomy (BIRA-IASB), Brussels, Belgium
[5]Netherlands Organization for Applied Scientific Research (TNO), Utrecht, the Netherlands
[6]National Institute for Public Health and the Environment (RIVM), Bilthoven, the Netherlands
[7]LuftBlick, Kreith, Austria
[8]Institute of Atmospheric and Cryospheric Sciences, University of Innsbruck, Innsbruck, Austria
[9]Airyx GmbH, Eppelheim, Germany
[a]now at: Institute for protection of maritime infrastructures, Bremerhaven, Germany

Correspondence to: Tim Bösch (tim.boesch@iup.physik.uni-bremen.de)

Abstract. We present a new MAX-DOAS profiling algorithm for aerosols and trace gases, BOREAS, which utilizes an iterative solution method including Tikhonov regularization and the optimal estimation technique. The aerosol profile retrieval is based on a novel approach in which the absorption depth of O_4 is directly used in order to retrieve extinction coefficient profiles instead of the commonly used perturbation theory method. The retrieval of trace gases is done with the frequently used optimal estimation method but significant improvements on how to deal with wrongly weighted a priori constraints and for scenarios in which the a priori profile is inaccurate are presented.

Performance tests are separated into two parts. First, we address the general sensitivity of the retrieval on the example of synthetic data calculated with the radiative transfer model SCIATRAN. In ~~a~~ the second part of the study, we demonstrate BOREAS profiling accuracy by validating results with the help of ancillary measurements carried out during the CINDI-2 campaign in Cabauw, the Netherlands in 2016.

The synthetic sensitivity tests indicate, that the regularization between measurement and a priori constraints is insufficient when knowledge of the true state of the atmosphere is poor. We demonstrate a priori pre-scaling and extensive regularization tests as a tool for the optimization of retrieved profiles. The comparison of retrieval results with in situ, ceilometer, NO_2 LIDAR, sonde and long path DOAS measurements during the CINDI-2 campaign always shows high correlations with coefficients greater than ~~0.79~~0.75. The largest differences can be found in the morning hours, when the planetary boundary layer is not yet fully developed and the concentration of trace gases and aerosol, as a result of a low night-time boundary layer having formed, is focused in a shallow, surface near layer.

1 Introduction

Aerosols and trace gases play an important role for life on Earth as high concentrations have adverse impacts on human health and climate. Furthermore, aerosols impact on Earth's energy budget by radiative forcing. They interact with solar radiation by scattering and absorption processes. Additionally, they have an impact on the formation of clouds when acting as cloud condensation nuclei (CCN). Despite considerable efforts by the scientific community, uncertainties on aerosol radiative forcing are still high (Stocker, 2014).

In addition to aerosols, atmospheric trace gases are of importance in an increasingly urbanized world as they impact on human health, agriculture, acid deposition, and climate (e.g. Lelieveld et al. (2002)). Trace gases in the troposphere such as nitrogen dioxide and sulfur dioxide (NO_2, SO_2), nitrous acid (HONO), formaldehyde (HCHO) and glyoxal (CHOCHO) need to be measured to assess their impact on air quality and because their spatial and temporal inhomogeneous distribution provides information on different emission sources e.g. the combustion of fossil fuels, biomass burning and agriculture (Wittrock et al., 2004; Irie et al., 2011; Pinardi et al., 2013; Hendrick et al., 2014). The separation and identification of anthropogenic from natural sources as well as measurements of their temporal variability improves the understanding of their effects on climate and life on Earth. The current lack of knowledge leads to uncertainties in temporal and spatial emission patterns of trace gases and aerosols and limits our ability to fully understand atmospheric processes. This results in a need for comprehensive measurements to fill these gaps.

For more than 15 years, Multi-Axis Differential Optical Absorption Spectroscopy (MAX-DOAS) measurements have been used to investigate the chemical composition of the troposphere (Hönninger and Platt, 2002; Bobrowski et al., 2003; Leser H. et al., 2003; Wittrock et al., 2004; Wagner et al., 2004; van Roozendael et al., 2004). This passive remote sensing method is based on absorption spectroscopy applied to measurements of scattered sunlight. The advantages of ground-based MAX-DOAS when compared to satellite observations are the high sensitivity for the lowermost layers of the troposphere, the high temporal and spatial resolution of measurements, and the lower cost.

The strength of the absorption signal detected in scattered sunlight depends on the absorber amounts and their vertical distribution but also on the length of the light path. In general, this length in a certain altitude layer is a function of the measurement geometry. Therefore, a set of MAX-DOAS radiance measurements taken at different elevation angles (lines of sight, LOS) contains information about the vertical distribution of trace gases, which can be retrieved. However, the retrieval of absorber profiles from MAX-DOAS measurements is an ill posed problem that needs additional constraints (see Section 3.2). Thus, the inversion, which is applied for retrieving vertical ~~profile concentrations~~ concentration profiles, is done by elaborated mathematical methods such as optimal estimation (OE). In addition to the trace gas profile, the aerosol extinction profile needs to be retrieved as well as it has a non-linear effect on the trace gas retrieval and it is too variable to be approximated by climatologies. In contrast to the trace gas retrievals, aerosol retrievals are strongly non-linear, necessitating iterative inversion schemes such as the Gauss-Newton algorithm or the Levenberg Marquardt algorithm (Rodgers, 2004).

Profile retrieval algorithms used in the scientific community are either inversion algorithms or parametrized approaches. Inversion algorithms directly link the measurement quantity to the vertical profile of the target absorber with the help of a forward

model (Wittrock et al., 2004; Hendrick et al., 2004; Wagner et al., 2004; Frieß et al., 2006; Wittrock, 2006; Clémer et al., 2010; Wang et al., 2017). This model is usually calculated with a radiative transfer model (RTM) assuming a selected set of atmospheric conditions. For trace gases, the model also includes a sensitivity matrix which can be considered as derivative of the measurement quantity with respect to the trace gas concentration for each altitude level. For aerosols, this sensitivity matrix

5 is normally calculated via perturbation theory. This perturbation approach is shortly summarized as follows: by consideration of a trace gas with a well known vertical distribution such as the oxygen dimer O_2-O_2 (or short O_4), the aerosol extinction for each layer is changed gradually and the resulting modelled observations for different LOS are compared with measurements until the iteration converges (e.g. the difference between measurement and modelled quantity is small enough).

Parametrization on the other hand means, that a forward model, based on a limited set of parameters, is used to describe the

10 measurement quantity. Frequently used forward model parameters are integrated values and profile information such as shape and height of certain absorber layers (Sinreich et al., 2005; Lee et al., 2009; Li et al., 2010; Vlemmix et al., 2011; Wagner et al., 2011; Sinreich et al., 2013). The forward model results are calculated with an RTM and are least squares fitted to the measurements. Generally, look up tables (LUT) are pre-calculated for a set of different scenarios, parameters and geometries covering all relevant atmospheric conditions, avoiding high computational efforts during near real time calculations.

15 Inversion algorithms have the advantage that they are not limited to the scenarios used when creating the LUT but unrealistic profiles are possible when the measurement, inversion, or regularization (weighting between the information from measurements and a priori informations) is poor. On the other hand, parametrized approaches evaluate profiles much faster, as the slow forward model computation was already done when creating the LUT.

Although efforts for deriving concentration profiles from MAX-DOAS measurements have been made for more than one de-

20 cade, profiling is still a difficult task and results of different algorithms can differ strongly when the absorber of interest is highly variable and inhomogeneous on spatial and temporal scales (Zieger et al., 2011; Vlemmix et al., 2015; Frieß et al., 2016). Comparison studies of different profiling algorithms for synthetic as well as for real data summarizing the current state of the art and including results from the algorithm introduced here will be reported by Frieß et al. (2018) and Tirpitz et al. (2018).

25 The purpose of this study is the introduction of IUP Bremen's new MAX-DOAS profile retrieval algorithm for aerosols and trace gases BOREAS (Bremen Optimal estimation REtrieval for Aerosols and trace gaseS) which has been developed to improve on the earlier profile retrieval algorithm (Wittrock, 2006). BOREAS uses a novel approach for the retrieval of aerosols but a similar optimal estimation technique for the retrieval of trace gases. In contrast to perturbation based inversion algorithms, BOREAS uses the change (from an a priori state) of depth in an absorption band to get information on the aerosol content which

30 caused this change. To the authors' knowledge, this approach has never been used within an operational profiling algorithm and it complements the variety of methods with another promising technique. In order to improve the standard OE method for trace gases, a simple way of changing the weighting between a priori and measurement constraints is introduced by varying a regularization factor so that oscillations are minimized. Additionally, the usage of a priori pre-scaling is highlighted as one way of improving results when the a priori profile is far away from the real atmosphere.

35

The development of BOREAS aimed at several key properties:

1. Flexibility: the algorithm should retrieve aerosol and trace gas profiles from any MAX-DOAS measurement with pre-filtering options for the data.

2. Accuracy/stability: the algorithm should be stable in terms of varying atmospheric conditions when retrieving profiles for several years of data. The profiling results (modelled observation) should fit the measured observations with a high accuracy.

3. Automation: the retrieval should respond to problematic data/settings (e.g. low information content, wrong regularization) automatically with an included problem solution scheme.

4. Fast: the algorithm should be fast enough to allow near real time profile retrievals.

The manuscript is organised as follow: in the first section, a typical MAX-DOAS measurement and its information content are shortly described. The next section focuses on the theoretical background of the retrieval algorithm. This section is followed by a detailed sensitivity study. The 4th section is divided into an analysis of synthetic data, a discussion of error sources and an example of application to real measurements which shows that BOREAS is able to retrieve profiles with high reliability and accuracy. The final section 5 concludes and summarizes the results presented in this study.

2 MAX-DOAS measurements and the DOAS retrieval

Modern ground-based MAX-DOAS instruments are capable of measuring scattered sunlight in the ultraviolet (UV) and visible (VIS) spectral range with a full azimuthal and elevation angle coverage of the hemisphere (see Figure 1). In general, the spectral least-squares fit of absorption cross sections and a polynomial to the slant optical thickness (logarithm of a sun normalized radiance at a certain LOS, also called slant optical thickness, SOT) $\tau = -\ln(I/I_0)$ (DOAS fit) provides integrated concentrations ρ along the light path L, the so called slant column densities S (or SCD) (Platt and Stutz, 2008).

$$S = \int_0^L \rho(s)ds$$

The length of the light path L depends on the sun position, the scattering properties of the atmosphere and on the viewing geometry. For ground based measurements, the extraterrestrial solar spectrum I_0 is usually replaced by an intensity spectrum measured in zenith direction I_{ref} (reference spectrum) to compensate for Fraunhofer lines and instrumental issues (e.g. temperature dependent wavelength shifts). As this zenith spectrum itself is usually contaminated by the absorber of interest to some extent, the difference of the two SCDs, ΔS is retrieved and referred to as differential SCD. The differential optical thickness $\Delta \tau_j$ of a certain absorber j only, is defined as

$$\Delta \tau_j(\lambda, \mathbf{\Omega}) = \sigma_j(\lambda) \Delta S_j(\mathbf{\Omega}), \tag{1}$$
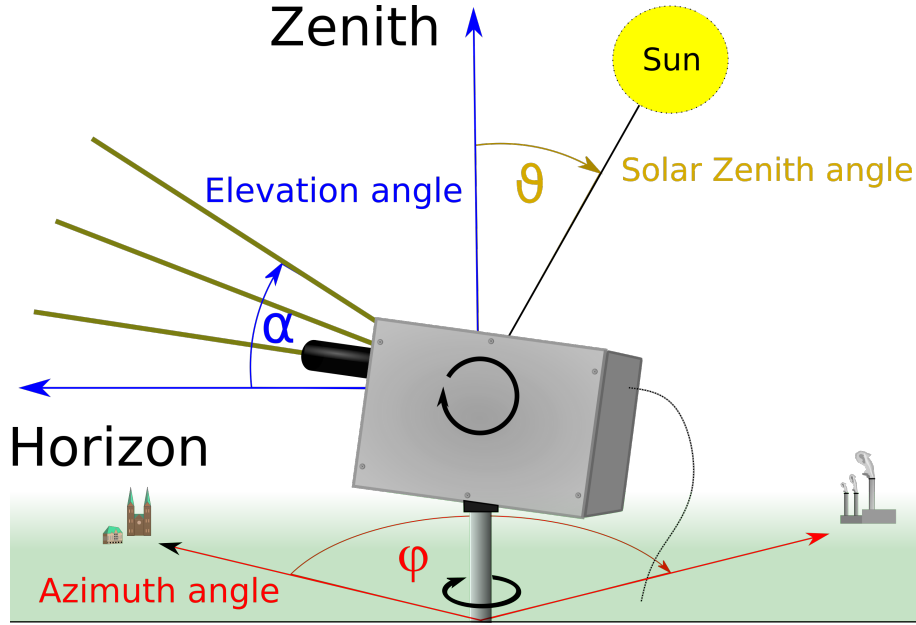
4

Figure 1. Schematic representation of typical MAX-DOAS measurement geometries.

where $\sigma_j(\lambda)$ is the spectral absorption cross section and $\boldsymbol{\Omega} = \{\alpha, \varphi, \vartheta\}$ represents the angular variables. Here, α is the elevation angle (or LOS), φ is the relative azimuth angle (RAA) between sun and viewing azimuth, and ϑ is the solar zenith angle (SZA). When using a single zenith spectrum measured around noon as I_{ref}, the tropospheric signal in I_{ref} is minimised but for absorbers which are also present in the stratosphere, stratospheric absorption contributes significantly to ΔS in the morning

5   and evening. This is due to diurnal variations in the stratospheric amounts of some absorbers such as NO_2 and the change in light paths through the stratosphere because of a varying SZA (see e.g. Leser H. et al. (2003)). To minimise the stratospheric signal, a reference spectrum measured close in time to the intensity I for a certain geometry is applied. Usually, a scan of measurements in different elevation angles is followed by a measurement in zenith direction so that the whole scan can be fitted with the same reference spectrum.

10   The ratio of slant column density S and the vertically integrated absorber concentration $V = \int_0^H \rho(z)dz$ (vertical column density V) is called air mass factor M (AMF).

$$M(\boldsymbol{\Omega}) \equiv \frac{S(\boldsymbol{\Omega})}{V} \tag{2}$$

Generally, this value depends on the radiative transfer through the atmosphere and on parameters such as SZA, surface albedo, wavelength, and the profiles of aerosols and gaseous absorbers. For trace gases in the boundary layer, it can in first

15   approximation be described by the geometric air mass factor

$$M_{geom}(\alpha) = \frac{S(\alpha)}{V} = \frac{1}{\sin(\alpha)}, \tag{3}$$

5

assuming that the trace gas layer is located below the last scattering point (Hönninger et al., 2004). The differential AMF (dAMF), assuming a zenith reference spectrum, is then $\Delta M = S/V - S_{ref}/V = (1 - \sin(\alpha))/\sin(\alpha)$. The difference between geometric and true AMF depends strongly on the wavelength, elevation angle, relative azimuth angle and aerosols.

Because of the altitude depending concentration of absorbers, there is a need for a similar quantity describing the ratio of S and V in a certain layer. The concept of box air mass factor $\mathscr{M}_z$ (BAMF) introduces this height dependence by defining the ratio for each altitude layer z:

$$\mathscr{M}_z(\boldsymbol{\Omega}) = \frac{S_z(\boldsymbol{\Omega})}{V_z} \tag{4}$$

Here, $\mathscr{M}_z$ depends on the altitude in contrast to the total AMF M. Box air mass factors are calculated by radiative transfer models and can be understood as sensitivity of the partial slant column to the partial vertical column at a certain altitude. On the other hand, multiplication of a profile of partial vertical columns with $\mathscr{M}_z$ leads to the corresponding slant column density.

3 Retrieval algorithm description

The profile retrieval algorithm BOREAS was developed in order to retrieve aerosol and trace gas vertical profiles from MAX-DOAS measurements. The aerosol retrieval is fully implemented within the RTM SCIATRAN (Rozanov et al., 2014) to decrease computation time for the iterative minimization scheme. BOREAS is a Python written analysis script which calls SCIATRAN for the aerosol retrieval and for calculations of BAMF matrices which are then used within an optimal estimation based trace gas retrieval. A flow chart depicting BOREAS is shown in Figure 2. In the next subsections, we give an overview of the individual steps of the algorithm.

3.1 Retrieval of aerosol profiles

The standard DOAS fit does not provide direct information about aerosols present in the atmosphere. However, the scattering and absorption properties of aerosols have an impact on the measured differential slant column density $\Delta S(\boldsymbol{\Omega})$ because scattering processes can significantly modify the light path. ~~In general, the absorption of photons by aerosols plays a small role in contrast to scattering effects, which lead to the modification in photon path length. The~~ Since the single scattering albedo ω (SSA)

$$\omega = \frac{\sigma_s}{\sigma_e} = \frac{\sigma_s}{\sigma_s + \sigma_a}$$

~~quantifies the ratio of scattering σ_s to total extinction efficiency σ_e. Here, σ_e is the sum of scattering and absorption efficiency $\sigma_e = \sigma_s + \sigma_a$. For urban pollution, SSA values are in the range of 0.90 to 0.99 for the visible spectral range (see e.g. Dubovik et al. (2002)) and they stay~~ stays more or less constant when the aerosol type does not change over time and altitude~~. Therefore, the SSA~~, it is not a quantity to be retrieved in BOREAS and is kept constant with typical values for the prevalent aerosol type (e.g. urban pollution: $SSA = 0.92$). The angular scattering distribution of aerosols is fully quantified by the scattering phase function. Within BOREAS, we use the Henyey-Greenstein approximation (Henyey and Greenstein, 1941) with constant values for the
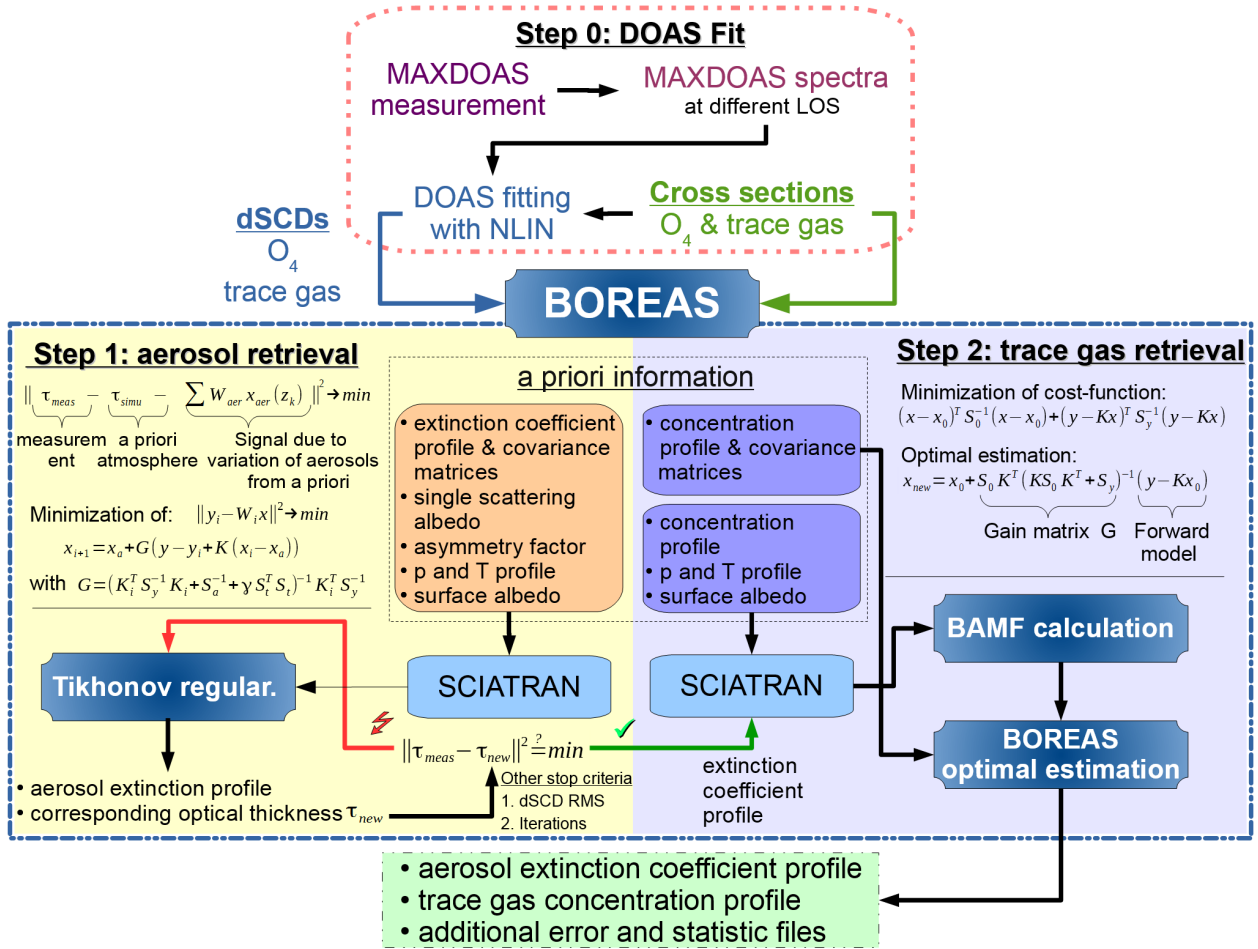
6

Step 0: DOAS Fit

MAXDOAS measurement → MAXDOAS spectra at different LOS

DOAS fitting with NLIN ← **Cross sections** O_4 & trace gas

dSCDs O_4 trace gas

BOREAS

Step 1: aerosol retrieval

$\| \underbrace{\tau_{meas}}_{\text{measurem ent}} - \underbrace{\tau_{simu}}_{\text{a priori atmosphere}} - \underbrace{\sum W_{aer} x_{aer}(z_k)}_{\text{Signal due to variation of aerosols from a priori}} \|^2 \to min$

Minimization of: $\|y_i - W_i x\|^2 \to min$

$x_{i+1} = x_a + G(y - y_i + K(x_i - x_a))$

with $G = (K_i^T S_y^{-1} K_i + S_a^{-1} + \gamma S_t^T S_t)^{-1} K_i^T S_y^{-1}$

a priori information

- extinction coefficient profile & covariance matrices
- single scattering albedo
- asymmetry factor
- p and T profile
- surface albedo

- concentration profile & covariance matrices
- concentration profile
- p and T profile
- surface albedo

Step 2: trace gas retrieval

Minimization of cost-function:
$(x - x_0)^T S_0^{-1}(x - x_0) + (y - Kx)^T S_y^{-1}(y - Kx)$

Optimal estimation:
$x_{new} = x_0 + S_0 K^T (KS_0 K^T + S_y)^{-1}(y - Kx_0)$

Gain matrix G   Forward model

Tikhonov regular.

SCIATRAN

SCIATRAN

BAMF calculation

$\|\tau_{meas} - \tau_{new}\|^2 \overset{?}{=} min$

Other stop criteria
1. dSCD RMS
2. Iterations

extinction coefficient profile

BOREAS optimal estimation

- aerosol extinction profile
- corresponding optical thickness τ_{new}

- aerosol extinction coefficient profile
- trace gas concentration profile
- additional error and statistic files

Figure 2. BOREAS analysis flow chart. The algorithm is separated into two steps. Step 1: Aerosol retrieval within a Tikhonov-Regularization. Step 2: Optimal estimation based trace gas retrieval.

asymmetry factor g which quantifies the amount of forward and backward scattering (e.g. urban pollution: $g = 0.68$). In this parametrization, the optical properties of aerosols are fully defined with g, SSA and an extinction coefficient profile $\sigma_e(z)$. The latter is the retrieval parameter for BOREAS aerosol retrievals. Note, that the usage of measured phase functions will be implemented in BOREAS in the future, since Henyey-Greenstein is in some situations not an accurate representation of the
5 atmospheric aerosol scattering distribution.

If $\sigma_e(z)$ is known, then the aerosol optical thickness (AOT) can be determined as $\tau_{aer} = \int_0^H \sigma_e(z)dz$, where the integration is performed over the entire atmosphere. If the vertical profile of an absorber number density is known, differences between modelled and measured S for this absorber are the result of differences between the assumed and real aerosol profile. As observations at different LOS have varying sensitivity to the presence of aerosols at different altitudes, this can be used to retrieve
10 an aerosol profile.

7

Generally, the vertical profiles of species in the troposphere are unknown because of the temporal and spatial variability of emission sources, transport and conversion processes. However, the oxygen monomer O_2 is in this respect an exceptional species because it only depends on pressure and temperature. Furthermore, as the oxygen dimer O_4 concentration is proportional to the squared monomer concentration, its profile is exponentially decreasing with altitude as well. The O_4 slant column density can easily be determined, because O_4 has spectral absorption features in the wavelength regions of most DOAS fits. Detailed sensitivity studies of O_4 $\Delta S(\mathbf{\Omega})$ measurements regarding changes in atmospheric aerosol properties can be found in Wagner et al. (2004) and Frieß et al. (2006).

In the BOREAS aerosol retrieval algorithm, the difference between modelled and measured O_4 differential slant optical thickness's $\Delta\tau(\lambda,\mathbf{\Omega})$ (DSOT) is used to retrieve aerosol extinction profiles in an iterative process. The measured $\Delta\tau(\lambda,\mathbf{\Omega})$ is calculated using Eq. (1), where $\Delta S_i(\mathbf{\Omega})$ is the DSCD retrieved in the framework of the standard DOAS fit, and the simulated O_4 DSOT ($\Delta\tilde{\tau}(\lambda,\mathbf{\Omega})$) is calculated as follows:

$$\Delta\tilde{\tau}(\lambda,\mathbf{\Omega},N_a(z)) \;=\; \ln\frac{I(\lambda,\mathbf{\Omega},N_a(z))}{I_{ref}(\lambda,N_a(z))}\,, \tag{5}$$

where $I(\lambda,\mathbf{\Omega},N_a(z))$ and $I_{ref}(\lambda,N_a(z))$ are the intensities calculated using SCIATRAN under the assumption that O_4 is the only absorber. The dependency on the reference geometry $\mathbf{\Omega}_{ref}$ is summarized with the index ref and will be neglected from now on. The vertical profiles of pressure and temperature are used according to the US standard atmosphere model (NASA, 1976) but can be replaced by measured atmospheric conditions when available. The aerosol loading is described using an a priori concentration number density vertical profile $N_a(z)$.

The inverse problem with respect to the aerosol optical depth is then formulated as

$$\left\| \Delta\tau(\lambda,\mathbf{\Omega}) \;-\; \Delta\tilde{\tau}(\lambda,\mathbf{\Omega},N_a(z)) \;-\; P(\lambda,\mathbf{\Omega}) \right\|^2 \;\longrightarrow\; \min\,, \tag{6}$$

where $P(\lambda,\mathbf{\Omega})$ is a polynomial of lower order and its argument $\mathbf{\Omega}$ emphasises that polynomial coefficients depend on the LOS angle. The assumptions made in this formulation are that 1) the O_4 absorption derived from the measurements does not depend on the concentration of other trace gases and 2) that the optical depth in an atmosphere without other absorbers can be described as the sum of the O_4 optical depth and a low order polynomial.

Since $\Delta\tilde{\tau}(\lambda,\mathbf{\Omega},N_a(z))$ is a non-linear and complicated functional of $N_a(z)$, an analytical solution of this minimization problem does not exist. To simplify the solution of the minimization problem given by Eq. (6), let us consider the variation of DSOT caused by the variation of the aerosol number density. The variation of DSOT in a linear approximation can be represented in the form of the following functional Tailor series (Rozanov and Rozanov, 2010):

$$\Delta\tilde{\tau}(\lambda,\mathbf{\Omega},N_a(z)) \;=\; \Delta\tilde{\tau}(\lambda,\mathbf{\Omega},\bar{N}_a(z)) \;+\; \int_0^H W(\lambda,\mathbf{\Omega},z)\,\delta N_a(z)\,dz \;+\; \varepsilon_{lin}(\lambda)\,, \tag{7}$$

where

$$W(\lambda,\mathbf{\Omega},z) \;=\; \left.\frac{\delta\,\Delta\tilde{\tau}(\lambda,\mathbf{\Omega},N_a(z))}{\delta\,N_a(z)}\right|_{\bar{N}_a}$$

8

is a functional derivative of DSOT with respect to the aerosol number density profile $N_a(z)$ around the initial guess $\bar{N}_a(z)$. $W(\lambda, \mathbf{\Omega}, z)$ is usually referred to as weighting function and $\varepsilon_{lin}(\lambda)$ is the linearisation error.

It follows that the weighting function provides a linear relationship between the variation of DSOT and the variation of an aerosol number density N_a around the initial guess $\bar{N}_a$. Substituting now Eq. (7) into (6) and approximating the integral with a finite sum, we have

$$\left\| \Delta\tau(\lambda, \mathbf{\Omega}) \;-\; \Delta\tilde{\tau}(\lambda, \mathbf{\Omega}, \bar{N}_a(z)) \;-\; \sum_{k=1}^{L} \mathcal{W}(\lambda, \mathbf{\Omega}, z_k)(x_k - \bar{x}_k) \;-\; P(\lambda, \mathbf{\Omega}) \right\|^2 \longrightarrow \min . \tag{8}$$

Here, $\Delta x = x_k - \bar{x}_k = N_a(z_k) - \bar{N}_a(z_k)$, L is the number of altitude levels, and $\mathcal{W}(\lambda, \mathbf{\Omega}, z_k)$ is defined to satisfy the trapezoidal integration rule.

The solution of the minimization problem given by Eq. (8) is performed on a discrete wavelength grid. In fact, only five wavelengths over the O_4 absorption band centred at e.g. 477 nm are used.

The minimization problem can be reformulated in the following vector-matrix form:

$$\left\| \Delta\mathbf{y} \;-\; \mathbf{K}\Delta\mathbf{x} \right\|^2 \longrightarrow \min . \tag{9}$$

Here, the vector $\Delta\mathbf{y} = \mathbf{y} - \bar{\mathbf{y}} = |\Delta\mathbf{y}_1, \Delta\mathbf{y}_2, ..., \Delta\mathbf{y}_N|^T$ has the dimension ~~$N \cdot M \times 1$~~ $N \cdot M$ and describes the difference between measured and simulated DSOT at N LOS angles and M wavelengths. The m-th element of vectors $\mathbf{y}_n$ and $\bar{\mathbf{y}}_n$ is the differential slant optical depth of O_4 at wavelength m, given by

$$\{\mathbf{y}_n\}_m \;=\; \Delta\tau^-(\lambda_m, \mathbf{\Omega}_n), \; m \;=\; 1, \ldots, M , \tag{10}$$

$$\{\bar{\mathbf{y}}_n\}_m \;=\; \Delta\tilde{\tau}^-(\lambda_m, \mathbf{\Omega}_n, \bar{N}_a(z)) , \tag{11}$$

where the superscript "-" denotes that a polynomial is subtracted. The state vector $\Delta\mathbf{x}$ has the dimension ~~$L \times 1$~~ L and matrix $\mathbf{K}$ has the dimension ~~$N \cdot M \times L$~~ $(N \cdot M) \times L$, i.e., the matrix consists of $N \cdot M$ rows and L columns. The r-th row of matrix $\mathbf{K}$ is then given by

$$\{\mathbf{K}\}_r \;=\; \left\{ \mathcal{W}^-(\lambda_m, \mathbf{\Omega}_n, z_1), \mathcal{W}^-(\lambda_m, \mathbf{\Omega}_n, z_2), \ldots, \mathcal{W}^-(\lambda_m, \mathbf{\Omega}_n, z_L) \right\} \qquad \text{with} \qquad r = (n-1)M + m \tag{12}$$

and contains weighting functions for the m-th wavelength, n-th LOS in L layers.

The minimization problem given by Eq. (9) is solved employing an iterative Tikhonov regularization technique (Rodgers, 2004):

$$\mathbf{x}_{i+1} = \mathbf{x}_0 + (\mathbf{K}_i^T \mathbf{S}_y^{-1} \mathbf{K}_i + \mathbf{S}_0^{-1} + \gamma \mathbf{S}_t^T \mathbf{S}_t)^{-1} \mathbf{K}_i^T \mathbf{S}_y^{-1} (\mathbf{y} - \mathbf{y}_i + \mathbf{K}_i(\mathbf{x}_i - \mathbf{x}_0)) \tag{13}$$

Here, i is the iteration number, $\mathbf{S}_0$ and $\mathbf{S}_y$ are the a priori and measurement covariance matrices, $\mathbf{K}_i$ is the weighting function matrix calculated using the estimated aerosol number density profile $\mathbf{x}_i$, $\mathbf{S}_t$ is the first order derivative matrix with ~~Thikonov~~ Tikhonov parameter γ and $\mathbf{x}_0 = \bar{\mathbf{x}}$ and $\mathbf{y}_0 = \bar{\mathbf{y}}$ are the a priori profile and the representing a priori measurement vector, respectively. Equation 13 is solved in the logarithmic space in order to avoid negative values.

There are three criteria to stop the iteration process:

- Convergence in parameter space, i.e., the maximum difference between the components of the state vector at two subsequent iterative steps does not exceed the selected criterion (e.g. $0.0001 \, \mathrm{km}^{-1}$).

- The root mean square difference between measured and simulated O_4 DSOT is less than selected (e.g. 0.001).

- The maximum number of iterations is reached.

5 In addition to the equations above, we introduce here other quantities which are useful to describe the retrieval. The gain matrix

$$\mathbf{G}_i = (\mathbf{K}_i^T \mathbf{S}_y^{-1} \mathbf{K}_i + \mathbf{S}_0^{-1} + \gamma \mathbf{S}_t^T \mathbf{S}_t)^{-1} \mathbf{K}_i^T \mathbf{S}_y^{-1} \tag{14}$$

describes the sensitivity of the solution to the measurement. Note, that this formulation includes also the Tikhonov term, leading to differences for $\gamma \neq 0$ with the definition given in Rodgers (2004). The averaging kernel $\mathbf{A}_i = \mathbf{G}_i \mathbf{K}_i$ (AK) characterizes the sensitivity of the solution to the true state. The trace of AK quantifies the degrees of freedom of the signal $d_s = \mathrm{tr}(\mathbf{A})$ (DOF).

10 This quantity is commonly understood as the number of individual pieces of information which, can be retrieved.

3.2 Retrieval of trace gas concentration profiles

Compared to aerosols, the inverse problem for trace gases is easier to solve because, under the assumption of an optically thin atmosphere, the relationship between trace gas concentration and measured differential slant column density is linear. Then, the forward model $\mathbf{F}(\mathbf{x}, \mathbf{b})$ is equal to a set of measurements $\mathbf{y}$,

15 $$\mathbf{y} = \mathbf{F}(\mathbf{x}, \mathbf{b}) + \epsilon \tag{15}$$

where ϵ includes the error of measurement and forward model. $\mathbf{F}(\mathbf{x}, \mathbf{b})$ depends on the retrieval quantity vector $\mathbf{x}$ (trace gas concentration profile) and on an additional parameter vector $\mathbf{b}$. The latter one includes quantities which have an impact on the measurement and are known with some accuracy (e.g. a priori information).

From the perspective of MAX-DOAS, this relationship is strongly ill-posed as the number of retrieval parameters is usually

20 much higher than the number of measurements. Furthermore, as the light paths of two geometrically close elevation angles traverse similar vertical layers near the surface, measurements cannot be considered as independent. Consequently, the retrieval parameter vector $\mathbf{x}$ is not fully constrained by the input vector $\mathbf{y}$ which introduces the need for additional a priori knowledge which constrains the solution. With the assumption of a Gaussian error distribution, the optimal estimation method (OE) is often used to prevent unstable solutions when dealing with ill-posed problems (Rodgers, 2004).

$$\mathbf{x}_n = \mathbf{x}_0 + (\mathbf{K}^T \mathbf{S}_y^{-1} \mathbf{K} + g^{-1} \mathbf{S}_0^{-1})^{-1} \mathbf{K}^T \mathbf{S}_y^{-1} (\mathbf{y} - \mathbf{K} \mathbf{x}_0) \qquad \text{or}$$

25 $$= \mathbf{x}_0 + \mathbf{S}_0 \mathbf{K}^T (\mathbf{K} \mathbf{S}_0 \mathbf{K}^T + g \mathbf{S}_y)^{-1} (\mathbf{y} - \mathbf{K} \mathbf{x}_0) \tag{16}$$

Again, $\mathbf{S}_0$ and $\mathbf{S}_y$ are the covariance matrices, $\mathbf{y}$ is the measurement and $\mathbf{x}_0$ is the a priori profile. Equation 16 is solved in the linear space. Negative values are possible but can be avoided by applying appropriate a priori constraints. Note that we introduced a scaling factor g which gives the possibility of regulating the weighting between a priori and measurement information.

Here, the matrix $\mathbf{K}$ consists of BAMF values for every layer and measuring geometry (Eq. (4)) instead of weighting functions. The covariance matrix of measurements has only diagonal elements which are the absolute errors of the spectral DOAS fit of this absorber. $\mathbf{S}_0$ has constant variances on its diagonal elements but consists of additional non-diagonal elements based on a Gaussian distribution which accounts for a possible correlation of different profile layers (Barret et al., 2002).

4   Results and Discussion

In this section, we first present and discuss results of synthetic sensitivity studies. For this purpose, noise free differential slant columns densities of different aerosol and NO_2 scenarios were simulated with SCIATRAN. Subsequently, these datasets were used as input for BOREAS, and results are compared with the true profiles. In the next subsection, we discuss the error sources of the retrieval before, in the last section, results of data measured during the CINDI-2 campaign (2nd Cabauw Intercomparison of Nitrogen Dioxide measuring Instruments, 2016) are shown. These results are validated by comparison with different ancillary measurements (sondes, LIDAR, long path DOAS, ceilometer, AERONET, Pandora and in situ).

4.1   Sensitivity study with synthetic data

A synthetic dataset of differential slant column densities of NO_2 and O_4 was created using SCIATRAN's spherical mode including multiple scattering. The settings in Table 1 were chosen to describe conditions as they can be found in urban areas like the city of Bremen. Pressure and temperature profiles were taken from a U.S. standard atmosphere (NASA, 1976). The vertical grid was set to 25 m steps from the surface up to 6 km, 250 m steps up to 10 km and 1 km steps up to 60 km. The LOS angles were chosen as a representation of a typical MAX-DOAS measurement with more angles for the lower elevations, where the sensitivity is highest. Both, solar zenith angle and relative azimuth angle were kept constant. The trace gas and aerosol profiles

Table 1. SCIATRAN settings for the calculation of differential slant column densities

trace gases	wavelength (nm)	albedo	SZA (°)	RAA (°)	LOS (°)	asymmetry factor	SSA	climatology
O_4, NO_2	477	0.06	40	90	1, 2, 3, 4, 5, 6, 8, 15, 30	0.68	0.92	US standard

in Table 2 (see also Fig. 3, 6, A1 and A8) were chosen to assess BOREAS retrieval capability under simple (exponential profiles with scale height SH = 1 km) and non-ideal conditions (box profiles, which are not similar to the exponential a priori profiles). The NO_2 scenarios did not include aerosols to avoid the mixture of uncertainties from the trace gas retrieval and inaccuracies within the aerosol retrieval. The box profiles are shown and shortly discussed in appendix A.

11

Table 2. Parameters for aerosol and NO_2 profiles used in the synthetic sensitivity study.

	Exp. profiles (SH = 1 km)			Box profiles (appendix)		
	E1	E2	E3	B1	B2	B3
AOT	0.2	0.6	1.0	0.4	0.4	0.4
VCD (10^{15} molec/cm^2)	5	10	20	10	10	10
maximum altitude (km)	6	6	6	0.5	1	2

4.1.1 Sensitivity of the aerosol retrieval

Figure 3 shows the true exponential extinction coefficient profiles (see Table 1) with aerosol optical thickness's of 0.2, 0.6
25 and 1.0. In addition, an a priori profile with the same scale height (SH = 1 km) but with AOT = 0.18 is depicted. In general, an a priori profile should comprise known information of the true atmosphere. Ancillary measurements are frequently used to gather information for a mean profile. Here, we try to evaluate the performance of the algorithm by using an a priori profile close to the true profile (E1) but also for atmospheres with highly varying aerosol loads (E2, E3).

Figure 3. Exponential aerosol profiles for the synthetic sensitivity study. Also shown is the a priori profile for the aerosol retrieval (dashed line).

The retrieval uses vertical grid steps of 50 m for synthetic data because smaller step widths introduce retrieval noise, whereas
5 larger steps result in vertical structure being overly smoothed. Since the retrieval tends to overestimate the upper layers due to missing sensitivity (see Fig. 9), a height depending a priori variance was used for the preparation of the a priori covariance matrix S_a. The measurement covariance matrix S_e consists of a constant signal to noise (SNR) value which is multiplied with

the measurement for each LOS to get absolute covariances. The Tikhonov parameter is changed in the first examples to demonstrate the retrieval response on this parameter. The iterations stop when convergence is reached or after 60 steps. Convergence in parameter space was set to $0.0001\,\mathrm{km^{-1}}$. In addition, convergence of the RMS of measured and simulated DSOT differences was set to 0.001.

On the left side in Figure 4 the retrieval results for different Tikhonov parameters γ are shown. E1, which is close to the a priori profile (dashed grey line) is retrieved well for all γ values. In general, smaller Tikhonov parameters give too much weight to the measurement by reducing smoothing and introducing retrieval noise which leads to oscillations. Large values smooth the solution in the direction of the a priori profile. When the true atmosphere is far away from the a priori profile, the algorithm does not perform satisfyingly. For E2, strong smoothing (large γ values) leads to more or less straight lines in which insufficient curvature can be found, whereas weak (or no) smoothing means the beginning of oscillations indicated by the reduction of the bottom extinction. No parameter value is able to retrieve the proper bottom extinction. This can be found in the same way for E3 where all results show a clear lack in accuracy. This is not surprising as the a priori profile cannot be understood as the best guess or median of the atmosphere any more.
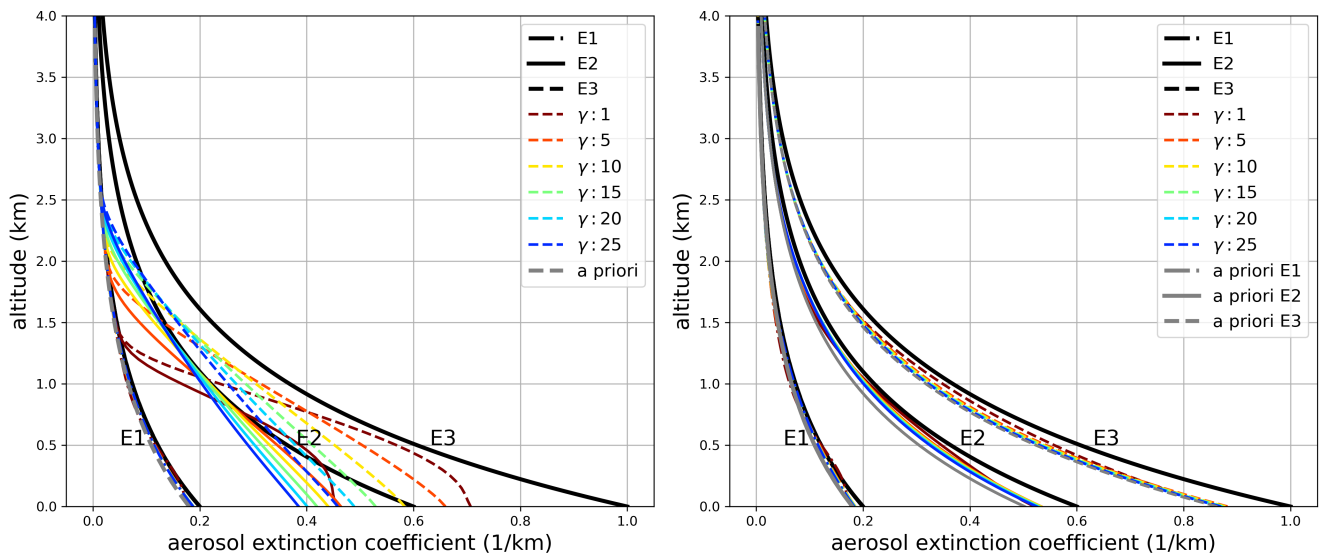
Figure 4. Retrieval results with a fixed (left) and a pre-scaled a priori profile (right) with varying Tikhonov parameters γ for SNR = 3000. Small γ values mean less smoothing of the resulting profiles.

Several authors have already highlighted retrieval problems from MAX-DOAS measurements under highly variable (in time and space) atmospheric conditions (e.g. Vlemmix et al. (2011); Wagner et al. (2011); Vlemmix et al. (2015); Frieß et al. (2016)). Nevertheless, studies that focus on improvements of the regularization (Eriksson, 2000; Hartl and Wenig, 2013) or a priori information (Frieß et al., 2006; Clémer et al., 2010; Hendrick et al., 2014) are rare, with respect to MAX-DOAS

retrievals. Here, we use a priori pre-scaling to cope with strong deviations of the true atmosphere from the a priori estimate. For this purpose, the BOREAS aerosol retrieval is started on a reduced vertical and spectral grid from a zero profile (all a priori extinction values were set to be zero) as a priori information. In Equation 15, the a priori profile x_0 is set to 0 but the remaining terms stay unchanged in order to retrieve a reliable AOT value without limiting the solution by a certain profile shape. Since the retrieval works directly on O_4 absorption, aerosol optical thickness is in general the most reliable retrieval quantity. The AOT from this pre-calculation is used to scale the a priori profile for the ~~true run~~ main run by calculating a scaling factor from the initial a priori AOT and the new value which is applied to all initial extinction coefficients before the main inversion.

5   Note, that the only a priori information used both within the pre-run and within the main run is the Tikhonov parameter. This method performs well when the a priori shape is similar to the true atmospheric profile shape (right side of Fig. 4). However, no improvement is found when the shape of the a priori profile deviates strongly from the true atmospheric condition but no deterioration either (see box profiles in appendix ~~A~~A). On the right-hand side of Figure 4, clear improvements can be seen in both overall shape and bottom extinction. Nevertheless, the profiles tend to deviate stronger at the surface, especially when

10   the aerosol load is higher which was also found by Frieß et al. (2006). The relative differences of retrieved AOT are high for the unscaled retrieval but can be significantly reduced with a priori pre-scaling (see Table 3). Further improvements could be made by increasing the allowed number of iterations together with stronger convergence criteria (not shown) but the average retrieval time would increase as well.

Table 3. True and retrieved AOT for SNR = 3000, $\gamma = 1.0$ with and without a priori pre-scaling including relative differences to the true profile in brackets.

AOT	true value	fix a priori	result	scaled a priori	result
E1	0.2	0.18	0.183 (-8.6%)	0.161	0.179 (-10.4%)
E2	0.6	0.18	0.439 (-26.9%)	0.493	0.535 (-10.6%)
E3	1.0	0.18	0.626 (-37.4%)	0.847	0.895 (-11.1%)

A comparison of all three profiles and their optimal γ ranges with and without pre-scaling indicates that each combination

15   of a priori and true profile has a specific optimal Tikhonov parameter which might differ strongly between each scenario. In addition, the signal to noise is another quantity which has a large impact on the retrieval. In general, SNR values might differ strongly throughout a day, because dynamic ranges of exposure and integration times are frequently used to operate the CCD in the ideal saturation range when the number of photons might differ strongly (e.g. due to different viewing geometries). In Figure 5 we varied SNR (as a representation of the measurement error) and Tikhonov parameter γ from 500 to 5000 and from

20   0.25 to 30 respectively, to find the best parameter range for the optimization of AOT and the bottom extinction (BOT). The figure shows results for the strong aerosol scenario E3 (E1, E2 and the box scenarios are shown in the appendix). Colour coded are the relative differences to the true value with bright spots indicating better retrievals. For scenario E3, high γ (or low SNR) values apply too much smoothing (not enough weight on the measurement) which ends in strong AOT/BOT underestimations of
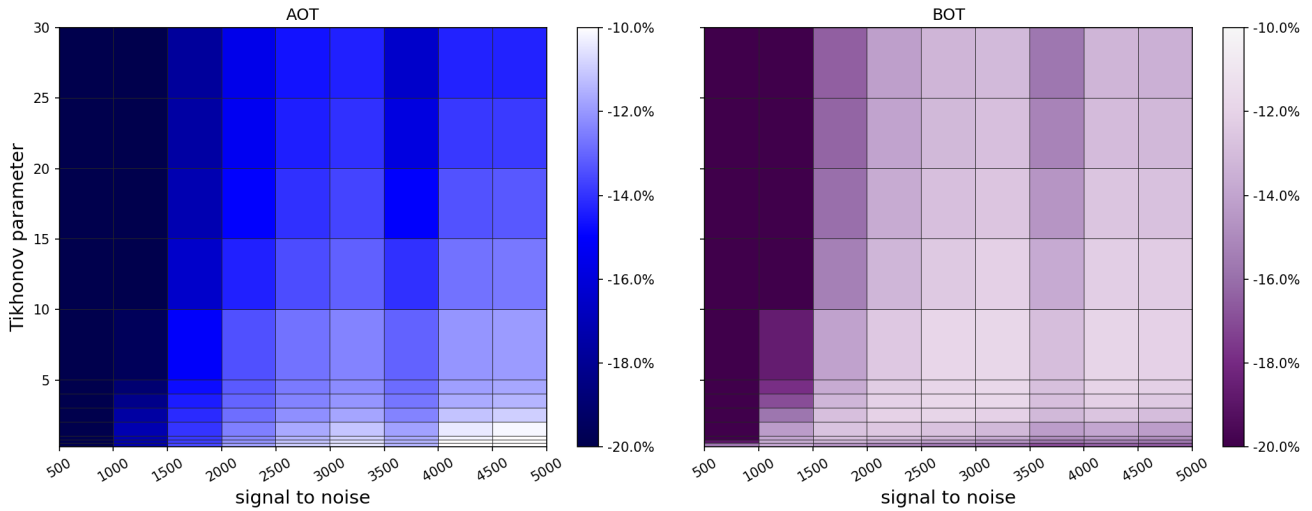
14

Figure 5. Variation of the relative difference of AOT and bottom extinction (BOT) to the true value as a function of signal to noise and Tikhonov parameter, colour coded for scenario E3 with a priori pre-scaling.

the retrieval results. Furthermore, there is an ideal range of SNR values for $\gamma \leq 2$ where the AOT relative difference is $\leq 10\%$. In this specific SNR/γ range, the bottom values do not show the best results. On the other hand, BOT values are optimized for $3 \leq \gamma \leq 10$ for SNR $= 2500$ and SNR $= 3000$ where the AOT does not have the lowest difference. As a consequence, due to unequal vertical sensitivity, choice of a priori constraints and parametrization, in some cases either AOT or the shape of the profile can be optimized. Stable solutions for the optimization of both profile characteristics could not be identified in the range of parametrization, regularization and convergence. As a result, a reasonable compromise for optimum values with respect to both AOT and BOT would be in the range SNR = 2000-3000 with low Tikhonov values $2 \leq \gamma \leq 5$. Note that the SNR range between 3500 and 4000 has larger relative deviations than the surrounding settings which could not be found for other scenarios. This is assumed to be either a unique solution, where the range of settings leads to poor retrieval results, or a numerical instability.

In contrast to this pragmatic approach, the so-called L-curve approach (Hansen, 1992; Engl and Grever, 1994) was found to be insufficient as it already assumes a good regularisation, i.e. the data residual and the parameter norm ($\| \mathbf{x} - \mathbf{x_a} \|$) can be described well by a specific regularisation parameter (Hartl and Wenig, 2013), which was not found for the application of MAX-DOAS profiling.

4.1.2 Sensitivity of the trace gas retrieval

The optimal estimation based trace gas profile retrieval faces similar problems as the regularization difficulties discussed for the aerosol retrieval in the previous section. In many studies, an a priori variance of a fixed percentage of the a priori profile in

combination with the differential slant column density errors from the DOAS fit are used to constrain the solution (e.g. Frieß et al. (2016)). Here, we show that this is an insufficient approach, since the fitting errors might be too small, giving too much weight to the measurement, when the NO_2 concentration is high and the a priori profile is not a good estimate of the true atmosphere.

Again, a priori pre-scaling is used to achieve a better estimate of the true atmospheric conditions. In contrast to the aerosol retrieval which needed a pre-run for a better first guess, the trace gas a priori pre-scaling is achieved using the 30° elevation angle measurement. In the geometric approximation (see Eq. (3)), the differential AMF is 1 which leads to $\Delta S_{30} = V$. This

5 vertical column density V is used as a pre-scaling value for the a priori profile.

The different NO_2 exponential profiles, based on the parameters in Table 2, are shown in Figure 6 together with the a priori profile (box profiles can be found in appendix A). Note that we used an a priori profile close to E2. These profiles are a good representation of the daily variability in an urban region, where high NO_2 concentrations are found during phases of commuter traffic (rush hours) in the morning and late afternoon and low NO_2 loads in between.

Figure 7 depicts the profiling results without a priori pre-scaling on the left side and with pre-scaling on the right side. Different
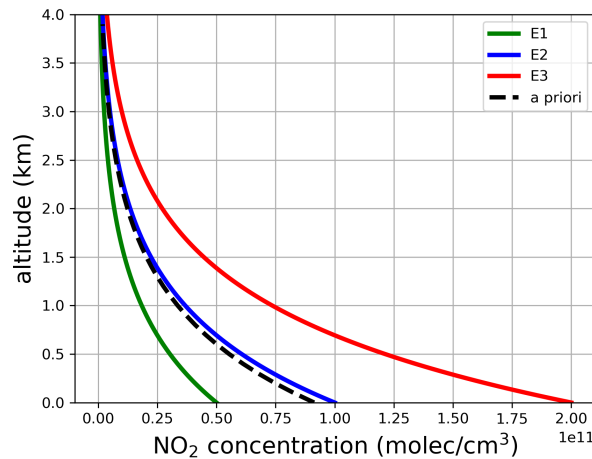
Figure 6. Exponential NO_2 profiles for the synthetic sensitivity study. Also shown, the a priori profile for the aerosol retrieval (dashed line).

10

regularization ratios are achieved by varying parameter g in Eq. (16) which varies the measurement error by $\sqrt{g}$. The retrieval is done on the same vertical grid as in the previous section with similar variances for the a priori covariance matrix. In contrast to a constant signal to noise ratio, we use variances in the range of typical DOAS fit errors of NO_2 for the measurement covariance matrix, which can be understood as the standard approach of the MAX-DOAS profiling community. For small

15 elevation angles and high NO_2 concentrations, the relative ΔS error is often lower than 1% and sometimes even lower than 0.3%, indicating a high reliability in the measurement but neglecting errors due to pointing inaccuracies of the telescope or horizontal inhomogeneities which affect the profiling result but not the measurement.

The results show again the importance of pre-scaling. Whereas the E2 scenario is well retrieved for all g-ranges without pre-

scaling, the other scenarios tend to oscillate or underestimate the profile. Note, that the standard regularization ratio ($g = 1$)

20   does not lead to satisfying results for E3. Applying pre-scaling leads to more accurate profiles especially for E3.

The specific optimal g-range for each scenario depends not only on the a priori profile and the true atmosphere but also on
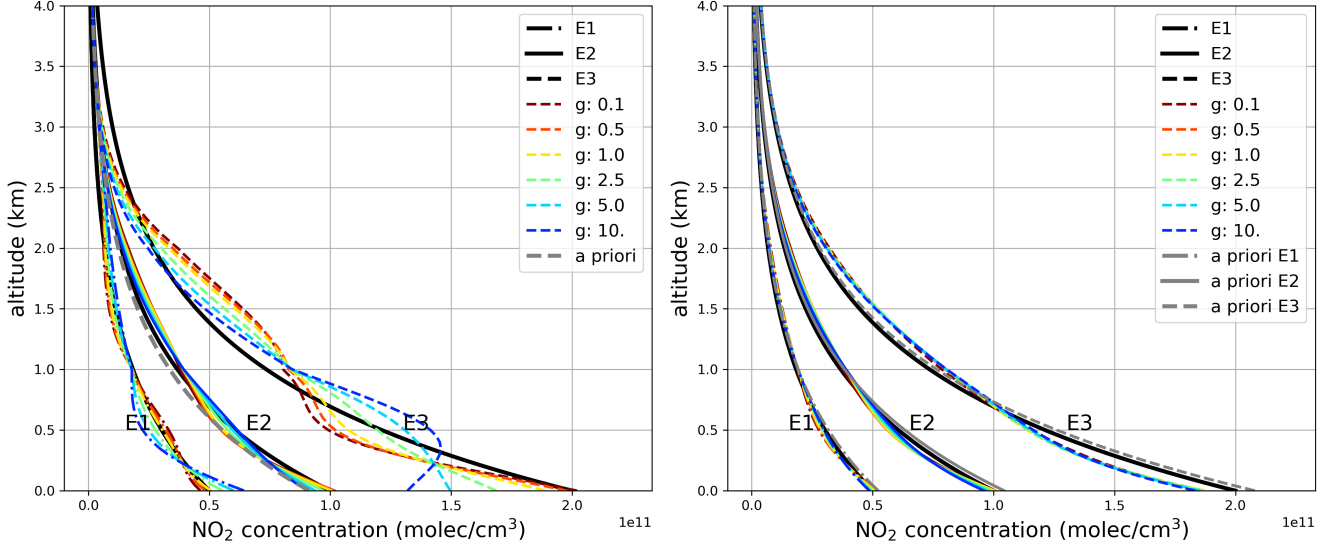

Figure 7. Retrieval results with a fix (left) and a pre-scaled a priori profile (right) with g factors. Small g values mean less measurement weighting for the resulting profiles.

the variance values, their height dependencies and the definition of off-diagonal elements. However, the quantification of this optimal range is a difficult task for real data due to the lack of knowledge about the true atmosphere. Manual variations of g as well as iterative approaches are conceivable. Possible criteria for finding the best g values are e.g. the RMS between measurement and retrieval quantity or ancillary measurements. Here, we used fixed values which were chosen to decrease

5   oscillations while maintaining the best surface concentration.

4.2   Discussion of error sources and information content

The total error of both aerosol and trace gas retrieval can be separated into three different error sources (Rodgers, 2004).

$$\mathbf{S}_{tot} = \mathbf{S}_{sm} + \mathbf{S}_{fw} + \mathbf{S}_{ns} \tag{17}$$

The first error term describes the smoothing error $\mathbf{S}_{sm} = (\mathbf{A} \text{ - } \mathbf{I})\mathbf{S}_e(\mathbf{A} \text{ - } \mathbf{I})^T$ which can be understood as error for the averaging

10   kernel smoothed estimate of the true state of the atmosphere. $\mathbf{A}$ and $\mathbf{I}$ are the averaging kernel and identity matrix respectively. The second term of $\mathbf{S}_{tot}$ is the forward model error $\mathbf{S}_{fw}$, which is hard to quantify in real retrievals, because it needs the true state of the atmosphere. For near linear problems, this error source can be neglected, when the forward model parameters are well estimated. The last error is called retrieval noise $\mathbf{S}_{ns} = \mathbf{G}\mathbf{S}_e\mathbf{G}^T$ (G: gain matrix, see e.g. Eq. (14) and denotes the

17

uncertainty of the retrieved profile due to measurement errors.

15 Figure 8 shows smoothing, retrieval and total error for the before mentioned scenarios of the aerosol retrieval (left) and the trace gas retrieval (right).
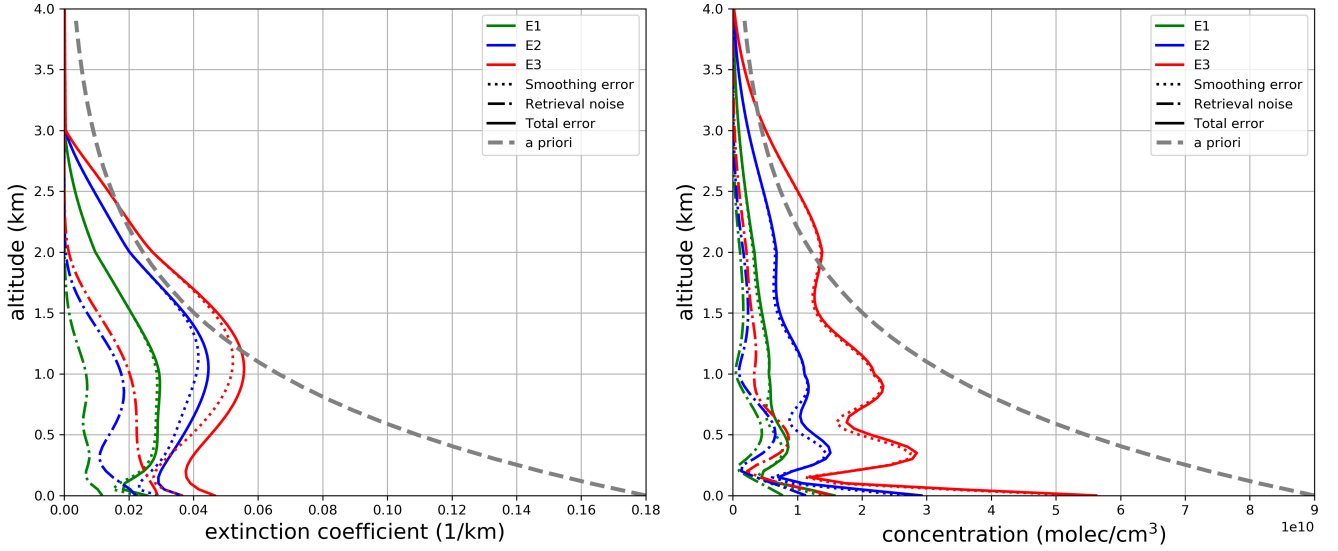
Figure 8. Retrieval errors for E1-E3 of the synthetic aerosol (left) and NO_2 study (right). Aerosol results are shown for SNR = 3000 and Tikhonov parameter $\gamma = 2$. Trace gas errors are depicted without additional regularization (g = 1). Pre- scaling was used.

The total errors for both aerosol and trace gas retrieval are dominated by the smoothing error with negligibly small retrieval noise. This shows, that the measurement itself can be considered as a small error source in contrast to the generally limited

5 information content of MAX-DOAS measurements. Note, that the error components of the NO_2 profile show small oscillations which also indicates that larger constraints are needed. For the aerosol retrieval, the largest errors can be found in an altitude were the sensitivity is low with an additional increase near the surface. The errors are nearly zero for higher altitudes because of the height depending variances which were chosen in order to reduce possible retrieval instabilities in altitude regimes where the sensitivity is lowest. In general, NO_2 shows also larger errors for higher altitudes but the surface error is dominant here,

10 indicating a reduced sensitivity or poor parametrization. The errors for $z \geq 3$ are close to zero because the smallest a priori covariance is used as boundary condition for the highest altitudes, where the sensitivity is low.

For the quantification of the vertical sensitivity of the retrieval, Figure 9 shows the averaging kernels AK (see Eq. (14) and text) for the aerosol scenarios E1-E3 calculated for a Tikhonov parameter $\gamma = 0.25$ and SNR = 3000. We used a small γ to demonstrate the general vertical sensitivity rather than the smoothed one. Larger γ values would lead to peaks at lower altitudes

15 with slightly reduced peak sizes. Within an ideal retrieval, the AK matrix should be equal to the identity matrix (Rodgers, 2004). Then, delta peaks in every layer would indicate a perfect sensitivity of the retrieval to the true state of the atmosphere.

18

For MAX-DOAS retrievals, AK are much broader with peaks close to the surface. Here, the sensitivity is highest and the kernels for a certain layer show correlations with neighbouring layers due to the finite width of each kernel. The comparison of AK for E1-E3 reveals, that besides the surface kernel, all peaks are reduced in size and width for higher aerosol loads. This demonstrates the smaller sensitivity due to both, an insufficient a priori estimate and the additional aerosol load which reduces the general number of photons scattered into the light path (for specific geometries, e.g. RAA = $90°$). The area of the AK should ideally be 1 over a large range of altitudes. Here we find, that only within the first kilometer, the overall sensitivity is high. Note, that especially for E2 and E3 the surface area value is much smaller than 1 due to the negative area of the lowermost kernels for higher altitudes. Negative kernel values indicate, that an additional aerosol load in this altitude would decrease the retrieved solution close to the surface. The FWHM of averaging kernels are a measure of the vertical retrieval resolution with the lowest values close to the surface. In the right hand side plot of Figure 9 we show FWHM at the nominal altitudes (coloured lines) and the altitudes of their individual maxima (black lines). The calculation was done by using the individual AK instead of the FWHM of fitted Gaussian distributions. The limited vertical extent of the black curves indicate, that a theoretical vertical resolution with values between 500 m and 1 km is available for all kernel levels but the specific sensitivity for all layers lies within the lowest kilometer.

Figure 9. Averaging kernels of the aerosol retrievals for scenarios E1-E3 (first three figures on the left side). Also shown are the area and FWHM of the AK on the right side. FWHM are depicted on their nominal heights (coloured) and on the height of their individual peaks (black).

The trace of the averaging kernel matrix (degrees of freedom, DOF) is often discussed as the number of independent pieces of information for a retrieval. Hartl and Wenig (2013) already pointed out, that this number is not necessarily a strict limitation of the retrieval and might differ strongly depending on the regularization.

In Figure 10, we depicted the RMS between measured and retrieved O_4 ΔS and the DOF for scenario E3. Giving the retrieval

more freedom will increase the degrees of freedom and decrease the RMS which might be understood as more information used for a better measurement assimilation. However, in Section 4.3.1 we already demonstrated, that profiles with high DOF and low RMS might oscillate. DOF only state the maximum number of independent pieces of information for the current regularization parameters without considering if the retrieved profiles are optimal. Therefore, we do not use this quantity for the description of retrieval results.

Figure 10. RMS between measured and simulated O_4 ΔS and the matching degrees of freedom (DOF) for the specific retrievals for different SNR and γ values.

5   In Figure 11, we show averaging kernel, area and FWHM of the NO_2 retrieval for scenarios E1-E3. Similar conclusions can be drawn as for the aerosol retrieval for the shape and altitude variation of AK. The area is closer to 1 for all altitudes which is due to the missing smoothing of the Tikhonov term. The FWHM shows again a lower vertical sensitivity for higher layers. On the other hand, the FWHM curves at their specific peak heights (black) show a larger vertical spread in comparison to the aerosol curves which indicates a larger sensitivity for higher altitudes in the NO_2 retrieval. The DOF for the trace gas
10 retrieval lie in the range between 2.3 and 3.2 but decrease significantly when applying values of $g \neq 1$. In addition to the above mentioned errors and resolution properties, further error sources and problems should be noted. For real measurements, the true meteorological conditions are mostly unknown. Wang et al. (2017) pointed out, that wrong O_4 profiles might lead to strong deviations between retrieved and true aerosol profile. Furthermore, we did not implement the instruments field of view (FOV) in the retrieval because it will increase run time. However, larger differences can be expected for concentrations/extinctions
15 in the lowermost layers, when parts of the FOV might gather photons reflected on Earth's surface. Additionally, we assume a linearity between measurement and concentration which might be inaccurate for high aerosol loads and NO_2 concentrations when the telescope points along the horizon.
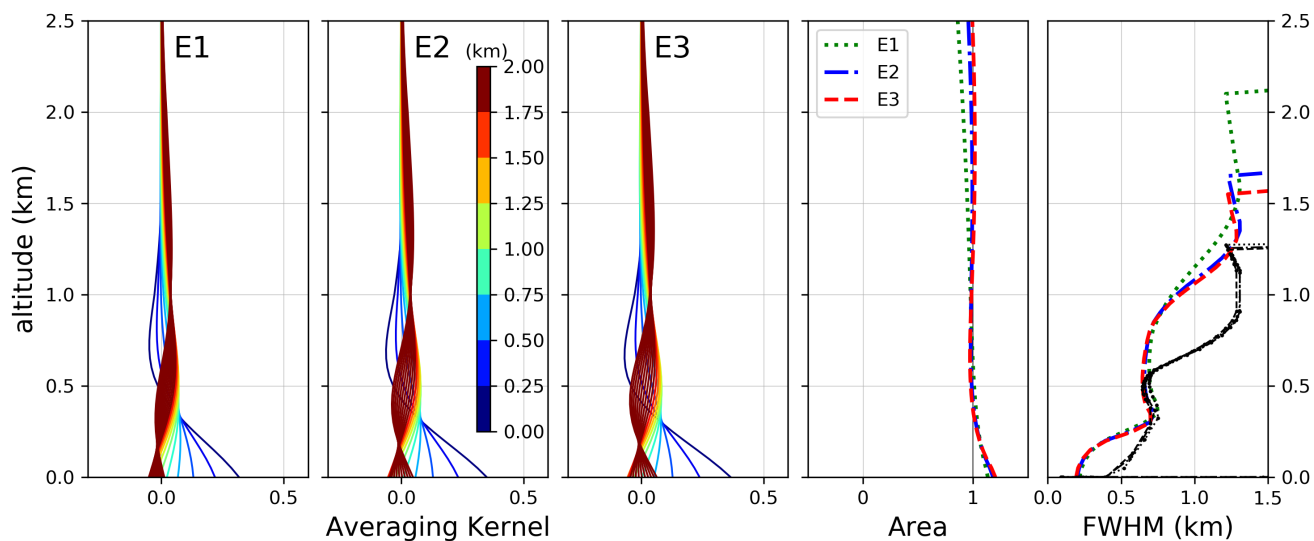
20

Figure 11. Averaging kernels of the NO_2 retrievals for scenarios E1-E3 (first three figures on the left side). Also shown are the area and FWHM of the AK on the right side. FWHM are depicted on their nominal heights (coloured) and on the height of their individual peaks (black).

4.3 Retrieval of profiles during the ~~CINDI2~~ CINDI-2 campaign

The 2nd Cabauw Intercomparison of Nitrogen Dioxide Measuring Instruments campaign (CINDI-2) took place in Cabauw (the Netherlands) from 25.08 - 07.10.2016 and was funded by the European Space Agency (ESA) and the research groups participating. The campaign goals were the characterization of differences between NO_2 measurements by various instruments and approaches, and the evaluation of the resulting datasets for the validation of the Copernicus satellite, Sentinel 5 Precursor (S5P). Over 40 different instruments operated by 30 groups from all over the world provided an outstanding ensemble of datasets for this task. The campaign was a successor of CINDI which was held in Cabauw from 16.06 - 24.06.2009 (see e.g. Piters et al. (2012); Pinardi et al. (2013); Zieger et al. (2011)).

The measurement site Cabauw is located in a rural region dominated by agriculture but is surrounded by four of the largest cities of the Netherlands (Rotterdam, Amsterdam, Den Haag and Utrecht). Thus, depending on the wind direction, long range transport from highly industrialized areas is likely which results in high pollution events. Here, three of the five investigated days show a more or less steady wind from south-easterly directions with a change in wind direction in the evening of the 15th of September (see Fig. 12). On the 23rd, wind came from the west whereas one day later the wind came mostly from southerly directions.

In this study, the instrumental set-up for the validation of aerosol and trace gas profiles consists of in situ and remote sensing instruments. Near-surface concentration/extinction values are provided by ceilometer, NO_2-LIDAR, long path DOAS (LP DOAS) and in situ samplers (ICAD/CAPS, NAQMN). Integrated values are provided by Pandora and AERONET direct sun
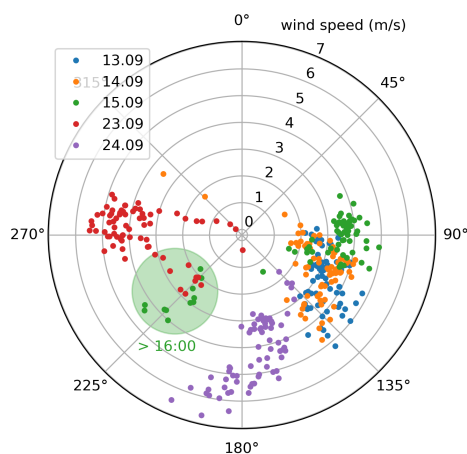
Figure 12. Wind speed and direction for the investigated days (CESAR, 2018) resampled to 5 minute values from 06:00 - 17:00 UTC.

instruments. Besides the MAX-DOAS measurements, the only routinely retrieved profiling information comes from ceilometer and NO_2-LIDAR data. In addition, three NO_2-sondes were launched on one of the days investigated here (15.09.2016). The profile validation is realized on two cloud free days (13. - 14.09.2016) and three days with broken clouds (15.09 and 23. - 24.09.2016). The operators of MAX-DOAS instruments were asked to perform elevation scans on the beginning of each hour

5 and at 11:15 and 11:45 UTC every day. The ancillary measurements introduced in the following subsections were resampled or averaged on this time interval to prevent discrepancies due to time lags between two observations. Each scan took around 8 minutes and consisted of the following elevation angles: $1°$, $2°$, $3°$, $4°$, $5°$, $6°$, $8°$, $15°$, $30°$. The telescope pointed into the western direction with a viewing azimuth angle of $107°$ from the south.

In this section, BOREAS retrievals were performed on data from the IUPB MAX-DOAS instrument on a 100 m step width

10 vertical grid from the surface up to 4 km. The aerosol retrieval uses the a priori pre-scaling option with an exponential a priori profile described by a 1 km scale height and an aerosol optical thickness of 0.18. Asymmetry factor and single scattering albedo were chosen as 0.92 and 0.68, respectively. The SNR was set to 2500 with a Tikhonov-parameter of 2. The a priori variance was decreasing with altitude from 1.5 at the surface to 0.01 at 4 ~~km.~~ km. This definition was chosen to improve the profiling results for lower altitudes where the main aerosol load/concentration can be expected and in order to suppress instabilities at the

15 upper grid boundary where the sensitivity is lowest. The trace gas retrieval uses again a priori pre-scaling with an exponentially decreasing profile with a scale height of 1 km and a vertical column density of $9x10^{15}$ molecules/cm^2. The a priori covariance matrix uses the same variances as the aerosol retrieval but includes Gaussian distributed side diagonal elements to account for correlations between individual layers (Barret et al., 2002). The measurement covariance matrix for NO_2 consists of the total differential slant column error on the diagonal elements only. Vertical profiles of pressure and temperature were created by

20 taking the mean of 16 different sonde measurements taken during the years 2013-2015 in De Bilt (the Netherlands).

22

4.3.1 Validation of aerosol retrievals

Instrumentation for the aerosol validation

Aerosol profiles were validated using three different instruments. The retrieved AOT was compared with values from an AE-
RONET station (AErosol RObotic NETwork, Dubovik et al. (2000); Holben et al. (1998)). The Level 2 AOT at 440 nm was
5   scaled with the Angström Exponent from the ratio 440 nm/675 nm to calculate the AOT at 477 nm (see Fig. 13). Due to measu-
rement intervals varying between 4 and 30 minutes, we decided to resample the AERONET signal. The errors from AERONET
instruments are usually in the range of 0.01 (VIS, IR) to 0.02 (UV) (Sayer et al., 2013). Here, we used a constant error of 0.01.
The bottom extinction coefficient of the retrieved aerosol profiles was compared with in situ PM10 concentrations from the
National Air Quality Monitoring Network (NAQMN) operated by the Dutch National Institute for Public Health and the Envi-
10   ronment (RIVM). The NAQMN measurement site Wielsekade is located at a distance of around 900 m from the MAX-DOAS
station. The site is listed as a regional background station and the PM10 measurement principle is beta attenuation (Thermo
Fisher Scientific FH62I-R). The instrument provides data on one minute intervals but only the hourly values are validated by
RIVM. These hourly values were resampled on the MAX-DOAS times and the minute values were used to calculate the errors
as standard deviation for the data points shown (see Fig. 14).
15   Furthermore, we used AERONET scaled ceilometer near surface extinction as a further validation dataset. The ceilometer
(CHM15k Nimbus) was operated by the Royal Netherlands Meteorological Institute (KNMI) and sampled backscattering sig-
nals every hour at a wavelength of 1064 nm. The integrated backscattering signal was divided by the 1020 nm AERONET AOD
to get a conversion factor which was applied to the backscattering signal for the conversion into extinction coefficients. This
new ceilometer profile was again scaled with AERONETs AOT at 477 nm. The error is expressed as the standard deviation
20   calculated from the temporal and vertical averaging.

Comparison of aerosol retrieval parameters

Figure 13 shows the time series and the scatter plot of AERONET and BOREAS derived AOT. The BOREAS data was filtered
for profiles which reached the iteration limit during the retrieval. Grey areas indicate clouds within the specified time period.
25   In the scatter plot, BOREAS errorbars were calculated by integrating the total error (Eq. (17)) vertically. On the first two cloud
free days, the temporal variability shows a similar pattern with a slight offset between both instruments most likely introduced
by an underestimation of the AOT by BOREAS. Due to the limited sensitivity of MAX-DOAS profiling for higher altitudes
(see Fig. 9), elevated aerosols do not contribute to BOREAS AOT but can be measured by direct sun instruments like AERO-
NET sunphotometers.
30   In the evening, results of both instruments vary more. Different reasons for this finding are possible. First, a developing pla-
netary boundary layer (PBL) might exceed the vertical extension where BOREAS has sufficient sensitivity. Second, when
pointing towards the sun, saturation of the CCD becomes a problem leading to low integration times which decrease SNR and
fitting quality. In addition, RTM calculations might introduce uncertainties at high SZA, when the aerosol load is high and
the light path is strongly increased. Furthermore, the aerosol phase function used leads to uncertainties as the forward scatte-
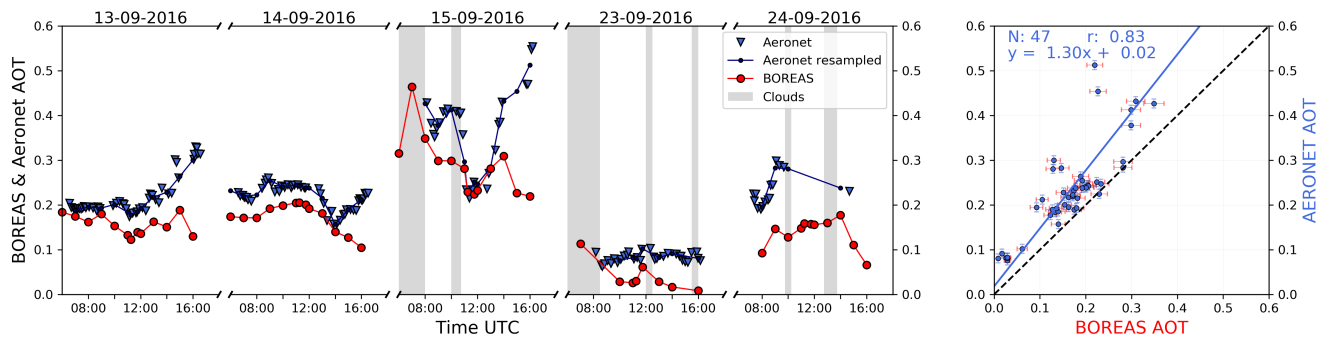
Figure 13. Left: time series of AERONET (blue) and BOREAS AOT (red). Small triangles show the original AERONET measurement, small dots with connecting lines depict the resampled data. Grey areas indicate clouds. Right: scatter plot of both datasets including parameters of the orthogonal regression and Pearsons correlation coefficient.

ring peak might be underestimated by the Henyey-Greenstein parametrization. The other days show a higher variability due to an increase in cloudy scenes. Note that especially in the morning and around noon, clouds may influence the instruments in various ways because of their different azimuthal viewing directions. BOREAS profile retrieval cannot be considered as reliable when one or several elevation angles pointed into clouds during the measurements, as intensity and light path vary in
5   unpredictable ways. This might also lead to large iteration numbers or to no convergence at all. On the 15th of September, the temporal patterns of the two instruments differ strongly. Although the extinction values around noon agree well, AERONETs decrease before and the increase afterwards cannot be found this strongly by BOREAS. Especially in the evening, both curves deviate, indicating highly variable atmospheric conditions which might also be introduced by a change in wind direction (see Fig. 12). The aerosol load on the last two days is much lower because of rainfalls in the time between 16.09 and 22.09. In the
10   morning of the 23rd, several profiles were discarded due to exceeded iteration limits.

The correlation coefficient of ~~0.81~~ 0.83 is high and shows the general good agreement at three of five days. The regression line indicates the before mentioned small underestimation of the AOT by BOREAS.

Figure 14 shows the comparison of near-surface aerosol values. Extinction coefficients from BOREAS and ceilometer are
15   depicted together with PM10 concentrations of the NAQMN in situ instrument. Note that the y-axis for PM10 concentrations was chosen to match the results of BOREAS on the 14th of September. The NAQMN in situ sampler and BOREAS show a good temporal agreement within the first three days. Only in the morning hours at the 13th and 15th, data from the two instruments show a larger spread. This deviation is most likely due to the insufficient vertical resolution of MAX-DOAS profile retrievals when the PBL has not yet evolved and near surface aerosol loads are dominant (see Fig. 9 and 15 for further details).
20   On the 15th, early morning clouds might also have an impact on the deviation. Again, a larger variability for BOREAS results can be found for the last two days, when the retrieval was influenced by broken clouds. The in situ instruments show a smoother daily variation here. The ceilometer bottom extinction shows a good agreement with BOREAS and NAQMN on the first day

24

and an underestimation on the second day. On the 15th of September, bottom values are influenced by thick clouds which might interfere with the backscattering signal of altitude ranges below the clouds (see Fig. 16). The 23rd shows more variability than the first two days but this can be found for the other instruments as well.

The correlation of BOREAS bottom extinctions with data from both validation instruments is high, indicating the good agreement on cloud free days. The correlation with ceilometer near-surface values is high as well but the regression line shows a general underestimation of ceilometer near surface values in comparison to BOREAS.

Figure 14. Left: time series of BOREAS (red), ceilometer (green) and NAQMN in situ (blue) and near surface aerosol parameters. Small triangles show the original hourly NAQMN measurements, small dots with connecting lines depict the resampled data. Green squares show ceilometer near-surface extinction values evaluated by averaging the 10 - 50 m coefficients. Grey areas indicate clouds. Right: scatter plot including parameters of the orthogonal regression and Pearsons correlation coefficients.

Figure 15 shows the aerosol layer height found by the ceilometer for all days. Especially during the first three days, an upward extending PBL can be identified from noon to the late afternoon. Only on the 15th, a more or less stable residual PBL seems to exist in the morning hours. The other days show a high variability in the morning with layer heights from 200 m to 600 m with more or less individual high signals which might be produced by smaller clouds at higher altitudes. The 24th of September shows a stable layer around 200 m and a diffuse developing PBL in the afternoon.

The underlying extinction coefficient profiles for the above discussed bottom extinction and AOT values can be seen in Figure 16. In the top row, temporal and vertically averaged ceilometer profiles are depicted. In the mid row, this data was smoothed to the MAX-DOAS vertical resolution by the application of BOREAS averaging kernels ($\mathbf{x}_{new} = \mathbf{x}_{apri} + \mathbf{A}(\mathbf{x}_{ceilo} - \mathbf{x}_{apri})$ see Rodgers and Connor (2003)). The first day shows a good agreement of BOREAS and ceilometer near surface extinction with a small offset between both curves. In the morning, both instruments find the aerosol load mainly located in the lowermost layers. Beginning around noon, the PBL starts developing with a maximum height of 2 km in the afternoon found by the ceilometer. BOREAS can not resolve this increasing PBL as well as the averaged ceilometer but the AK smoothed data indicate that the reason might be a limited sensitivity for the top boundary of the PBL.

On the 15th of September, the averaged ceilometer data show high and thick clouds in the morning and a rising PBL in the afternoon. In the AK smoothed data, these clouds can not be identified anymore. BOREAS introduces elevated aerosol
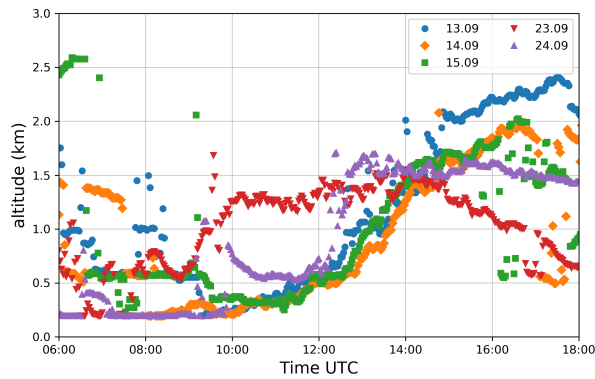
25

Figure 15. ceilometer aerosol layer height within the planetary boundary layer.

layers which can be understood as a retrieval artefact due to these cloudy scenes. In the afternoon, BOREAS finds an upward expansion in the PBL similar to the ceilometer with the exception of the last profile which was influenced by the telescope pointing towards the sun. BOREAS extinction values are smaller in the PBL which is a consequence of the already explained underestimation of BOREAS AOT to AERONETs AOT which was used for the backscatter signal scaling.

Figure 16. Comparison of aerosol extinction coefficient profiles from BOREAS and ceilometer for the 13.09.2016 (left) and 15.09.2016 (right).

4.3.2 Validation of nitrogen dioxide profiles

Instrumentation for the NO_2 validation

Several instruments were used for the validation of BOREAS nitrogen dioxide profiling results. The VCD results were validated with the help of a Pandora instrument (#128) operated by LuftBlick (Herman et al., 2009) and a NO_2 LIDAR from RIVM. In addition, three NO_2 sondes launched on the 15th of September by KNMI were also used.

The Pandora instrument was used with its direct sun capability to retrieve total nitrogen dioxide columns on hourly timesteps (see Fig. 17). Since the measurement time did not match to BOREAS scans, Pandora values were resampled. The stratospheric column was subtracted based on the approach of Knepp et al. (2015) by using OMI stratospheric columns during the Cabauw overpass (L2 OVP NASA (2018)). The data was quality filtered and the errors were provided by LuftBlick and are based on Herman et al. (2009).

The NO_2 LIDAR (Brinksma et al., 2008) measured not as frequently as Pandora and MAX-DOAS instruments but performed several measurements on the 15th of September. One LIDAR scan took approximately 30 minutes with the temporal midpoints of the scans on a non-regular temporal grid which necessitated resampling. The scan was done on different elevation angles which enabled the retrieval of vertical profiles with altitude points up to 2.5 km. For the VCD calculation, these profiles were vertically integrated. Errors were provided by the RIVM team and Gaussian error propagation was applied for the calculation of VCD errors. In addition to the remote sensing instrument, NO_2 sondes were launched on the 15th around 5:15, 8:04 and 10:25 UTC. The sondes provide NO_2 VMR as well as pressure, temperature and altitude data for the conversion to concentrations which were vertically integrated up to 4 km.

Near surface concentration validation was done with the help of in situ (NAQMN, ICAD, CAPS) and remote sensing instruments (LIDAR and LP DOAS). The in situ samplers NAQMN, CAPS and ICAD were operated by RIVM, the Royal Belgian Institute for Space Aeronomy (BIRA-IASB) and the institute for environmental physics in Heidelberg (IUPH), respectively. In addition to the aerosol bottom concentration, NAQMN provided also NO_2 concentrations (Teledyne API 200E, see Section 4.3.1 for details on data handling). IUPH and BIRA-IASB created a common NO_2 in situ dataset from IUPHs ICAD (Iterative CAvity DOAS, (Pöhler et al., 2017)) and BIRAs CAPS (Environment SA, AS32M- CAPS, Cavity Attenuated Phase Shift, (Kebabian et al., 2008)). This joint dataset filled gaps in the individual measurement series and fixed a scaling issue for CAPS. BIRA-IASB operated two different CAPS instruments which were installed at the 27 m and 200 m level of the Cabauw measurement tower. The joint ICAD/CAPS dataset as well as the 200 m CAPS data were averaged over 15 minutes time steps. For both instruments (ICAD/CAPS) an error of 1 ppb was assumed.

In addition to the in situ instruments, a long path DOAS (LP DOAS) provided by IUPH (Pöhler et al., 2010) was used for the validation. Four reflectors attached on different altitude levels of the measurement tower (12.7 m, 47 m, 107 m and 207 m) provided unique and well-defined light paths which enabled the calculation of concentration on several altitudes. The instruments elevation measurements lead to profiles every 30 minutes. Errors were calculated by the IUPH team.

Nitrogen dioxide profiles were provided only by the NO_2 LIDAR and sonde launches. The LP DOAS did not cover enough altitude levels for a comparison. The conversion from trace gas VMR to concentrations for all datasets was done with the

meteorological data from the CESAR observatory (CESAR, 2018).

Comparison of NO_2 retrieval parameters

Figure 17 depicts the comparison of VCD for different instruments. The agreement with Pandora is good on all days with
larger deviations in the morning and on the 15th of September in general with the exception around noon. Deviations in the
morning might be (similar to the AERONET comparison) due to spatial differences in the NO_2 distribution, when Pandora
points to the east and MAX-DOAS to the west. This argument is supported by the LIDAR measurement on the 15th that agreed
well with BOREAS and shared the same azimuthal viewing direction. In the afternoon of that day, BOREAS VCD increase
faster than Pandora and LIDAR with a strong overestimation for the last profile at 16:00 when the sun was low. Here, we can
exclude horizontal gradients as a reason for differences, because of the same viewing direction of LIDAR and MAX-DOAS.
On the same day, NO_2 sondes proved the BOREAS VCD only during the ascend (triangle with edge to the top) of the second
launch correct. The matching descend (triangle with edge to the bottom) for the first flight was approximately 38 km into the
northwestern direction between Amsterdam and Rotterdam and agrees more with Pandora columns indicating differences due
to azimuthal viewing directions. The strong differences in VCD for ascend and descend of the first and second sonde launches
show a high temporal and spatial variability of the NO_2 concentration which is supported by all remote sensing instruments.
The correlation with Pandora is slightly better than with LIDAR but the regression parameter shows, that Pandora VCDs are
higher than those from BOREAS whereas the LIDAR regression is closer to one.
In Figure 18, near surface NO_2 concentrations are depicted. Both in situ datasets (NAQMN and ICAD/CAPS) agree well with

Figure 17. Left: time series of Pandora, LIDAR and BOREAS NO_2-VCD. Blue diamonds show the original Pandora measurements, green
squares the LIDAR datapoints. Small dots with connecting lines depict the resampled datasets of Pandora and LIDAR. BOREAS is shown as
red circles. Grey areas indicate clouds. The plot includes orange triangles as the representation of the integrated NO_2 sondes measurements
with the ascend and descend separated in different triangles with the edge to the top or to the bottom respectively. Right: scatter plot of the
datasets including parameters of the orthogonal regression and Pearsons correlation coefficients.

each other and show larger differences only in the morning of the 14th of September. The LP DOAS profiles at 12.7 m and 47 m
show similar concentrations as the in situ instruments. Differences in the morning of the first two days between the lower and

28

the higher LP DOAS values indicate a strong vertical inhomogeneity which was also found for the aerosols (see Section 4.3.1). BOREAS surface concentrations agree very well with all datasets except during the morning hours. On the 13th of September, in addition to the ICAD/CAPS data at the 27 m level (blue), the 200 m points are shown (green). The anti-correlated behaviour in the morning hours confirms the strong inhomogeneity and proves that nitrogen dioxide was mainly concentrated close to the

5   surface at that time. The mean values of both CAPS instruments (yellow line) show a better agreement with BOREAS than the 27 m and 200 m data.

It seems that BOREAS cannot fully resolve this thin near-surface layer and retrieves rather smooth profiles instead of sharp concentration peaks (see also the discussion about vertical sensitivity in subsection 4.2). This is again in agreement with LP DOAS results on the 24th of September, where the 200 m level LP DOAS finds similar concentrations as BOREAS. Note, that

10 the NO_2 LIDAR has a finer resolution within the lowest 100 m which might be the reason, why it depicts similar concentration numbers as the other instruments in the morning hours of the 15th of September. As a rough estimation of the thickness of the individual thin layers in the morning, we divided BOREAS VCD by the ICAD/CAPS concentration and found, that the layer height lies around 200 m (06:00 - 08:00), 300 m (09:00) and 400 m (10:00) on the 13th of September. The mean AK FWHM for the surface layer on that day is 214 m indicating that the lowermost layer can be resolved only from around 09:00 UTC

15 where the curves approach each other. A good agreement is found at 10:00 UTC when the concentration is focused in a layer twice as thick as BOREAS surface resolution.

The correlations are high for all instruments with the highest value for NAQMN and the NO_2 LIDAR. The in situ instruments show similar correlations but a slight underestimation of BOREAS can be found with slopes between ~~1.24 and 1.45~~1.22 and 1.44.

Figure 19 depicts NO_2 profiles for BOREAS, LIDAR and sondes on the 15th of September. Similar to the aerosol profile
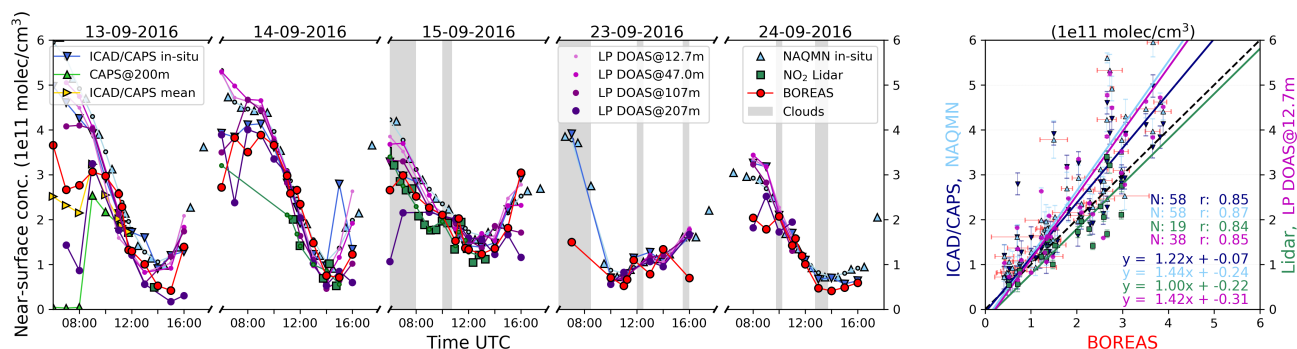

Figure 18. Left: time series of in situ and remote sensing NO_2 near surface concentrations. Triangles show in situ instruments for NAQMN (bright blue, triangles pointing upwards) and for ICAD/CAPS (dark blue, triangles pointing downwards). In addition, on the 13.09.2016, CAPS at the 200 m level is depicted as green triangles with the edge up and the mean values of both CAPS with the edge to the side (yellow). The NO_2 LIDAR is plotted as green squares and the LP DOAS as different sized circles in shades of magenta (lowest altitude as smallest circle). BOREAS is shown as large red circles. Right: scatter plot of the datasets including parameters of the orthogonal regression and Pearsons correlation coefficients.

comparison, averaging kernels were applied to LIDAR and sondes measurements. The vertical profiles of the unsmoothed LIDAR show the previously discussed high vertical inhomogeneity. We can clearly identify a high concentration close to the surface and another elevated NO_2 layer with altitudes varying between 100 m and 500 m. The unsmoothed sondes agree well with the LIDAR measurements only at the ascend of the second launch. After the application of averaging kernels, the two

5 distinct layers with high concentrations are smoothed to one layer with NO_2 concentrated at the surface indicating again a lower vertical sensitivity of MAX-DOAS profiling. In addition, smoothed and unsmoothed LIDAR find larger concentrations for altitudes over 500 m before 8:00 UTC which was not found by BOREAS and the sonde profiles.

Figure 19. Comparison of NO_2 concentration profiles from BOREAS and LIDAR and sonde measurements for the 15.09.2016.

5 Conclusions

In this study, we introduced BOREAS, a new profiling algorithm for MAX-DOAS measurements. BOREAS retrieves aerosol

10 extinction coefficient profiles around O_4 absorption bands from the oxygen dimers differential slant column densities. In contrast to existing inversion algorithms which are based on perturbation theory, BOREAS directly minimises the difference of modelled and measured optical depth by varying aerosol extinction coefficient profiles in an iterative Tikhonov regularization scheme. In addition, trace gas concentration profiles are retrieved via optimal estimation using the aerosol properties determined in the first step. For both retrieval parts, we introduced a priori pre-scaling as a simple method for improving results under

variable atmospheric conditions.

The retrieval performance was demonstrated on the example of synthetic data calculated with SCIATRAN and with real measurements performed during the CINDI-2 campaign in Cabauw 2016. The synthetic scenarios were chosen to work as a stress test for BOREAS. One fix a priori profile was used for the retrieval of different large aerosol loads and NO_2 concentrations. The results are good when the scenario is relatively close to the a priori profile but fail for strong loads/concentrations. In a comprehensive variation of parameters we showed that, in non-ideal situations, either the shape/near-surface value or the integrated quantity can be optimized. The information content of a MAX-DOAS scan with degrees of freedom between ≈ 1 and ≈ 3.5 is not enough for a perfect retrieval. Furthermore, the frequently utilized assumption of using the trace gas errors from DOAS fits only as measurement variance was found to be insufficient since the regularisation ratio might be wrongly weighted. We suggest a manual change in measurement errors or an iterative approach for finding the best ratio.

In the second part of this study, BOREAS retrieval results from measurements of the IUPB MAX-DOAS instrument during the CINDI-2 campaign were validated with ancillary measurements. The agreement for all parameters was good with correlations equal or higher than 0.75. Systematic offsets or deviations depending on geometry, atmospheric condition and investigated air mass indicate limitations due to the specific measurement characteristics which were also found in earlier MAX-DOAS profiling studies. The correlation with AERONET AOT is ~~0.81~~ 0.83 with an underestimation by BOREAS leading to a regression slope of ~~1.37~~1.30. The bottom value correlation is 0.75 for the ceilometer near surface extinction and ~~0.8~~ 0.81 for NAQMN in situ measurements. The total column of NO_2 shows a good agreement with Pandora and LIDAR with correlations of ~~0.83~~ 0.86 and 0.79 respectively. In contrast to the underestimation of BOREAS integrated aerosol, Pandora nitrogen dioxide columns are overestimated, especially in the morning hours. The correlations for near surface NO_2 concentrations are high with values larger than ~~0.83~~0.84. Stronger deviations between BOREAS and in situ were found in the morning. This was explained by the limited vertical resolution of BOREAS, while in the morning the highest concentrations are found close to the surface.

As a conclusion, BOREAS profiling capabilities are strong which was proven by high correlations with all validating instruments. Discrepancies were found due to different azimuthal viewing directions of the instruments and the limited vertical resolution of MAX-DOAS profiling when aerosol load or concentration is close to the surface in layers thinner than the BOREAS vertical resolution. Comparison of BOREAS results to the performance of other MAX-DOAS profiling algorithms will be discussed in two upcoming papers (Frieß et al. (2018) and Tirpitz et al. (2018)).

Appendix A: Additional plots and retrieval of box profiles

A1 Additional aerosol scenarios and plots

The retrieval results for the box scenarios in Figure A1 are shown in Figure A2 for different Tikhonov parameters and SNR = 3000. A priori pre-scaling leads only for scenario B3 to a clear improvement since the bottom extinction is reached. For B2 and B3, the resulting profile shapes change slightly which indicates the before mentioned lack in improvements through pre-scaling, when the a priori profile shape differs strongly from the true atmosphere. Nevertheless, since exponential profiles are improved a lot and box profiles show no degradation we highly recommend the usage of better and more flexible a priori profiles.

Figure A1. Box aerosol profiles for the synthetic sensitivity study. Also shown, the a priori profile for the aerosol retrieval (dashed line).

Figures A3 till A5 show the SNR and Tikhonov variation for the three aerosol box profiles. One can see, that for B2 the smallest γ values lead to the best bottom value, whereas for scenario B1 these values would result in an overestimation. Also the optimal SNR/γ range for the AOT differs strongly for all box profiles which show again, that regularization should be considered as a flexible choice of parameters, depending on the specific atmospheric conditions.

Figures A6 and A7 show the SNR/Tikhonov variation for the exponential profiles E1 and E2. Note that for E1 all parameter combinations lead to good profiling results because the a priori profile is close to the true atmosphere. In comparison to E3, E2 shows a better adaptation of AOT with a coincidently similar performance for the bottom extinction.
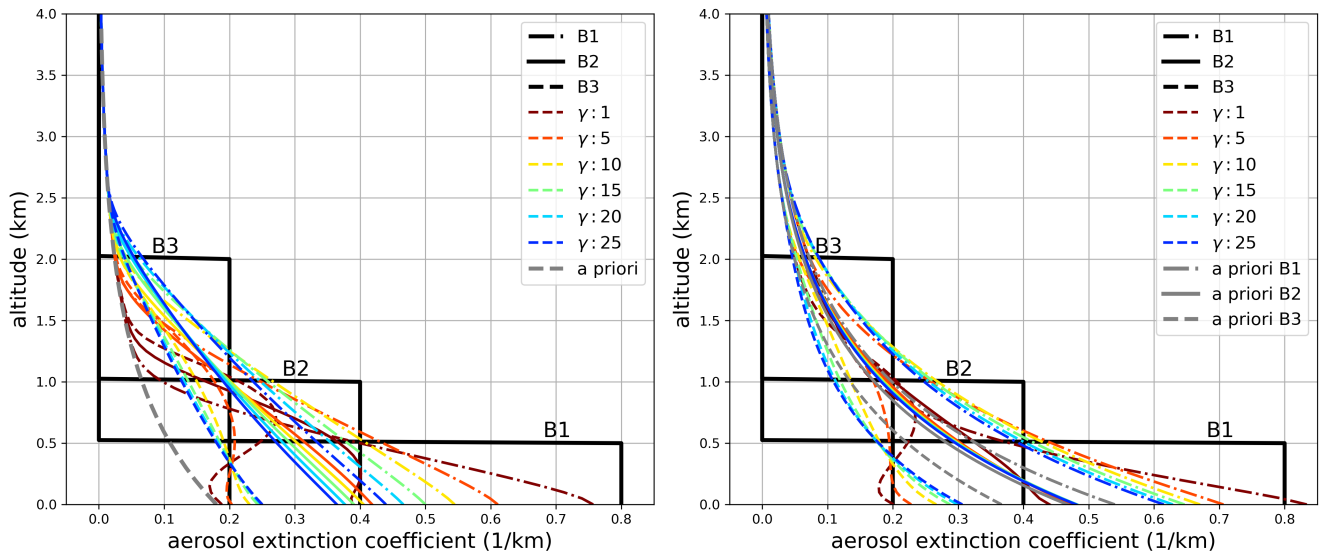
32

Figure A2. Retrieval results with a fix (left) and a pre-scaled a priori profile (right) with varying Tikhonov parameters γ for SNR = 3000. Small γ values mean less smoothing of the resulting profiles.
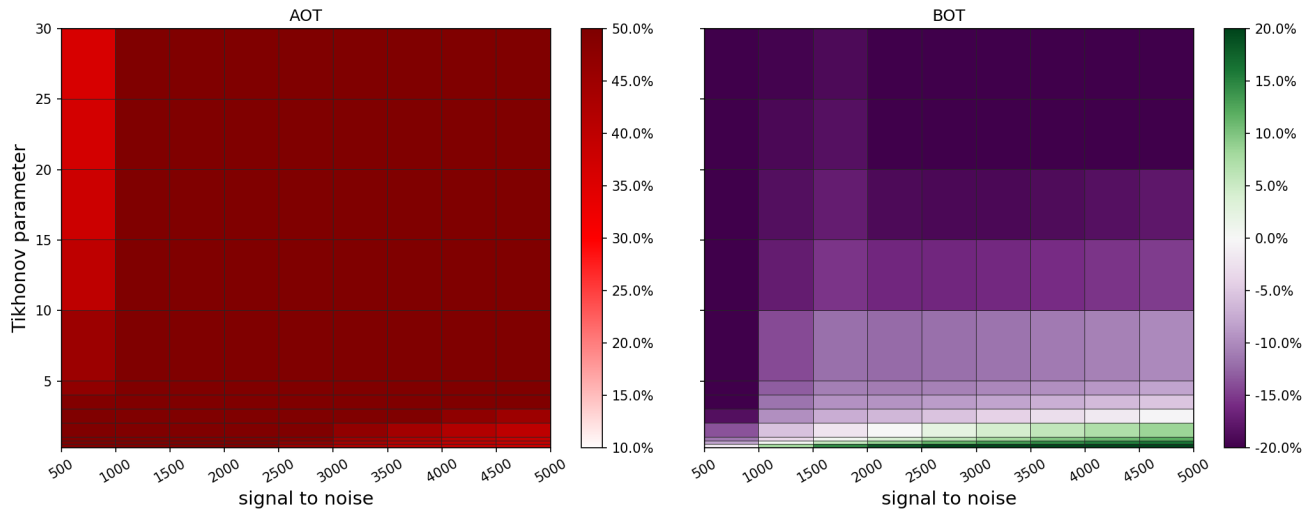

Figure A3. Variation of signal to noise and Tikhonov parameter with the relative difference of AOT and bottom extinction to the true value, colour coded for scenario B1 with a priori pre-scaling.
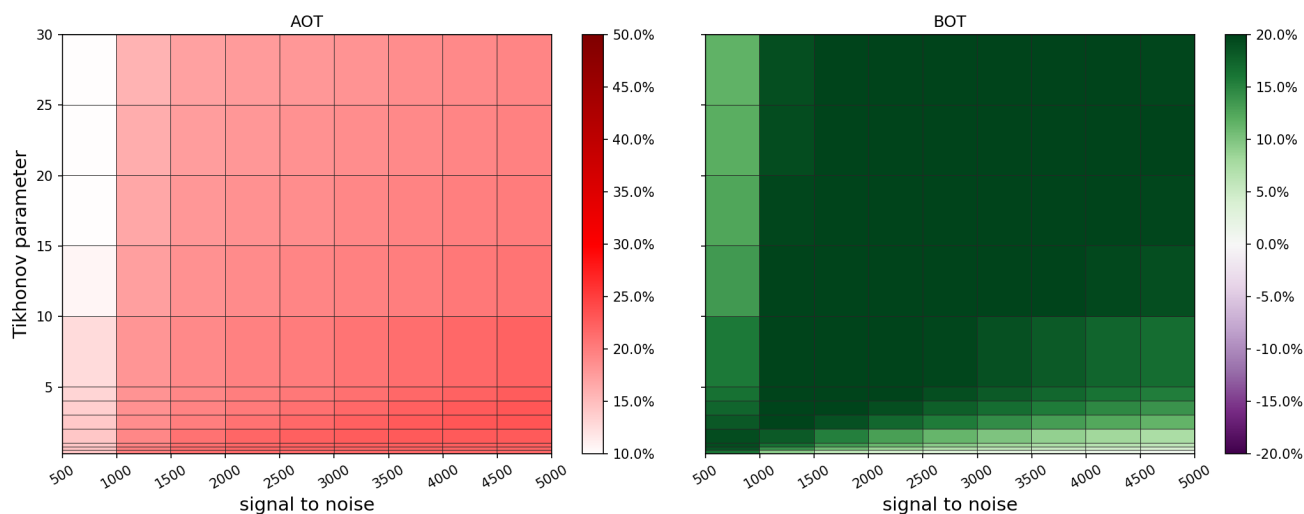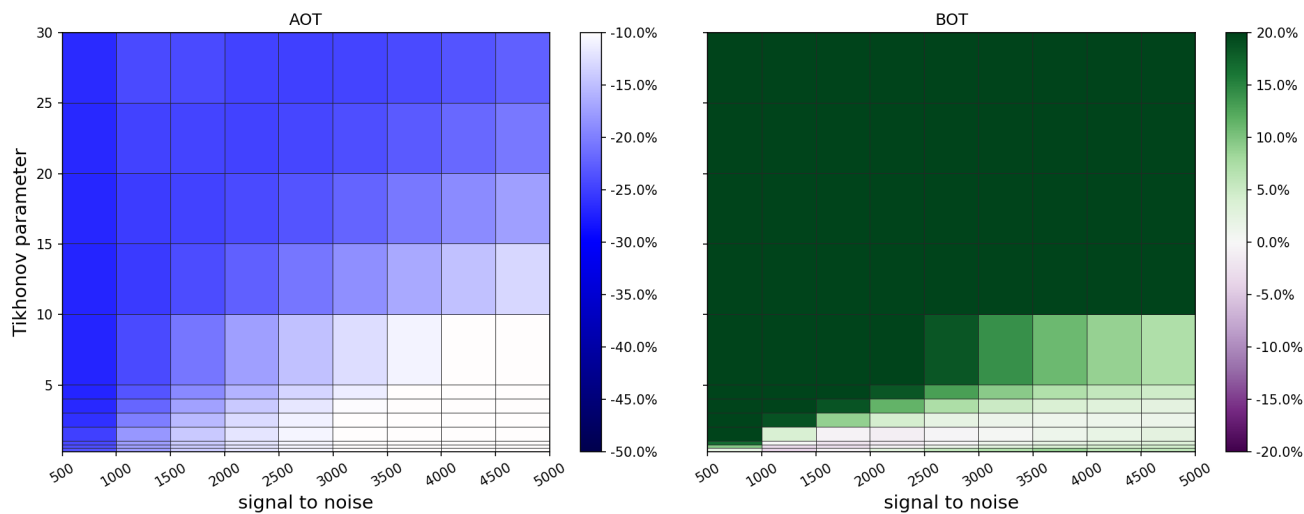
Figure A4. Same as figure A3 but for scenario B2.

Figure A5. Same as Figure A3 but for scenario B3.

A2   Additional NO₂ scenarios and plots

Figure A8 shows the box NO_2 scenarios which are retrieved for different g values in Figure A9. The standard regularisation ratio for $g = 1$ is again found to be oscillating without reaching the proper bottom concentrations for E2 and E3. Higher g factors show an improvement for both, fix a priori and pre-scaled initial guess.
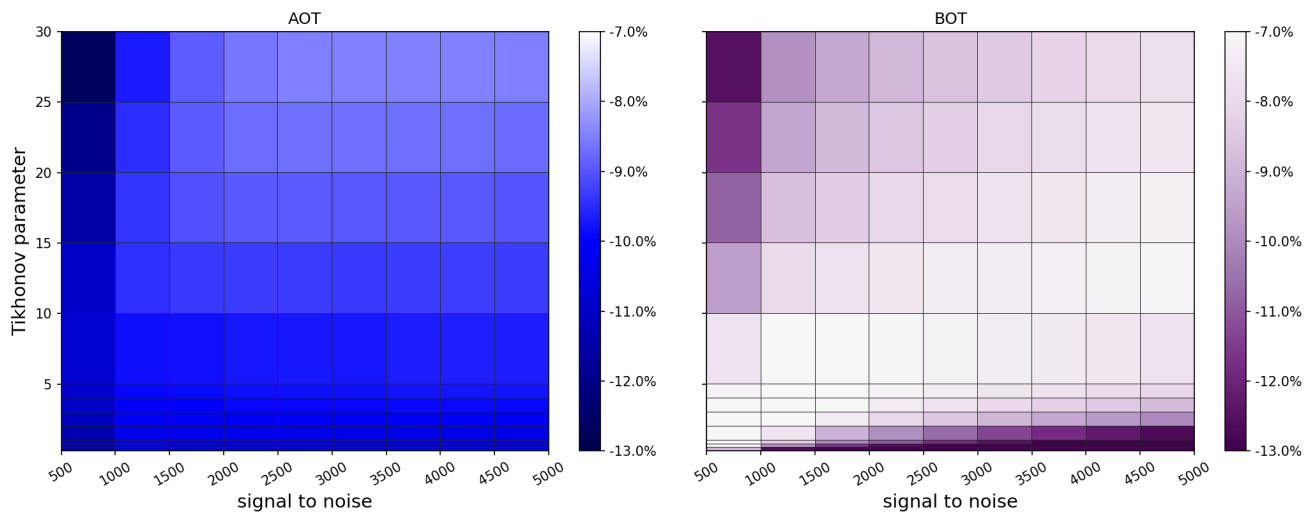
Figure A6. Same as Figure 5 but for scenario E1.
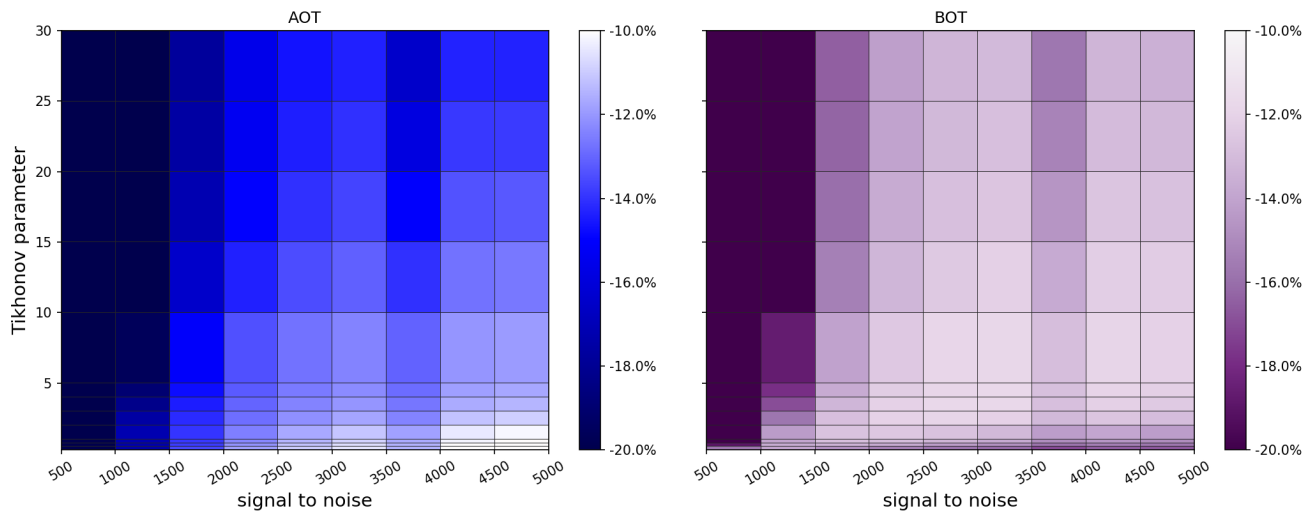
Figure A7. Same as Figure 5 but for scenario E2.

References

Barret, B., De Mazière, M., and Demoulin, P.: Retrieval and Characterization of Ozone Profiles from Solar Infrared Spectra at the Jungfrau-joch, Journal of Geophysical Research: Atmospheres, 107, 4788, doi:10.1029/2001JD001298, 2002.
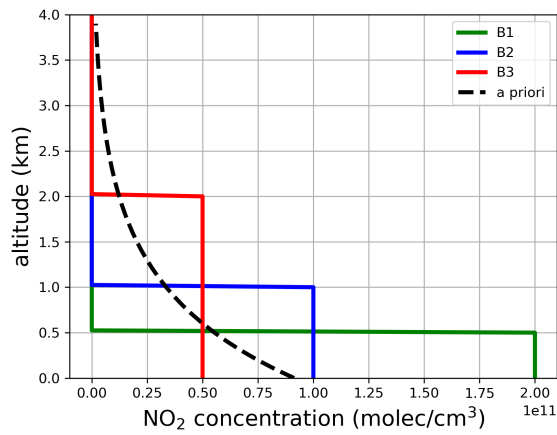
Figure A8. Box NO_2 profiles for the synthetic sensitivity study. Also shown, the a priori profile for the aerosol retrieval (dashed line).
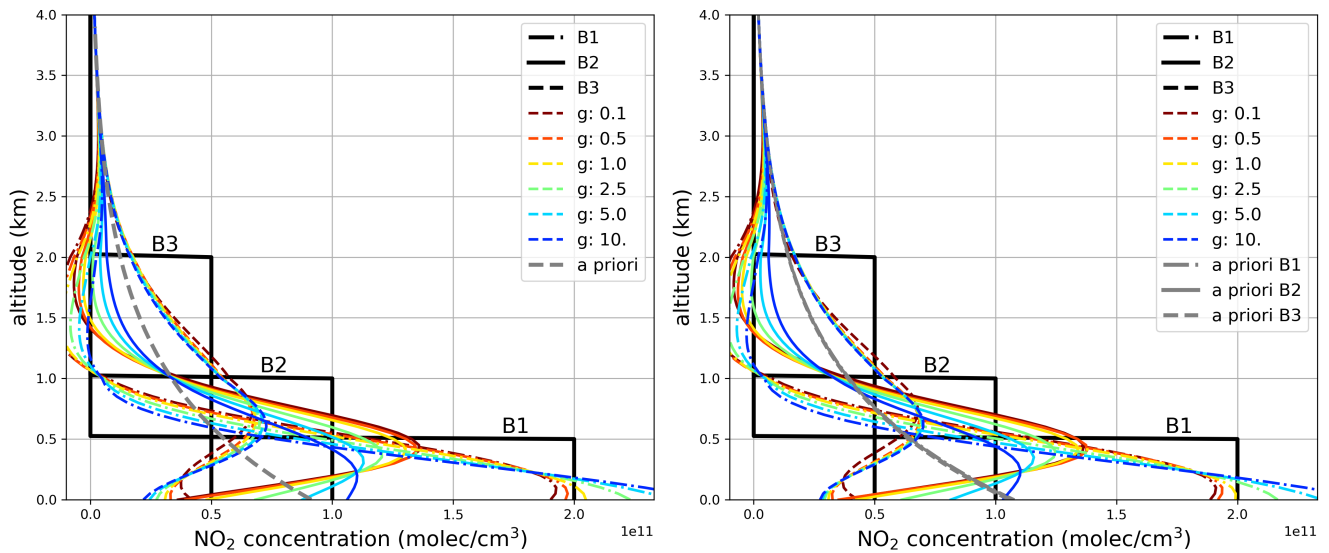

Figure A9. Retrieval results with a fix (left) and a pre-scaled a priori profile (right) with g factors. Small g values mean less measurement weighting for the resulting profiles.

Bobrowski, N., Hönninger, G., Galle, B., and Platt, U.: Detection of Bromine Monoxide in a Volcanic Plume, Nature, 423, 273–276, doi:10/bv8hq8, 2003.

Brinksma, E. J., Pinardi, G., Volten, H., Braak, R., Richter, A., Schönhardt, A., van Roozendael, M., Fayt, C., Hermans, C., Dirksen, R. J., Vlemmix, T., Berkhout, A. J. C., Swart, D. P. J., Oetjen, H., Wittrock, F., Wagner, T., Ibrahim, O. W., de Leeuw, G., Moerman, M., Curier, R. L., Celarier, E. A., Cede, A., Knap, W. H., Veefkind, J. P., Eskes, H. J., Allaart, M., Rothe, R., Piters, A. J. M., and Le-

velt, P. F.: The 2005 and 2006 DANDELIONS NO$_2$ and Aerosol Intercomparison Campaigns, Journal of Geophysical Research, 113, doi:10.1029/2007JD008808, 2008.

CESAR: Cesar Observatory, http://www.cesar-observatory.nl/index.php, 2018.

Clémer, K., Van Roozendael, M., Fayt, C., Hendrick, F., Hermans, C., Pinardi, G., Spurr, R., Wang, P., and De Mazière, M.: Multiple Wavelength Retrieval of Tropospheric Aerosol Optical Properties from MAXDOAS Measurements in Beijing, Atmospheric Measurement Techniques, 3, 863–878, doi:10.5194/amt-3-863-2010, 2010.

Dubovik, O., Smirnov, A., Holben, B. N., King, M. D., Kaufman, Y. J., Eck, T. F., and Slutsker, I.: Accuracy Assessments of Aerosol Optical Properties Retrieved from Aerosol Robotic Network (AERONET) Sun and Sky Radiance Measurements, Journal of Geophysical Research: Atmospheres, 105, 9791–9806, doi:10.1029/2000JD900040, 2000.

Dubovik, O., Holben, B., Eck, T. F., Smirnov, A., Kaufman, Y. J., King, M. D., Tanré, D., and Slutsker, I.: Variability of Absorption and Optical Properties of Key Aerosol Types Observed in Worldwide Locations, Journal of the Atmospheric Sciences, 59, 590–608, doi:10/cdvdp3, 2002.

Engl, H. W. and Grever, W.: Using the L–Curve for Determining Optimal Regularization Parameters, Numerische Mathematik, 69, 25–31, doi:10/bdzkp4, 1994.

Eriksson, P.: Analysis and Comparison of Two Linear Regularization Methods for Passive Atmospheric Observations, Journal of Geophysical Research: Atmospheres, 105, 18 157–18 167, doi:10.1029/2000JD900172, 2000.

Frieß, U., Monks, P. S., Remedios, J. J., Rozanov, A., Sinreich, R., Wagner, T., and Platt, U.: MAX-DOAS O$_4$ Measurements: A New Technique to Derive Information on Atmospheric Aerosols: 2. Modeling Studies, Journal of Geophysical Research, 111, doi:10.1029/2005JD006618, 2006.

Frieß, U., Klein Baltink, H., Beirle, S., Clémer, K., Hendrick, F., Henzing, B., Irie, H., de Leeuw, G., Li, A., Moerman, M. M., van Roozendael, M., Shaiganfar, R., Wagner, T., Wang, Y., Xie, P., Yilmaz, S., and Zieger, P.: Intercomparison of Aerosol Extinction Profiles Retrieved from MAX-DOAS Measurements, Atmospheric Measurement Techniques, 9, 3205–3222, doi:10.5194/amt-9-3205-2016, 2016.

Hansen, P.: Analysis of Discrete Ill-Posed Problems by Means of the L-Curve, SIAM Review, 34, 561–580, doi:10/c2dntc, 1992.

Hartl, A. and Wenig, M. O.: Regularisation Model Study for the Least-Squares Retrieval of Aerosol Extinction Time Series from UV/VIS MAX-DOAS Observations for a Ground Layer Profile Parameterisation, Atmospheric Measurement Techniques, 6, 1959–1980, doi:10.5194/amt-6-1959-2013, 2013.

Hendrick, F., Barret, B., van Roozendael, M., Boesch, H., Butz, A., De Mazière, M., Goutail, F., Hermans, C., Lambert, J.-C., Pfeilsticker, K., and Pommereau, J.-P.: Retrieval of Nitrogen Dioxide Stratospheric Profiles from Ground-Based Zenith-Sky UV-Visible Observations: Validation of the Technique through Correlative Comparisons, Atmospheric Chemistry and Physics, 4, 2091–2106, 2004.

Hendrick, F., Müller, J.-F., Clémer, K., Wang, P., De Mazière, M., Fayt, C., Gielen, C., Hermans, C., Ma, J. Z., Pinardi, G., Stavrakou, T., Vlemmix, T., and Van Roozendael, M.: Four Years of Ground-Based MAX-DOAS Observations of HONO and NO$_2$ in the Beijing Area, Atmospheric Chemistry and Physics, 14, 765–781, doi:10.5194/acp-14-765-2014, 2014.

Henyey, L. G. and Greenstein, J. L.: Diffuse Radiation in the Galaxy, The Astrophysical Journal, 93, 70–83, doi:10.1086/144246, 1941.

Herman, J., Cede, A., Spinei, E., Mount, G., Tzortziou, M., and Abuhassan, N.: NO$_2$ Column Amounts from Ground-Based Pandora and MFDOAS Spectrometers Using the Direct-Sun DOAS Technique: Intercomparisons and Application to OMI Validation, Journal of Geophysical Research: Atmospheres, 114, D13 307, doi:10.1029/2009JD011848, 2009.

Holben, B. N., Eck, T. F., Slutsker, I., Tanré, D., Buis, J. P., Setzer, A., Vermote, E., Reagan, J. A., Kaufman, Y. J., Nakajima, T., Lavenu, F., Jankowiak, I., and Smirnov, A.: AERONET—A Federated Instrument Network and Data Archive for Aerosol Characterization, Remote Sensing of Environment, 66, 1–16, doi:10.1016/S0034-4257(98)00031-5, 1998.

Hönninger, G. and Platt, U.: Observations of BrO and Its Vertical Distribution during Surface Ozone Depletion at Alert, Atmospheric Environment, 36, 2481–2489, doi:10/bkjbwh, 2002.

Hönninger, G., von Friedeburg, C., and Platt, U.: Multi Axis Differential Optical Absorption Spectroscopy (MAX-DOAS), Atmospheric Chemistry and Physics, 4, 231–254, 2004.

Irie, H., Takashima, H., Kanaya, Y., Boersma, K. F., Gast, L., Wittrock, F., Brunner, D., Zhou, Y., and Van Roozendael, M.: Eight-Component Retrievals from Ground-Based MAX-DOAS Observations, Atmospheric Measurement Techniques, 4, 1027–1044, doi:10.5194/amt-4-1027-2011, 2011.

Kebabian, P. L., Wood, E. C., Herndon, S. C., and Freedman, A.: A Practical Alternative to Chemiluminescence-Based Detection of Nitrogen Dioxide: Cavity Attenuated Phase Shift Spectroscopy, Environmental Science & Technology, 42, 6040–6045, doi:10/fs8pg7, 2008.

Knepp, T., Pippin, M., Crawford, J., Chen, G., Szykman, J., Long, R., Cowen, L., Cede, A., Abuhassan, N., Herman, J., Delgado, R., Compton, J., Berkoff, T., Fishman, J., Martins, D., Stauffer, R., Thompson, A. M., Weinheimer, A., Knapp, D., Montzka, D., Lenschow, D., and Neil, D.: Estimating Surface NO_2 and SO_2 Mixing Ratios from Fast-Response Total Column Observations and Potential Application to Geostationary Missions, Journal of Atmospheric Chemistry, 72, 261–286, doi:10.1007/s10874-013-9257-6, 2015.

Lee, H., Irie, H., Kim, Y. J., Noh, Y., Lee, C., Kim, Y., and Chun, K. J.: Retrieval of Aerosol Extinction in the Lower Troposphere Based on UV MAX-DOAS Measurements, Aerosol Science and Technology, 43, 502–509, doi:10.1080/02786820902769691, 2009.

Lelieveld, J., Berresheim, H., Borrmann, S., Crutzen, P. J., Dentener, F. J., Fischer, H., Feichter, J., Flatau, P. J., Heland, J., Holzinger, R., Korrmann, R., Lawrence, M. G., Levin, Z., Markowicz, K. M., Mihalopoulos, N., Minikin, A., Ramanathan, V., de Reus, M., Roelofs, G. J., Scheeren, H. A., Sciare, J., Schlager, H., Schultz, M., Siegmund, P., Steil, B., Stephanou, E. G., Stier, P., Traub, M., Warneke, C., Williams, J., and Ziereis, H.: Global Air Pollution Crossroads over the Mediterranean, Science, 298, 794–799, doi:10/fntp6v, 2002.

Leser H., Hönninger G., and Platt U.: MAX-DOAS Measurements of BrO and NO_2 in the Marine Boundary Layer, Geophysical Research Letters, 30, doi:10/fjm8bv, 2003.

Li, X., Brauers, T., Shao, M., Garland, R. M., Wagner, T., Deutschmann, T., and Wahner, A.: MAX-DOAS Measurements in Southern China: Retrieval of Aerosol Extinctions and Validation Using Ground-Based in-Situ Data, Atmospheric Chemistry and Physics, 10, 2079–2089, doi:10.5194/acp-10-2079-2010, 2010.

NASA: U.S. Standard Atmosphere, 1976, Office, U.S. Government Printing, Washington, D.C., 1976.

NASA: AVDC | DATA - AURA - NASA EOS -Aura Validation Data Center - Correlative Data, Field of View Predictions, Data Subsets, https://avdc.gsfc.nasa.gov/index.php?site=2045907950, 2018.

Pinardi, G., Van Roozendael, M., Abuhassan, N., Adams, C., Cede, A., Clémer, K., Fayt, C., Frieß, U., Gil, M., Herman, J., Hermans, C., Hendrick, F., Irie, H., Merlaud, A., Navarro Comas, M., Peters, E., Piters, A. J. M., Puentedura, O., Richter, A., Schönhardt, A., Shaiganfar, R., Spinei, E., Strong, K., Takashima, H., Vrekoussis, M., Wagner, T., Wittrock, F., and Yilmaz, S.: MAX-DOAS Formaldehyde Slant Column Measurements during CINDI: Intercomparison and Analysis Improvement, Atmospheric Measurement Techniques, 6, 167–185, doi:10.5194/amt-6-167-2013, 2013.

Piters, A. J. M., Boersma, K. F., Kroon, M., Hains, J. C., Van Roozendael, M., Wittrock, F., Abuhassan, N., Adams, C., Akrami, M., Allaart, M. A. F., Apituley, A., Beirle, S., Bergwerff, J. B., Berkhout, A. J. C., Brunner, D., Cede, A., Chong, J., Clémer, K., Fayt, C., Frieß, U., Gast, L. F. L., Gil-Ojeda, M., Goutail, F., Graves, R., Griesfeller, A., Großmann, K., Hemerijckx, G., Hendrick, F., Henzing, B., Herman,

J., Hermans, C., Hoexum, M., van der Hoff, G. R., Irie, H., Johnston, P. V., Kanaya, Y., Kim, Y. J., Klein Baltink, H., Kreher, K., de Leeuw, G., Leigh, R., Merlaud, A., Moerman, M. M., Monks, P. S., Mount, G. H., Navarro-Comas, M., Oetjen, H., Pazmino, A., Perez-Camacho, M., Peters, E., du Piesanie, A., Pinardi, G., Puentedura, O., Richter, A., Roscoe, H. K., Schönhardt, A., Schwarzenbach, B., Shaiganfar, R., Sluis, W., Spinei, E., Stolk, A. P., Strong, K., Swart, D. P. J., Takashima, H., Vlemmix, T., Vrekoussis, M., Wagner, T., Whyte, C., Wilson, K. M., Yela, M., Yilmaz, S., Zieger, P., and Zhou, Y.: The Cabauw Intercomparison Campaign for Nitrogen Dioxide Measuring Instruments (CINDI): Design, Execution, and Early Results, Atmospheric Measurement Techniques, 5, 457–485, doi:10.5194/amt-5-457-2012, 2012.

Platt, U. and Stutz, J.: Differential Optical Absorption Spectroscopy: Principles and Applications, Physics of Earth and space environments, Springer, Berlin, 2008.

Pöhler, D., Vogel, L., Frieß, U., and Platt, U.: Observation of Halogen Species in the Amundsen Gulf, Arctic, by Active Long-Path Differential Optical Absorption Spectroscopy, Proceedings of the National Academy of Sciences, 107, 6582–6587, doi:10/cqnpj4, 2010.

Pöhler, D., Lutz, E., Horbanski, M., Lampel, J., and Platt, U.: High Precision NO_2 and NO Measurements with the ICAD Instrument during S-b-s Campaign Hohenpeißenberg 2016, vol. 19, p. 14336, 2017.

Rodgers, C. D.: Inverse Methods for Atmospheric Sounding: Theory and Practice, no. 2 in Series on atmospheric oceanic and planetary physics, World Scientific, Singapore, reprinted edn., oCLC: 254137862, 2004.

Rodgers, C. D. and Connor, B. J.: Intercomparison of Remote Sounding Instruments, Journal of Geophysical Research: Atmospheres, 108, 4116, doi:10.1029/2002JD002299, 2003.

Rozanov, V. V. and Rozanov, A. V.: Differential Optical Absorption Spectroscopy (DOAS) and Air Mass Factor Concept for a Multiply Scattering Vertically Inhomogeneous Medium: Theoretical Consideration, Atmospheric Measurement Techniques, 3, 751–780, doi:10.5194/amt-3-751-2010, 2010.

Rozanov, V. V., Rozanov, A. V., Kokhanovsky, A. A., and Burrows, J. P.: Radiative Transfer through Terrestrial Atmosphere and Ocean: Software Package SCIATRAN, Journal of Quantitative Spectroscopy and Radiative Transfer, 133, 13–71, doi:10.1016/j.jqsrt.2013.07.004, 2014.

Sayer, A. M., Hsu, N. C., Bettenhausen, C., and Jeong, M.-J.: Validation and Uncertainty Estimates for MODIS Collection 6 "Deep Blue" Aerosol Data, Journal of Geophysical Research: Atmospheres, 118, 7864–7872, doi:10.1002/jgrd.50600, 2013.

Sinreich, R., Frieß, U., Wagner, T., and Platt, U.: Multi Axis Differential Optical Absorption Spectroscopy (MAX-DOAS) of Gas and Aerosol Distributions, Faraday Discussions, 130, 153, doi:10.1039/b419274p, 2005.

Sinreich, R., Merten, A., Molina, L., and Volkamer, R.: Parameterizing Radiative Transfer to Convert MAX-DOAS dSCDs into near-Surface Box-Averaged Mixing Ratios, Atmospheric Measurement Techniques, 6, 1521–1532, doi:10.5194/amt-6-1521-2013, 2013.

Stocker, T., ed.: Climate Change 2013: The Physical Science Basis: Working Group I Contribution to the Fifth Assessment Report of the Intergovernmental Panel on Climate Change, Cambridge University Press, New York, 2014.

van Roozendael, M., Fayt, C., Post, P., Hermans, C., and Lambert, J. C.: Retrieval of Tropospheric BrO and NO2</Subscript> from UV-Visible Observations, in: Sounding the Troposphere from Space, pp. 155–165, Springer, Berlin, Heidelberg, doi:10.1007/978-3-642-18875-6_19, 2004.

Vlemmix, T., Piters, A. J. M., Berkhout, A. J. C., Gast, L. F. L., Wang, P., and Levelt, P. F.: Ability of the MAX-DOAS Method to Derive Profile Information for NO_2: Can the Boundary Layer and Free Troposphere Be Separated?, Atmospheric Measurement Techniques, 4, 2659–2684, doi:10.5194/amt-4-2659-2011, 2011.

Vlemmix, T., Hendrick, F., Pinardi, G., De Smedt, I., Fayt, C., Hermans, C., Piters, A., Wang, P., Levelt, P., and Van Roozendael, M.: MAX-DOAS Observations of Aerosols, Formaldehyde and Nitrogen Dioxide in the Beijing Area: Comparison of Two Profile Retrieval Approaches, Atmospheric Measurement Techniques, 8, 941–963, doi:10.5194/amt-8-941-2015, 2015.

Wagner, T., Dix, B., v. Friedeburg, C., Frieß, U., Sanghavi, S., Sinreich, R., and Platt, U.: MAX-DOAS O_4 Measurements: A New Technique to Derive Information on Atmospheric Aerosols-Principles and Information Content: MAX-DOAS O $_4$ MEASUREMENTS OF AERO-SOLS, Journal of Geophysical Research: Atmospheres, 109, n/a–n/a, doi:10.1029/2004JD004904, 2004.

Wagner, T., Beirle, S., Brauers, T., Deutschmann, T., Frieß, U., Hak, C., Halla, J. D., Heue, K. P., Junkermann, W., Li, X., Platt, U., and Pundt-Gruber, I.: Inversion of Tropospheric Profiles of Aerosol Extinction and HCHO and NO_2 Mixing Ratios from MAX-DOAS Observations in Milano during the Summer of 2003 and Comparison with Independent Data Sets, Atmospheric Measurement Techniques, 4, 2685–2715, doi:10.5194/amt-4-2685-2011, 2011.

Wang, Y., Lampel, J., Xie, P., Beirle, S., Li, A., Wu, D., and Wagner, T.: Ground-Based MAX-DOAS Observations of Tropospheric Aerosols, NO_2, SO_2 and HCHO in Wuxi, China, from 2011 to 2014, Atmos. Chem. Phys., 17, 2189–2215, doi:10.5194/acp-17-2189-2017, 2017.

Wittrock, F.: The Retrieval of Oxygenated Volatile Organic Compounds by Remote Sensing Techniques, Dissertation, University of Bremen, Bremen, 2006.

Wittrock, F., Oetjen, H., Richter, A., Fietkau, S., Medeke, T., Rozanov, A., and Burrows, J. P.: MAX-DOAS Measurements of Atmospheric Trace Gases in Ny-Ålesund - Radiative Transfer Studies and Their Application, Atmospheric Chemistry and Physics, 4, 955–966, doi:10.5194/acp-4-955-2004, 2004.

Zieger, P., Weingartner, E., Henzing, J., Moerman, M., de Leeuw, G., Mikkilä, J., Ehn, M., Petäjä, T., Clémer, K., van Roozendael, M., Yilmaz, S., Frieß, U., Irie, H., Wagner, T., Shaiganfar, R., Beirle, S., Apituley, A., Wilson, K., and Baltensperger, U.: Comparison of Ambient Aerosol Extinction Coefficients Obtained from In-Situ, MAX-DOAS and LIDAR Measurements at Cabauw, Atmospheric Chemistry and Physics, 11, 2603–2624, doi:10.5194/acp-11-2603-2011, 2011.

BOREAS - a new MAX-DOAS profile retrieval algorithm for aerosols and trace gases

Tim Bösch[1], Vladimir Rozanov[1], Andreas Richter[1], Enno Peters[1,a], Alexei Rozanov[1], Folkard Wittrock[1], Alexis Merlaud[4], Johannes Lampel[3,9], Stefan Schmitt[3], Marijn de Haij[2], Stijn Berkhout[6], Bas Henzing[5], Arnoud Apituley[2], Mirjam den Hoed[2], Jan Vonk[6], Martin Tiefengraber[7,8], Moritz Müller[7,8], and John Philip Burrows[1]

[1]Institute of Environmental Physics, University of Bremen, Bremen, Germany
[2]Royal Netherlands Meteorological Institute (KNMI), De Bilt, the Netherlands
[3]Institute of Environmental Physics, University of Heidelberg, Heidelberg, Germany
[4]Royal Belgian Institute for Space Aeronomy (BIRA-IASB), Brussels, Belgium
[5]Netherlands Organization for Applied Scientific Research (TNO), Utrecht, the Netherlands
[6]National Institute for Public Health and the Environment (RIVM), Bilthoven, the Netherlands
[7]LuftBlick, Kreith, Austria
[8]Institute of Atmospheric and Cryospheric Sciences, University of Innsbruck, Innsbruck, Austria
[9]Airyx GmbH, Eppelheim, Germany
[a]now at: Institute for protection of maritime infrastructures, Bremerhaven, Germany

Correspondence to: Tim Bösch (tim.boesch@iup.physik.uni-bremen.de)

Abstract. We present a new MAX-DOAS profiling algorithm for aerosols and trace gases, BOREAS, which utilizes an iterative solution method including Tikhonov regularization and the optimal estimation technique. The aerosol profile retrieval is based on a novel approach in which the absorption depth of O_4 is directly used in order to retrieve extinction coefficient profiles instead of the commonly used perturbation theory method. The retrieval of trace gases is done with the frequently used optimal estimation method but significant improvements on how to deal with wrongly weighted a priori constraints and for scenarios in which the a priori profile is inaccurate are presented.

Performance tests are separated into two parts. First, we address the general sensitivity of the retrieval on the example of synthetic data calculated with the radiative transfer model SCIATRAN. In the second part of the study, we demonstrate BOREAS profiling accuracy by validating results with the help of ancillary measurements carried out during the CINDI-2 campaign in Cabauw, the Netherlands in 2016.

The synthetic sensitivity tests indicate, that the regularization between measurement and a priori constraints is insufficient when knowledge of the true state of the atmosphere is poor. We demonstrate a priori pre-scaling and extensive regularization tests as a tool for the optimization of retrieved profiles. The comparison of retrieval results with in situ, ceilometer, NO_2 LIDAR, sonde and long path DOAS measurements during the CINDI-2 campaign always shows high correlations with coefficients greater than 0.75. The largest differences can be found in the morning hours, when the planetary boundary layer is not yet fully developed and the concentration of trace gases and aerosol, as a result of a low night-time boundary layer having formed, is focused in a shallow, surface near layer.

1 Introduction

Aerosols and trace gases play an important role for life on Earth as high concentrations have adverse impacts on human health and climate. Furthermore, aerosols impact on Earth's energy budget by radiative forcing. They interact with solar radiation by scattering and absorption processes. Additionally, they have an impact on the formation of clouds when acting as cloud con-
5 densation nuclei (CCN). Despite considerable efforts by the scientific community, uncertainties on aerosol radiative forcing are still high (Stocker, 2014).

In addition to aerosols, atmospheric trace gases are of importance in an increasingly urbanized world as they impact on human health, agriculture, acid deposition, and climate (e.g. Lelieveld et al. (2002)). Trace gases in the troposphere such as nitrogen dioxide and sulfur dioxide (NO_2, SO_2), nitrous acid (HONO), formaldehyde (HCHO) and glyoxal (CHOCHO) need to be
10 measured to assess their impact on air quality and because their spatial and temporal inhomogeneous distribution provides information on different emission sources e.g. the combustion of fossil fuels, biomass burning and agriculture (Wittrock et al., 2004; Irie et al., 2011; Pinardi et al., 2013; Hendrick et al., 2014). The separation and identification of anthropogenic from natural sources as well as measurements of their temporal variability improves the understanding of their effects on climate and life on Earth. The current lack of knowledge leads to uncertainties in temporal and spatial emission patterns of trace gases
15 and aerosols and limits our ability to fully understand atmospheric processes. This results in a need for comprehensive measurements to fill these gaps.

For more than 15 years, Multi-Axis Differential Optical Absorption Spectroscopy (MAX-DOAS) measurements have been used to investigate the chemical composition of the troposphere (Hönninger and Platt, 2002; Bobrowski et al., 2003; Leser H. et al., 2003; Wittrock et al., 2004; Wagner et al., 2004; van Roozendael et al., 2004). This passive remote sensing method is ba-
20 sed on absorption spectroscopy applied to measurements of scattered sunlight. The advantages of ground-based MAX-DOAS when compared to satellite observations are the high sensitivity for the lowermost layers of the troposphere, the high temporal and spatial resolution of measurements, and the lower cost.

The strength of the absorption signal detected in scattered sunlight depends on the absorber amounts and their vertical distribution but also on the length of the light path. In general, this length in a certain altitude layer is a function of the measurement
25 geometry. Therefore, a set of MAX-DOAS radiance measurements taken at different elevation angles (lines of sight, LOS) contains information about the vertical distribution of trace gases, which can be retrieved. However, the retrieval of absorber profiles from MAX-DOAS measurements is an ill posed problem that needs additional constraints (see Section 3.2). Thus, the inversion, which is applied for retrieving vertical concentration profiles, is done by elaborated mathematical methods such as optimal estimation (OE). In addition to the trace gas profile, the aerosol extinction profile needs to be retrieved as well as it has
30 a non-linear effect on the trace gas retrieval and it is too variable to be approximated by climatologies. In contrast to the trace gas retrievals, aerosol retrievals are strongly non-linear, necessitating iterative inversion schemes such as the Gauss-Newton algorithm or the Levenberg Marquardt algorithm (Rodgers, 2004).

Profile retrieval algorithms used in the scientific community are either inversion algorithms or parametrized approaches. Inversion algorithms directly link the measurement quantity to the vertical profile of the target absorber with the help of a forward

2

model (Wittrock et al., 2004; Hendrick et al., 2004; Wagner et al., 2004; Frieß et al., 2006; Wittrock, 2006; Clémer et al., 2010; Wang et al., 2017). This model is usually calculated with a radiative transfer model (RTM) assuming a selected set of atmospheric conditions. For trace gases, the model also includes a sensitivity matrix which can be considered as derivative of the measurement quantity with respect to the trace gas concentration for each altitude level. For aerosols, this sensitivity matrix

5 is normally calculated via perturbation theory. This perturbation approach is shortly summarized as follows: by consideration of a trace gas with a well known vertical distribution such as the oxygen dimer O_2-O_2 (or short O_4), the aerosol extinction for each layer is changed gradually and the resulting modelled observations for different LOS are compared with measurements until the iteration converges (e.g. the difference between measurement and modelled quantity is small enough).

Parametrization on the other hand means, that a forward model, based on a limited set of parameters, is used to describe the

10 measurement quantity. Frequently used forward model parameters are integrated values and profile information such as shape and height of certain absorber layers (Sinreich et al., 2005; Lee et al., 2009; Li et al., 2010; Vlemmix et al., 2011; Wagner et al., 2011; Sinreich et al., 2013). The forward model results are calculated with an RTM and are least squares fitted to the measurements. Generally, look up tables (LUT) are pre-calculated for a set of different scenarios, parameters and geometries covering all relevant atmospheric conditions, avoiding high computational efforts during near real time calculations.

15 Inversion algorithms have the advantage that they are not limited to the scenarios used when creating the LUT but unrealistic profiles are possible when the measurement, inversion, or regularization (weighting between the information from measurements and a priori informations) is poor. On the other hand, parametrized approaches evaluate profiles much faster, as the slow forward model computation was already done when creating the LUT.

Although efforts for deriving concentration profiles from MAX-DOAS measurements have been made for more than one de-

20 cade, profiling is still a difficult task and results of different algorithms can differ strongly when the absorber of interest is highly variable and inhomogeneous on spatial and temporal scales (Zieger et al., 2011; Vlemmix et al., 2015; Frieß et al., 2016). Comparison studies of different profiling algorithms for synthetic as well as for real data summarizing the current state of the art and including results from the algorithm introduced here will be reported by Frieß et al. (2018) and Tirpitz et al. (2018).

25 The purpose of this study is the introduction of IUP Bremen's new MAX-DOAS profile retrieval algorithm for aerosols and trace gases BOREAS (Bremen Optimal estimation REtrieval for Aerosols and trace gaseS) which has been developed to improve on the earlier profile retrieval algorithm (Wittrock, 2006). BOREAS uses a novel approach for the retrieval of aerosols but a similar optimal estimation technique for the retrieval of trace gases. In contrast to perturbation based inversion algorithms, BOREAS uses the change (from an a priori state) of depth in an absorption band to get information on the aerosol content which

30 caused this change. To the authors' knowledge, this approach has never been used within an operational profiling algorithm and it complements the variety of methods with another promising technique. In order to improve the standard OE method for trace gases, a simple way of changing the weighting between a priori and measurement constraints is introduced by varying a regularization factor so that oscillations are minimized. Additionally, the usage of a priori pre-scaling is highlighted as one way of improving results when the a priori profile is far away from the real atmosphere.

35

The development of BOREAS aimed at several key properties:

1. Flexibility: the algorithm should retrieve aerosol and trace gas profiles from any MAX-DOAS measurement with pre-filtering options for the data.

2. Accuracy/stability: the algorithm should be stable in terms of varying atmospheric conditions when retrieving profiles for several years of data. The profiling results (modelled observation) should fit the measured observations with a high accuracy.

3. Automation: the retrieval should respond to problematic data/settings (e.g. low information content, wrong regularization) automatically with an included problem solution scheme.

4. Fast: the algorithm should be fast enough to allow near real time profile retrievals.

The manuscript is organised as follow: in the first section, a typical MAX-DOAS measurement and its information content are shortly described. The next section focuses on the theoretical background of the retrieval algorithm. This section is followed by a detailed sensitivity study. The 4th section is divided into an analysis of synthetic data, a discussion of error sources and an example of application to real measurements which shows that BOREAS is able to retrieve profiles with high reliability and accuracy. The final section 5 concludes and summarizes the results presented in this study.

2 MAX-DOAS measurements and the DOAS retrieval

Modern ground-based MAX-DOAS instruments are capable of measuring scattered sunlight in the ultraviolet (UV) and visible (VIS) spectral range with a full azimuthal and elevation angle coverage of the hemisphere (see Figure 1). In general, the spectral least-squares fit of absorption cross sections and a polynomial to the slant optical thickness (logarithm of a sun normalized radiance at a certain LOS, also called slant optical thickness, SOT) $\tau = -\ln(I/I_0)$ (DOAS fit) provides integrated concentrations ρ along the light path L, the so called slant column densities S (or SCD) (Platt and Stutz, 2008). The length of the light path L depends on the sun position, the scattering properties of the atmosphere and on the viewing geometry. For ground based measurements, the extraterrestrial solar spectrum I_0 is usually replaced by an intensity spectrum measured in zenith direction I_{ref} (reference spectrum) to compensate for Fraunhofer lines and instrumental issues (e.g. temperature dependent wavelength shifts). As this zenith spectrum itself is usually contaminated by the absorber of interest to some extent, the difference of the two SCDs, ΔS is retrieved and referred to as differential SCD. The differential optical thickness $\Delta \tau_j$ of a certain absorber j only, is defined as

$$\Delta \tau_j(\lambda, \boldsymbol{\Omega}) = \sigma_j(\lambda) \Delta S_j(\boldsymbol{\Omega}), \tag{1}$$

where $\sigma_j(\lambda)$ is the spectral absorption cross section and $\boldsymbol{\Omega} = \{\alpha, \varphi, \vartheta\}$ represents the angular variables. Here, α is the elevation angle (or LOS), φ is the relative azimuth angle (RAA) between sun and viewing azimuth, and ϑ is the solar zenith angle (SZA). When using a single zenith spectrum measured around noon as I_{ref}, the tropospheric signal in I_{ref} is minimised but for
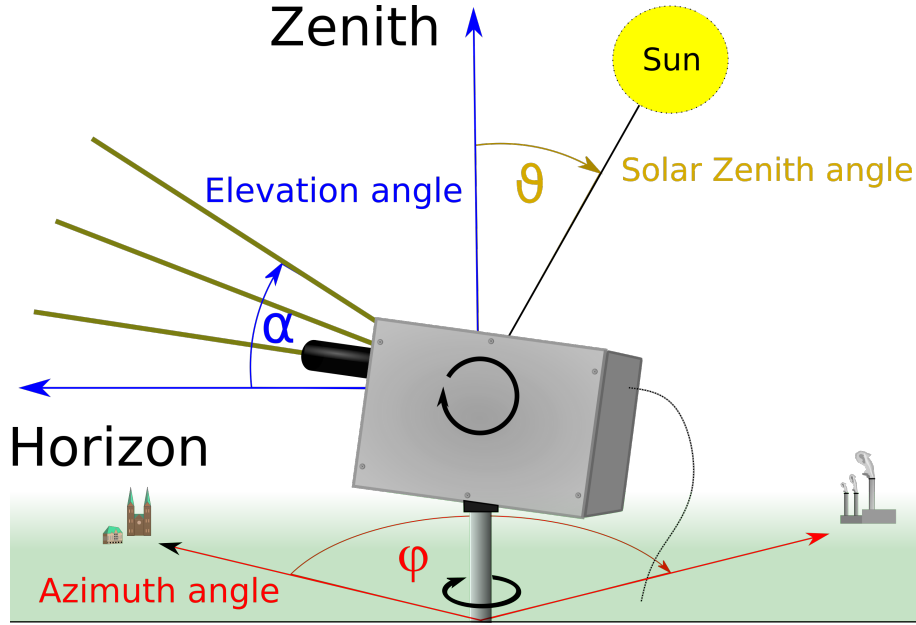
4

Figure 1. Schematic representation of typical MAX-DOAS measurement geometries.

absorbers which are also present in the stratosphere, stratospheric absorption contributes significantly to ΔS in the morning and evening. This is due to diurnal variations in the stratospheric amounts of some absorbers such as NO_2 and the change in light paths through the stratosphere because of a varying SZA (see e.g. Leser H. et al. (2003)). To minimise the stratospheric signal, a reference spectrum measured close in time to the intensity I for a certain geometry is applied. Usually, a scan of measurements in different elevation angles is followed by a measurement in zenith direction so that the whole scan can be fitted with the same reference spectrum.

The ratio of slant column density S and the vertically integrated absorber concentration $V = \int_0^H \rho(z)dz$ (vertical column density V) is called air mass factor M (AMF).

$$M(\mathbf{\Omega}) \equiv \frac{S(\mathbf{\Omega})}{V} \tag{2}$$

Generally, this value depends on the radiative transfer through the atmosphere and on parameters such as SZA, surface albedo, wavelength, and the profiles of aerosols and gaseous absorbers. For trace gases in the boundary layer, it can in first approximation be described by the geometric air mass factor

$$M_{geom}(\alpha) = \frac{S(\alpha)}{V} = \frac{1}{\sin(\alpha)}, \tag{3}$$

assuming that the trace gas layer is located below the last scattering point (Hönninger et al., 2004). The differential AMF (dAMF), assuming a zenith reference spectrum, is then $\Delta M = S/V - S_{ref}/V = (1 - \sin(\alpha))/\sin(\alpha)$. The difference between geometric and true AMF depends strongly on the wavelength, elevation angle, relative azimuth angle and aerosols.

5

Because of the altitude depending concentration of absorbers, there is a need for a similar quantity describing the ratio of S and V in a certain layer. The concept of box air mass factor $\mathscr{M}_z$ (BAMF) introduces this height dependence by defining the ratio for each altitude layer z:

$$\mathscr{M}_z(\mathbf{\Omega}) = \frac{S_z(\mathbf{\Omega})}{V_z} \tag{4}$$

5   Here, $\mathscr{M}_z$ depends on the altitude in contrast to the total AMF M. Box air mass factors are calculated by radiative transfer models and can be understood as sensitivity of the partial slant column to the partial vertical column at a certain altitude. On the other hand, multiplication of a profile of partial vertical columns with $\mathscr{M}_z$ leads to the corresponding slant column density.

3   Retrieval algorithm description

The profile retrieval algorithm BOREAS was developed in order to retrieve aerosol and trace gas vertical profiles from MAX-
10   DOAS measurements. The aerosol retrieval is fully implemented within the RTM SCIATRAN (Rozanov et al., 2014) to decrease computation time for the iterative minimization scheme. BOREAS is a Python written analysis script which calls SCIATRAN for the aerosol retrieval and for calculations of BAMF matrices which are then used within an optimal estimation based trace gas retrieval. A flow chart depicting BOREAS is shown in Figure 2. In the next subsections, we give an overview of the individual steps of the algorithm.

15   ### 3.1   Retrieval of aerosol profiles

The standard DOAS fit does not provide direct information about aerosols present in the atmosphere. However, the scattering and absorption properties of aerosols have an impact on the measured differential slant column density $\Delta S(\mathbf{\Omega})$ because scattering processes can significantly modify the light path. Since the single scattering albedo ω (SSA) stays more or less constant when the aerosol type does not change over time and altitude, it is not a quantity to be retrieved in BOREAS and
20   is kept constant with typical values for the prevalent aerosol type (e.g. urban pollution: $SSA = 0.92$). The angular scattering distribution of aerosols is fully quantified by the scattering phase function. Within BOREAS, we use the Henyey-Greenstein approximation (Henyey and Greenstein, 1941) with constant values for the asymmetry factor g which quantifies the amount of forward and backward scattering (e.g. urban pollution: $g = 0.68$). In this parametrization, the optical properties of aerosols are fully defined with g, SSA and an extinction coefficient profile $\sigma_e(z)$. The latter is the retrieval parameter for BOREAS aerosol
25   retrievals. Note, that the usage of measured phase functions will be implemented in BOREAS in the future, since Henyey-Greenstein is in some situations not an accurate representation of the atmospheric aerosol scattering distribution.

If $\sigma_e(z)$ is known, then the aerosol optical thickness (AOT) can be determined as $\tau_{aer} = \int_0^H \sigma_e(z)dz$, where the integration is performed over the entire atmosphere. If the vertical profile of an absorber number density is known, differences between modelled and measured S for this absorber are the result of differences between the assumed and real aerosol profile. As obser-
30   vations at different LOS have varying sensitivity to the presence of aerosols at different altitudes, this can be used to retrieve an aerosol profile.
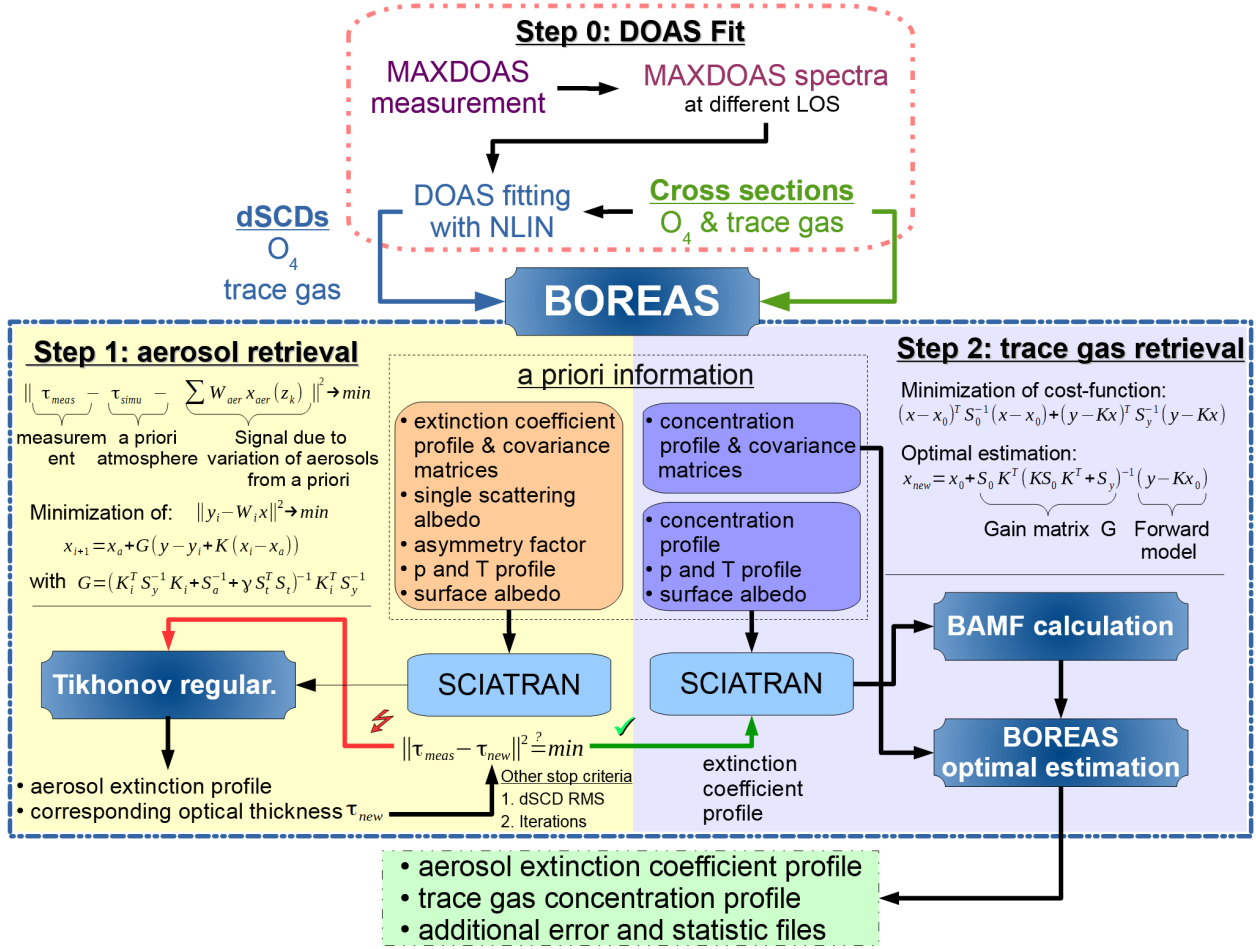
6

Figure 2. BOREAS analysis flow chart. The algorithm is separated into two steps. Step 1: Aerosol retrieval within a Tikhonov-Regularization. Step 2: Optimal estimation based trace gas retrieval.

Generally, the vertical profiles of species in the troposphere are unknown because of the temporal and spatial variability of emission sources, transport and conversion processes. However, the oxygen monomer O_2 is in this respect an exceptional species because it only depends on pressure and temperature. Furthermore, as the oxygen dimer O_4 concentration is proportional to the squared monomer concentration, its profile is exponentially decreasing with altitude as well. The O_4 slant column

5   density can easily be determined, because O_4 has spectral absorption features in the wavelength regions of most DOAS fits. Detailed sensitivity studies of O_4 $\Delta S(\mathbf{\Omega})$ measurements regarding changes in atmospheric aerosol properties can be found in Wagner et al. (2004) and Frieß et al. (2006).

In the BOREAS aerosol retrieval algorithm, the difference between modelled and measured O_4 differential slant optical thickness's $\Delta\tau(\lambda,\mathbf{\Omega})$ (DSOT) is used to retrieve aerosol extinction profiles in an iterative process. The measured $\Delta\tau(\lambda,\mathbf{\Omega})$ is

10   calculated using Eq. (1), where $\Delta S_i(\mathbf{\Omega})$ is the DSCD retrieved in the framework of the standard DOAS fit, and the simulated

O_4 DSOT ($\Delta\tilde{\tau}(\lambda, \boldsymbol{\Omega})$) is calculated as follows:

$$\Delta\tilde{\tau}(\lambda, \boldsymbol{\Omega}, N_a(z)) = \ln \frac{I(\lambda, \boldsymbol{\Omega}, N_a(z))}{I_{ref}(\lambda, N_a(z))}, \tag{5}$$

where $I(\lambda, \boldsymbol{\Omega}, N_a(z))$ and $I_{ref}(\lambda, N_a(z))$ are the intensities calculated using SCIATRAN under the assumption that O_4 is the only absorber. The dependency on the reference geometry $\boldsymbol{\Omega}_{ref}$ is summarized with the index ref and will be neglected from now on. The vertical profiles of pressure and temperature are used according to the US standard atmosphere model (NASA, 1976) but can be replaced by measured atmospheric conditions when available. The aerosol loading is described using an a priori concentration number density vertical profile $N_a(z)$.

The inverse problem with respect to the aerosol optical depth is then formulated as

$$\left\| \Delta\tau(\lambda, \boldsymbol{\Omega}) - \Delta\tilde{\tau}(\lambda, \boldsymbol{\Omega}, N_a(z)) - P(\lambda, \boldsymbol{\Omega}) \right\|^2 \longrightarrow \min, \tag{6}$$

where $P(\lambda, \boldsymbol{\Omega})$ is a polynomial of lower order and its argument $\boldsymbol{\Omega}$ emphasises that polynomial coefficients depend on the LOS angle. The assumptions made in this formulation are that 1) the O_4 absorption derived from the measurements does not depend on the concentration of other trace gases and 2) that the optical depth in an atmosphere without other absorbers can be described as the sum of the O_4 optical depth and a low order polynomial.

Since $\Delta\tilde{\tau}(\lambda, \boldsymbol{\Omega}, N_a(z))$ is a non-linear and complicated functional of $N_a(z)$, an analytical solution of this minimization problem does not exist. To simplify the solution of the minimization problem given by Eq. (6), let us consider the variation of DSOT caused by the variation of the aerosol number density. The variation of DSOT in a linear approximation can be represented in the form of the following functional Tailor series (Rozanov and Rozanov, 2010):

$$\Delta\tilde{\tau}(\lambda, \boldsymbol{\Omega}, N_a(z)) = \Delta\tilde{\tau}(\lambda, \boldsymbol{\Omega}, \bar{N}_a(z)) + \int_0^H W(\lambda, \boldsymbol{\Omega}, z)\,\delta N_a(z)\,dz + \varepsilon_{lin}(\lambda), \tag{7}$$

where

$$W(\lambda, \boldsymbol{\Omega}, z) = \left. \frac{\delta\,\Delta\tilde{\tau}(\lambda, \boldsymbol{\Omega}, N_a(z))}{\delta\,N_a(z)} \right|_{\bar{N}_a}$$

is a functional derivative of DSOT with respect to the aerosol number density profile $N_a(z)$ around the initial guess $\bar{N}_a(z)$. $W(\lambda, \boldsymbol{\Omega}, z)$ is usually referred to as weighting function and $\varepsilon_{lin}(\lambda)$ is the linearisation error.

It follows that the weighting function provides a linear relationship between the variation of DSOT and the variation of an aerosol number density N_a around the initial guess $\bar{N}_a$. Substituting now Eq. (7) into (6) and approximating the integral with a finite sum, we have

$$\left\| \Delta\tau(\lambda, \boldsymbol{\Omega}) - \Delta\tilde{\tau}(\lambda, \boldsymbol{\Omega}, \bar{N}_a(z)) - \sum_{k=1}^L \mathcal{W}(\lambda, \boldsymbol{\Omega}, z_k)\,(x_k - \bar{x}_k) - P(\lambda, \boldsymbol{\Omega}) \right\|^2 \longrightarrow \min. \tag{8}$$

Here, $\Delta x = x_k - \bar{x}_k = N_a(z_k) - \bar{N}_a(z_k)$, L is the number of altitude levels, and $\mathcal{W}(\lambda, \boldsymbol{\Omega}, z_k)$ is defined to satisfy the trapezoidal integration rule.

The solution of the minimization problem given by Eq. (8) is performed on a discrete wavelength grid. In fact, only five wavelengths over the O_4 absorption band centred at e.g. 477 nm are used.

The minimization problem can be reformulated in the following vector-matrix form:

$$\left\| \Delta \mathbf{y} \, - \, \mathbf{K} \Delta \mathbf{x} \right\|^2 \longrightarrow \min . \tag{9}$$

Here, the vector $\Delta \mathbf{y} = \mathbf{y} - \bar{\mathbf{y}} = |\Delta \mathbf{y}_1, \Delta \mathbf{y}_2, ..., \Delta \mathbf{y}_N|^T$ has the dimension $N \cdot M$ and describes the difference between measured and simulated DSOT at N LOS angles and M wavelengths. The m-th element of vectors $\mathbf{y}_n$ and $\bar{\mathbf{y}}_n$ is the differential slant optical depth of O_4 at wavelength m, given by

$$\{\mathbf{y}_n\}_m \, = \, \Delta \tau^-(\lambda_m, \mathbf{\Omega}_n) \, , \, m \, = \, 1, \ldots, M \, , \tag{10}$$

$$\{\bar{\mathbf{y}}_n\}_m \, = \, \Delta \tilde{\tau}^-(\lambda_m, \mathbf{\Omega}_n, \bar{N}_a(z)) \, , \tag{11}$$

where the superscript "-" denotes that a polynomial is subtracted. The state vector $\Delta \mathbf{x}$ has the dimension L and matrix $\mathbf{K}$ has the dimension $(N \cdot M) \times L$, i.e., the matrix consists of $N \cdot M$ rows and L columns. The r-th row of matrix $\mathbf{K}$ is then given by

$$\{\mathbf{K}\}_r \, = \, \left\{ \mathcal{W}^-(\lambda_m, \mathbf{\Omega}_n, z_1), \mathcal{W}^-(\lambda_m, \mathbf{\Omega}_n, z_2), \ldots, \mathcal{W}^-(\lambda_m, \mathbf{\Omega}_n, z_L) \right\} \qquad \text{with} \qquad r = (n-1)M + m \tag{12}$$

and contains weighting functions for the m-th wavelength, n-th LOS in L layers.

The minimization problem given by Eq. (9) is solved employing an iterative Tikhonov regularization technique (Rodgers, 2004):

$$\mathbf{x}_{i+1} = \mathbf{x}_0 + (\mathbf{K}_i^T \mathbf{S}_y^{-1} \mathbf{K}_i + \mathbf{S}_0^{-1} + \gamma \mathbf{S}_t^T \mathbf{S}_t)^{-1} \mathbf{K}_i^T \mathbf{S}_y^{-1} (\mathbf{y} - \mathbf{y}_i + \mathbf{K}_i(\mathbf{x}_i - \mathbf{x}_0)) \tag{13}$$

Here, i is the iteration number, $\mathbf{S}_0$ and $\mathbf{S}_y$ are the a priori and measurement covariance matrices, $\mathbf{K}_i$ is the weighting function matrix calculated using the estimated aerosol number density profile $\mathbf{x}_i$, $\mathbf{S}_t$ is the first order derivative matrix with Tikhonov parameter γ and $\mathbf{x}_0 = \bar{\mathbf{x}}$ and $\mathbf{y}_0 = \bar{\mathbf{y}}$ are the a priori profile and the representing a priori measurement vector, respectively. Equation 13 is solved in the logarithmic space in order to avoid negative values.

There are three criteria to stop the iteration process:

– Convergence in parameter space, i.e., the maximum difference between the components of the state vector at two subsequent iterative steps does not exceed the selected criterion (e.g. $0.0001 \, \text{km}^{-1}$).

– The root mean square difference between measured and simulated O_4 DSOT is less than selected (e.g. 0.001).

– The maximum number of iterations is reached.

In addition to the equations above, we introduce here other quantities which are useful to describe the retrieval. The gain matrix

$$\mathbf{G}_i = (\mathbf{K}_i^T \mathbf{S}_y^{-1} \mathbf{K}_i + \mathbf{S}_0^{-1} + \gamma \mathbf{S}_t^T \mathbf{S}_t)^{-1} \mathbf{K}_i^T \mathbf{S}_y^{-1} \tag{14}$$

describes the sensitivity of the solution to the measurement. Note, that this formulation includes also the Tikhonov term, leading to differences for $\gamma \neq 0$ with the definition given in Rodgers (2004). The averaging kernel $\mathbf{A}_i = \mathbf{G}_i \mathbf{K}_i$ (AK) characterizes the sensitivity of the solution to the true state. The trace of AK quantifies the degrees of freedom of the signal $d_s = \text{tr}(\mathbf{A})$ (DOF). This quantity is commonly understood as the number of individual pieces of information which, can be retrieved.

3.2 Retrieval of trace gas concentration profiles

Compared to aerosols, the inverse problem for trace gases is easier to solve because, under the assumption of an optically thin atmosphere, the relationship between trace gas concentration and measured differential slant column density is linear. Then, the forward model $\mathbf{F}(\mathbf{x}, \mathbf{b})$ is equal to a set of measurements $\mathbf{y}$,

$$\mathbf{y} = \mathbf{F}(\mathbf{x}, \mathbf{b}) + \epsilon \tag{15}$$

where ϵ includes the error of measurement and forward model. $\mathbf{F}(\mathbf{x}, \mathbf{b})$ depends on the retrieval quantity vector $\mathbf{x}$ (trace gas concentration profile) and on an additional parameter vector $\mathbf{b}$. The latter one includes quantities which have an impact on the measurement and are known with some accuracy (e.g. a priori information).

From the perspective of MAX-DOAS, this relationship is strongly ill-posed as the number of retrieval parameters is usually much higher than the number of measurements. Furthermore, as the light paths of two geometrically close elevation angles traverse similar vertical layers near the surface, measurements cannot be considered as independent. Consequently, the retrieval parameter vector $\mathbf{x}$ is not fully constrained by the input vector $\mathbf{y}$ which introduces the need for additional a priori knowledge which constrains the solution. With the assumption of a Gaussian error distribution, the optimal estimation method (OE) is often used to prevent unstable solutions when dealing with ill-posed problems (Rodgers, 2004).

$$\mathbf{x}_n = \mathbf{x}_0 + (\mathbf{K}^T \mathbf{S}_y^{-1} \mathbf{K} + g^{-1} \mathbf{S}_0^{-1})^{-1} \mathbf{K}^T \mathbf{S}_y^{-1} (\mathbf{y} - \mathbf{K} \mathbf{x}_0) \qquad \text{or}$$

$$= \mathbf{x}_0 + \mathbf{S}_0 \mathbf{K}^T (\mathbf{K} \mathbf{S}_0 \mathbf{K}^T + g \mathbf{S}_y)^{-1} (\mathbf{y} - \mathbf{K} \mathbf{x}_0) \tag{16}$$

Again, $\mathbf{S}_0$ and $\mathbf{S}_y$ are the covariance matrices, $\mathbf{y}$ is the measurement and $\mathbf{x}_0$ is the a priori profile. Equation 16 is solved in the linear space. Negative values are possible but can be avoided by applying appropriate a priori constraints. Note that we introduced a scaling factor g which gives the possibility of regulating the weighting between a priori and measurement information. Here, the matrix $\mathbf{K}$ consists of BAMF values for every layer and measuring geometry (Eq. (4)) instead of weighting functions. The covariance matrix of measurements has only diagonal elements which are the absolute errors of the spectral DOAS fit of this absorber. $\mathbf{S}_0$ has constant variances on its diagonal elements but consists of additional non-diagonal elements based on a Gaussian distribution which accounts for a possible correlation of different profile layers (Barret et al., 2002).

4 Results and Discussion

In this section, we first present and discuss results of synthetic sensitivity studies. For this purpose, noise free differential slant columns densities of different aerosol and NO_2 scenarios were simulated with SCIATRAN. Subsequently, these datasets

were used as input for BOREAS, and results are compared with the true profiles. In the next subsection, we discuss the error sources of the retrieval before, in the last section, results of data measured during the CINDI-2 campaign (2nd Cabauw Intercomparison of Nitrogen Dioxide measuring Instruments, 2016) are shown. These results are validated by comparison with different ancillary measurements (sondes, LIDAR, long path DOAS, ceilometer, AERONET, Pandora and in situ).

4.1 Sensitivity study with synthetic data

A synthetic dataset of differential slant column densities of NO_2 and O_4 was created using SCIATRAN's spherical mode including multiple scattering. The settings in Table 1 were chosen to describe conditions as they can be found in urban areas like the city of Bremen. Pressure and temperature profiles were taken from a U.S. standard atmosphere (NASA, 1976). The vertical grid was set to 25 m steps from the surface up to 6 km, 250 m steps up to 10 km and 1 km steps up to 60 km. The LOS angles were chosen as a representation of a typical MAX-DOAS measurement with more angles for the lower elevations, where the sensitivity is highest. Both, solar zenith angle and relative azimuth angle were kept constant. The trace gas and aerosol profiles

Table 1. SCIATRAN settings for the calculation of differential slant column densities

trace gases	wavelength (nm)	albedo	SZA (°)	RAA (°)	LOS (°)	asymmetry factor	SSA	climatology
O_4, NO_2	477	0.06	40	90	1, 2, 3, 4, 5, 6, 8, 15, 30	0.68	0.92	US standard

in Table 2 (see also Fig. 3, 6, A1 and A8) were chosen to assess BOREAS retrieval capability under simple (exponential profiles with scale height SH = 1 km) and non-ideal conditions (box profiles, which are not similar to the exponential a priori profiles). The NO_2 scenarios did not include aerosols to avoid the mixture of uncertainties from the trace gas retrieval and inaccuracies within the aerosol retrieval. The box profiles are shown and shortly discussed in appendix A.

Table 2. Parameters for aerosol and NO_2 profiles used in the synthetic sensitivity study.

	Exp. profiles (SH = 1 km)			Box profiles (appendix)		
	E1	E2	E3	B1	B2	B3
AOT	0.2	0.6	1.0	0.4	0.4	0.4
VCD (10^{15} molec/cm^2)	5	10	20	10	10	10
maximum altitude (km)	6	6	6	0.5	1	2

4.1.1 Sensitivity of the aerosol retrieval

Figure 3 shows the true exponential extinction coefficient profiles (see Table 1) with aerosol optical thickness's of 0.2, 0.6 and 1.0. In addition, an a priori profile with the same scale height (SH = 1 km) but with AOT = 0.18 is depicted. In general,

11

an a priori profile should comprise known information of the true atmosphere. Ancillary measurements are frequently used to gather information for a mean profile. Here, we try to evaluate the performance of the algorithm by using an a priori profile close to the true profile (E1) but also for atmospheres with highly varying aerosol loads (E2, E3).
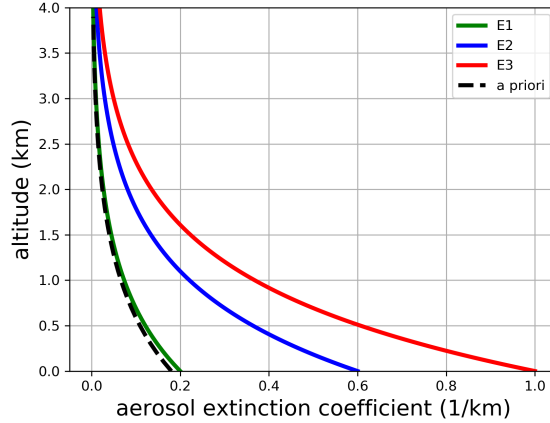
5

Figure 3. Exponential aerosol profiles for the synthetic sensitivity study. Also shown is the a priori profile for the aerosol retrieval (dashed line).

The retrieval uses vertical grid steps of 50 m for synthetic data because smaller step widths introduce retrieval noise, whereas larger steps result in vertical structure being overly smoothed. Since the retrieval tends to overestimate the upper layers due to missing sensitivity (see Fig. 9), a height depending a priori variance was used for the preparation of the a priori covariance matrix S_a. The measurement covariance matrix S_e consists of a constant signal to noise (SNR) value which is multiplied with

10   the measurement for each LOS to get absolute covariances. The Tikhonov parameter is changed in the first examples to demonstrate the retrieval response on this parameter. The iterations stop when convergence is reached or after 60 steps. Convergence in parameter space was set to $0.0001\,km^{-1}$. In addition, convergence of the RMS of measured and simulated DSOT differences was set to 0.001.

15   On the left side in Figure 4 the retrieval results for different Tikhonov parameters γ are shown. E1, which is close to the a priori profile (dashed grey line) is retrieved well for all γ values. In general, smaller Tikhonov parameters give too much weight to the measurement by reducing smoothing and introducing retrieval noise which leads to oscillations. Large values smooth the solution in the direction of the a priori profile. When the true atmosphere is far away from the a priori profile, the algorithm does not perform satisfyingly. For E2, strong smoothing (large γ values) leads to more or less straight lines in

20   which insufficient curvature can be found, whereas weak (or no) smoothing means the beginning of oscillations indicated by the reduction of the bottom extinction. No parameter value is able to retrieve the proper bottom extinction. This can be found

12

in the same way for E3 where all results show a clear lack in accuracy. This is not surprising as the a priori profile cannot be understood as the best guess or median of the atmosphere any more.
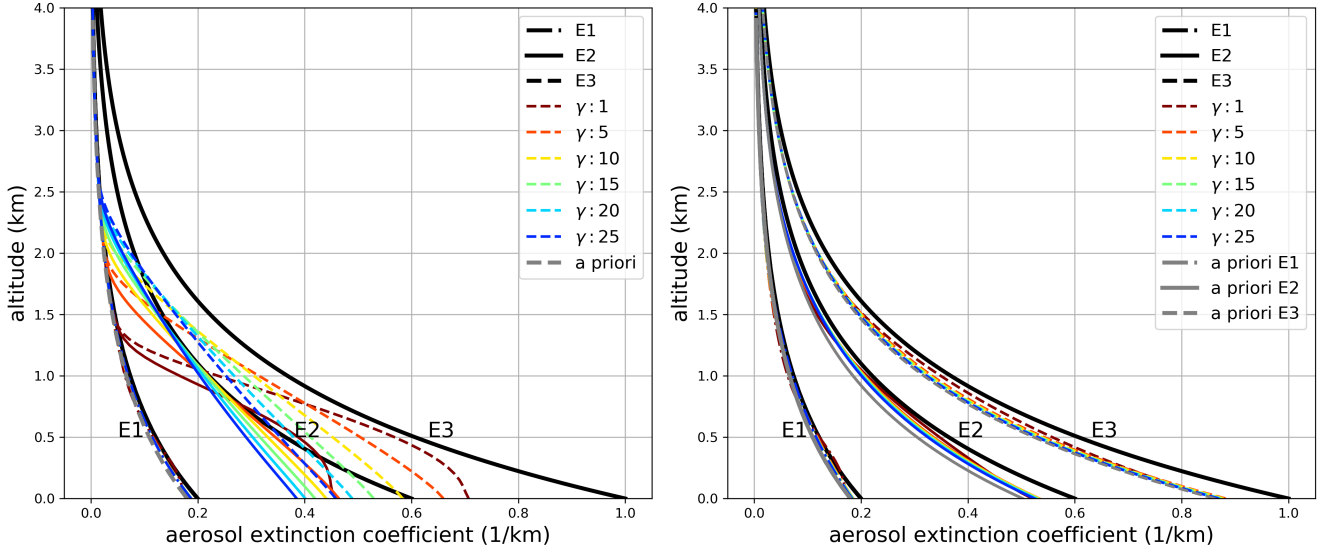

Figure 4. Retrieval results with a fixed (left) and a pre-scaled a priori profile (right) with varying Tikhonov parameters γ for SNR = 3000. Small γ values mean less smoothing of the resulting profiles.

Several authors have already highlighted retrieval problems from MAX-DOAS measurements under highly variable (in time
5   and space) atmospheric conditions (e.g. Vlemmix et al. (2011); Wagner et al. (2011); Vlemmix et al. (2015); Frieß et al. (2016)). Nevertheless, studies that focus on improvements of the regularization (Eriksson, 2000; Hartl and Wenig, 2013) or a priori information (Frieß et al., 2006; Clémer et al., 2010; Hendrick et al., 2014) are rare, with respect to MAX-DOAS retrievals. Here, we use a priori pre-scaling to cope with strong deviations of the true atmosphere from the a priori estimate. For this purpose, the BOREAS aerosol retrieval is started on a reduced vertical and spectral grid from a zero profile (all a priori
10 extinction values were set to be zero) as a priori information. In Equation 15, the a priori profile x_0 is set to 0 but the remaining terms stay unchanged in order to retrieve a reliable AOT value without limiting the solution by a certain profile shape. Since the retrieval works directly on O_4 absorption, aerosol optical thickness is in general the most reliable retrieval quantity. The AOT from this pre-calculation is used to scale the a priori profile for the main run by calculating a scaling factor from the initial a priori AOT and the new value which is applied to all initial extinction coefficients before the main inversion. Note, that the only
15 a priori information used both within the pre-run and within the main run is the Tikhonov parameter. This method performs well when the a priori shape is similar to the true atmospheric profile shape (right side of Fig. 4). However, no improvement is found when the shape of the a priori profile deviates strongly from the true atmospheric condition but no deterioration either (see box profiles in appendix A). On the right-hand side of Figure 4, clear improvements can be seen in both overall shape and bottom extinction. Nevertheless, the profiles tend to deviate stronger at the surface, especially when the aerosol load is

13

higher which was also found by Frieß et al. (2006). The relative differences of retrieved AOT are high for the unscaled retrieval but can be significantly reduced with a priori pre-scaling (see Table 3). Further improvements could be made by increasing the allowed number of iterations together with stronger convergence criteria (not shown) but the average retrieval time would increase as well.

Table 3. True and retrieved AOT for SNR = 3000, γ = 1.0 with and without a priori pre-scaling including relative differences to the true profile in brackets.

AOT	true value	fix a priori	result	scaled a priori	result
E1	0.2	0.18	0.183 (-8.6%)	0.161	0.179 (-10.4%)
E2	0.6	0.18	0.439 (-26.9%)	0.493	0.535 (-10.6%)
E3	1.0	0.18	0.626 (-37.4%)	0.847	0.895 (-11.1%)

5

A comparison of all three profiles and their optimal γ ranges with and without pre-scaling indicates that each combination of a priori and true profile has a specific optimal Tikhonov parameter which might differ strongly between each scenario. In addition, the signal to noise is another quantity which has a large impact on the retrieval. In general, SNR values might differ strongly throughout a day, because dynamic ranges of exposure and integration times are frequently used to operate the CCD

10 in the ideal saturation range when the number of photons might differ strongly (e.g. due to different viewing geometries). In Figure 5 we varied SNR (as a representation of the measurement error) and Tikhonov parameter γ from 500 to 5000 and from 0.25 to 30 respectively, to find the best parameter range for the optimization of AOT and the bottom extinction (BOT). The figure shows results for the strong aerosol scenario E3 (E1, E2 and the box scenarios are shown in the appendix). Colour coded are the relative differences to the true value with bright spots indicating better retrievals. For scenario E3, high γ (or low SNR)

15 values apply too much smoothing (not enough weight on the measurement) which ends in strong AOT/BOT underestimations of the retrieval results. Furthermore, there is an ideal range of SNR values for $\gamma \leq 2$ where the AOT relative difference is $\leq 10\%$. In this specific SNR/γ range, the bottom values do not show the best results. On the other hand, BOT values are optimized for $3 \leq \gamma \leq 10$ for SNR $= 2500$ and SNR $= 3000$ where the AOT does not have the lowest difference. As a consequence, due to unequal vertical sensitivity, choice of a priori constraints and parametrization, in some cases either AOT or the shape

20 of the profile can be optimized. Stable solutions for the optimization of both profile characteristics could not be identified in the range of parametrization, regularization and convergence. As a result, a reasonable compromise for optimum values with respect to both AOT and BOT would be in the range SNR = 2000-3000 with low Tikhonov values $2 \leq \gamma \leq 5$. Note that the SNR range between 3500 and 4000 has larger relative deviations than the surrounding settings which could not be found for other scenarios. This is assumed to be either a unique solution, where the range of settings leads to poor retrieval results, or a

25 numerical instability.

In contrast to this pragmatic approach, the so-called L-curve approach (Hansen, 1992; Engl and Grever, 1994) was found to be insufficient as it already assumes a good regularisation, i.e. the data residual and the parameter norm ($\left\| \mathbf{x} - \mathbf{x_a} \right\|$) can
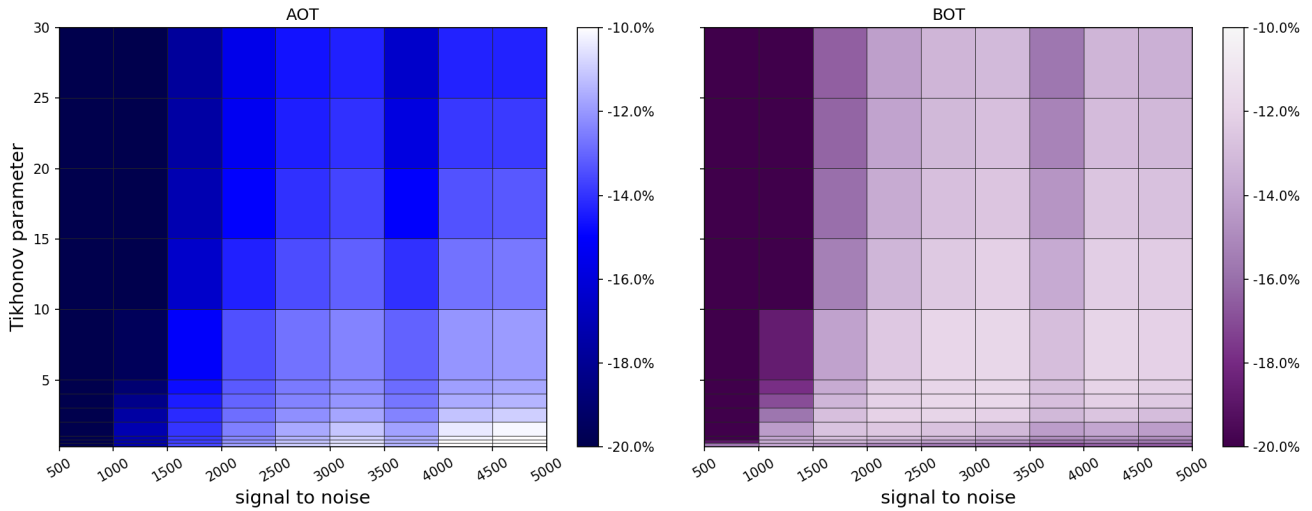
14

Figure 5. Variation of the relative difference of AOT and bottom extinction (BOT) to the true value as a function of signal to noise and Tikhonov parameter, colour coded for scenario E3 with a priori pre-scaling.

be described well by a specific regularisation parameter (Hartl and Wenig, 2013), which was not found for the application of MAX-DOAS profiling.

4.1.2 Sensitivity of the trace gas retrieval

5   The optimal estimation based trace gas profile retrieval faces similar problems as the regularization difficulties discussed for the aerosol retrieval in the previous section. In many studies, an a priori variance of a fixed percentage of the a priori profile in combination with the differential slant column density errors from the DOAS fit are used to constrain the solution (e.g. Frieß et al. (2016)). Here, we show that this is an insufficient approach, since the fitting errors might be too small, giving too much weight to the measurement, when the NO_2 concentration is high and the a priori profile is not a good estimate of the true

10 atmosphere.
Again, a priori pre-scaling is used to achieve a better estimate of the true atmospheric conditions. In contrast to the aerosol retrieval which needed a pre-run for a better first guess, the trace gas a priori pre-scaling is achieved using the 30° elevation angle measurement. In the geometric approximation (see Eq. (3)), the differential AMF is 1 which leads to $\Delta S_{30} = V$. This vertical column density V is used as a pre-scaling value for the a priori profile.

15 The different NO_2 exponential profiles, based on the parameters in Table 2, are shown in Figure 6 together with the a priori profile (box profiles can be found in appendix A). Note that we used an a priori profile close to E2. These profiles are a good representation of the daily variability in an urban region, where high NO_2 concentrations are found during phases of commuter traffic (rush hours) in the morning and late afternoon and low NO_2 loads in between.

15

Figure 7 depicts the profiling results without a priori pre-scaling on the left side and with pre-scaling on the right side. Different
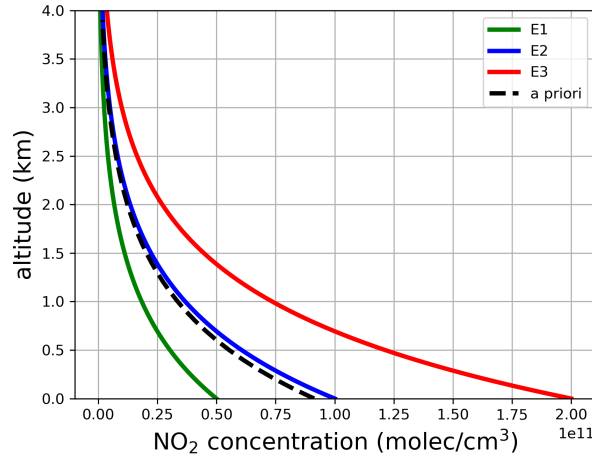

Figure 6. Exponential NO_2 profiles for the synthetic sensitivity study. Also shown, the a priori profile for the aerosol retrieval (dashed line).

regularization ratios are achieved by varying parameter g in Eq. (16) which varies the measurement error by $\sqrt{g}$. The retrieval is done on the same vertical grid as in the previous section with similar variances for the a priori covariance matrix. In contrast

5 to a constant signal to noise ratio, we use variances in the range of typical DOAS fit errors of NO_2 for the measurement covariance matrix, which can be understood as the standard approach of the MAX-DOAS profiling community. For small elevation angles and high NO_2 concentrations, the relative ΔS error is often lower than 1% and sometimes even lower than 0.3%, indicating a high reliability in the measurement but neglecting errors due to pointing inaccuracies of the telescope or horizontal inhomogeneities which affect the profiling result but not the measurement.

10 The results show again the importance of pre-scaling. Whereas the E2 scenario is well retrieved for all g-ranges without pre-scaling, the other scenarios tend to oscillate or underestimate the profile. Note, that the standard regularization ratio ($g = 1$) does not lead to satisfying results for E3. Applying pre-scaling leads to more accurate profiles especially for E3.

The specific optimal g-range for each scenario depends not only on the a priori profile and the true atmosphere but also on the variance values, their height dependencies and the definition of off-diagonal elements. However, the quantification of this

15 optimal range is a difficult task for real data due to the lack of knowledge about the true atmosphere. Manual variations of g as well as iterative approaches are conceivable. Possible criteria for finding the best g values are e.g. the RMS between measurement and retrieval quantity or ancillary measurements. Here, we used fixed values which were chosen to decrease oscillations while maintaining the best surface concentration.
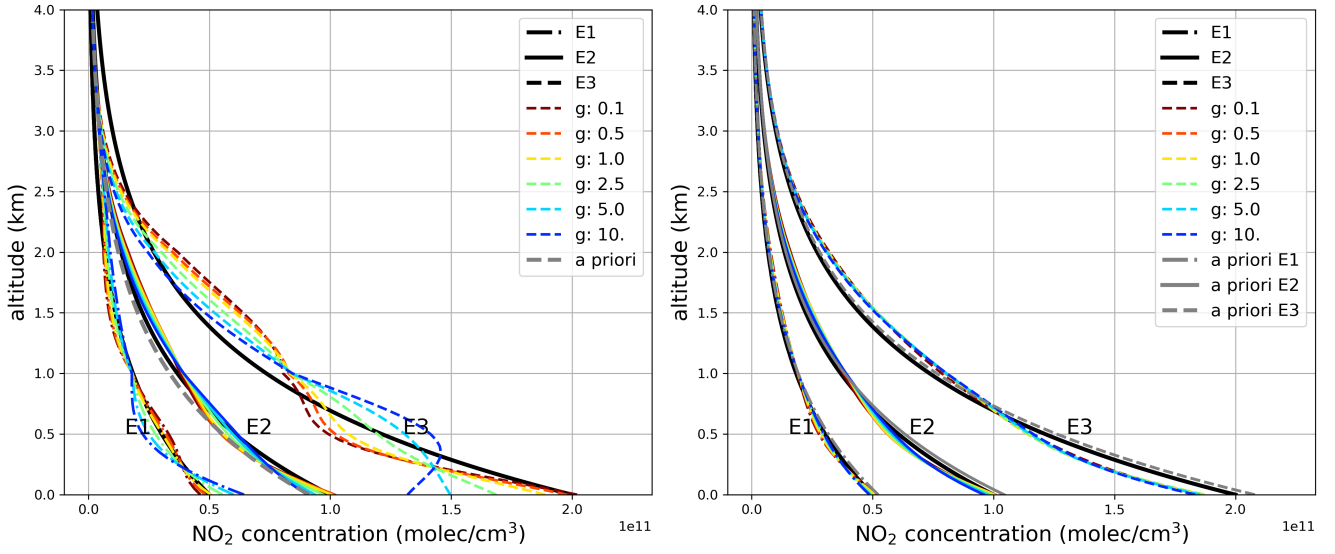
16

Figure 7. Retrieval results with a fix (left) and a pre-scaled a priori profile (right) with g factors. Small g values mean less measurement weighting for the resulting profiles.

4.2 Discussion of error sources and information content

The total error of both aerosol and trace gas retrieval can be separated into three different error sources (Rodgers, 2004).

$$\mathbf{S}_{tot} = \mathbf{S}_{sm} + \mathbf{S}_{fw} + \mathbf{S}_{ns} \tag{17}$$

5 The first error term describes the smoothing error $\mathbf{S}_{sm} = (\mathbf{A} - \mathbf{I})\mathbf{S}_e(\mathbf{A} - \mathbf{I})^T$ which can be understood as error for the averaging kernel smoothed estimate of the true state of the atmosphere. $\mathbf{A}$ and $\mathbf{I}$ are the averaging kernel and identity matrix respectively. The second term of $\mathbf{S}_{tot}$ is the forward model error $\mathbf{S}_{fw}$, which is hard to quantify in real retrievals, because it needs the true state of the atmosphere. For near linear problems, this error source can be neglected, when the forward model parameters are well estimated. The last error is called retrieval noise $\mathbf{S}_{ns} = \mathbf{G}\mathbf{S}_e\mathbf{G}^T$ (G: gain matrix, see e.g. Eq. (14) and denotes the
10 uncertainty of the retrieved profile due to measurement errors.

Figure 8 shows smoothing, retrieval and total error for the before mentioned scenarios of the aerosol retrieval (left) and the trace gas retrieval (right).

The total errors for both aerosol and trace gas retrieval are dominated by the smoothing error with negligibly small retrieval
15 noise. This shows, that the measurement itself can be considered as a small error source in contrast to the generally limited information content of MAX-DOAS measurements. Note, that the error components of the NO_2 profile show small oscillations which also indicates that larger constraints are needed. For the aerosol retrieval, the largest errors can be found in an altitude were the sensitivity is low with an additional increase near the surface. The errors are nearly zero for higher altitudes because
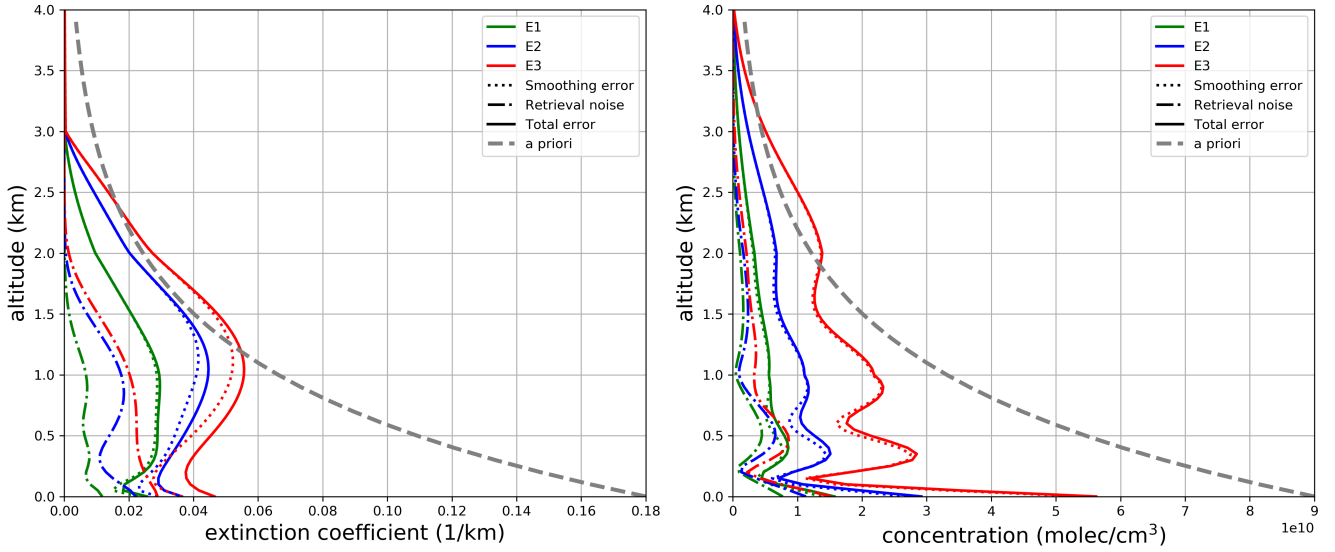
17

Figure 8. Retrieval errors for E1-E3 of the synthetic aerosol (left) and NO_2 study (right). Aerosol results are shown for SNR = 3000 and Tikhonov parameter $\gamma = 2$. Trace gas errors are depicted without additional regularization (g = 1). Pre- scaling was used.

of the height depending variances which were chosen in order to reduce possible retrieval instabilities in altitude regimes where the sensitivity is lowest. In general, NO_2 shows also larger errors for higher altitudes but the surface error is dominant here, indicating a reduced sensitivity or poor parametrization. The errors for $z \geq 3$ are close to zero because the smallest a priori covariance is used as boundary condition for the highest altitudes, where the sensitivity is low.

For the quantification of the vertical sensitivity of the retrieval, Figure 9 shows the averaging kernels AK (see Eq. (14) and text) for the aerosol scenarios E1-E3 calculated for a Tikhonov parameter $\gamma = 0.25$ and SNR = 3000. We used a small γ to demonstrate the general vertical sensitivity rather than the smoothed one. Larger γ values would lead to peaks at lower altitudes with slightly reduced peak sizes. Within an ideal retrieval, the AK matrix should be equal to the identity matrix (Rodgers, 2004). Then, delta peaks in every layer would indicate a perfect sensitivity of the retrieval to the true state of the atmosphere. For MAX-DOAS retrievals, AK are much broader with peaks close to the surface. Here, the sensitivity is highest and the kernels for a certain layer show correlations with neighbouring layers due to the finite width of each kernel. The comparison of AK for E1-E3 reveals, that besides the surface kernel, all peaks are reduced in size and width for higher aerosol loads. This demonstrates the smaller sensitivity due to both, an insufficient a priori estimate and the additional aerosol load which reduces the general number of photons scattered into the light path (for specific geometries, e.g. RAA = $90°$). The area of the AK should ideally be 1 over a large range of altitudes. Here we find, that only within the first kilometer, the overall sensitivity is high. Note, that especially for E2 and E3 the surface area value is much smaller than 1 due to the negative area of the lowermost kernels for higher altitudes. Negative kernel values indicate, that an additional aerosol load in this altitude would decrease the retrieved solution close to the surface. The FWHM of averaging kernels are a measure of the vertical retrieval resolution with

the lowest values close to the surface. In the right hand side plot of Figure 9 we show FWHM at the nominal altitudes (coloured lines) and the altitudes of their individual maxima (black lines). The calculation was done by using the individual AK instead of the FWHM of fitted Gaussian distributions. The limited vertical extent of the black curves indicate, that a theoretical vertical resolution with values between 500 m and 1 km is available for all kernel levels but the specific sensitivity for all layers lies within the lowest kilometer.

Figure 9. Averaging kernels of the aerosol retrievals for scenarios E1-E3 (first three figures on the left side). Also shown are the area and FWHM of the AK on the right side. FWHM are depicted on their nominal heights (coloured) and on the height of their individual peaks (black).

The trace of the averaging kernel matrix (degrees of freedom, DOF) is often discussed as the number of independent pieces of information for a retrieval. Hartl and Wenig (2013) already pointed out, that this number is not necessarily a strict limitation of the retrieval and might differ strongly depending on the regularization.

In Figure 10, we depicted the RMS between measured and retrieved O_4 ΔS and the DOF for scenario E3. Giving the retrieval more freedom will increase the degrees of freedom and decrease the RMS which might be understood as more information used for a better measurement assimilation. However, in Section 4.3.1 we already demonstrated, that profiles with high DOF and low RMS might oscillate. DOF only state the maximum number of independent pieces of information for the current regularization parameters without considering if the retrieved profiles are optimal. Therefore, we do not use this quantity for the description of retrieval results.

In Figure 11, we show averaging kernel, area and FWHM of the NO_2 retrieval for scenarios E1-E3. Similar conclusions can be drawn as for the aerosol retrieval for the shape and altitude variation of AK. The area is closer to 1 for all altitudes which is due to the missing smoothing of the Tikhonov term. The FWHM shows again a lower vertical sensitivity for higher
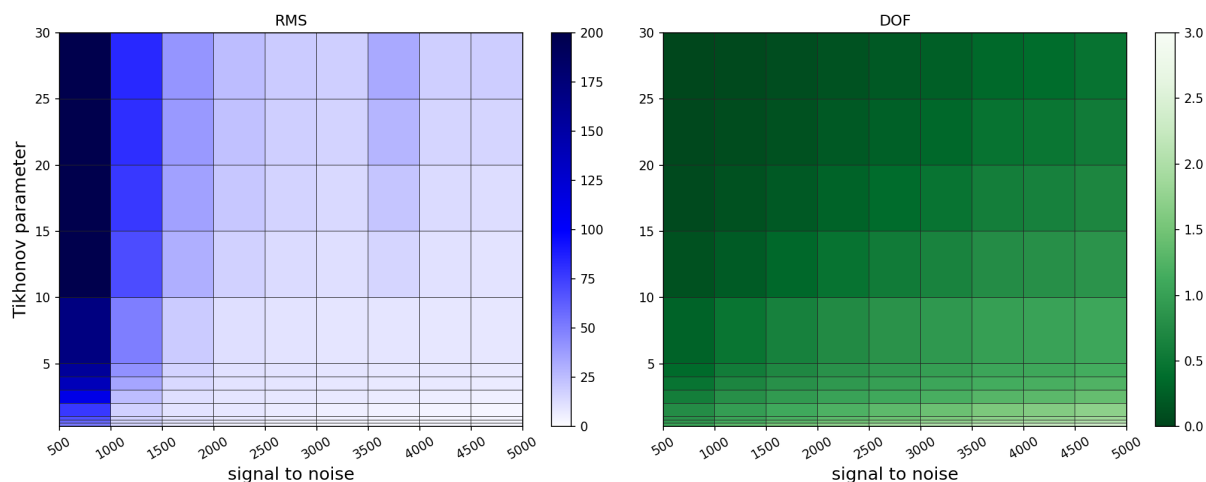
Figure 10. RMS between measured and simulated O_4 ΔS and the matching degrees of freedom (DOF) for the specific retrievals for different SNR and γ values.

layers. On the other hand, the FWHM curves at their specific peak heights (black) show a larger vertical spread in comparison to the aerosol curves which indicates a larger sensitivity for higher altitudes in the NO_2 retrieval. The DOF for the trace gas retrieval lie in the range between 2.3 and 3.2 but decrease significantly when applying values of $g \neq 1$. In addition to the above

5 mentioned errors and resolution properties, further error sources and problems should be noted. For real measurements, the true meteorological conditions are mostly unknown. Wang et al. (2017) pointed out, that wrong O_4 profiles might lead to strong deviations between retrieved and true aerosol profile. Furthermore, we did not implement the instruments field of view (FOV) in the retrieval because it will increase run time. However, larger differences can be expected for concentrations/extinctions in the lowermost layers, when parts of the FOV might gather photons reflected on Earth's surface. Additionally, we assume a

10 linearity between measurement and concentration which might be inaccurate for high aerosol loads and NO_2 concentrations when the telescope points along the horizon.

4.3 Retrieval of profiles during the CINDI-2 campaign

The 2nd Cabauw Intercomparison of Nitrogen Dioxide Measuring Instruments campaign (CINDI-2) took place in Cabauw (the Netherlands) from 25.08 - 07.10.2016 and was funded by the European Space Agency (ESA) and the research groups

15 participating. The campaign goals were the characterization of differences between NO_2 measurements by various instruments and approaches, and the evaluation of the resulting datasets for the validation of the Copernicus satellite, Sentinel 5 Precursor (S5P). Over 40 different instruments operated by 30 groups from all over the world provided an outstanding ensemble of datasets for this task. The campaign was a successor of CINDI which was held in Cabauw from 16.06 - 24.06.2009 (see e.g. Piters et al. (2012); Pinardi et al. (2013); Zieger et al. (2011)).
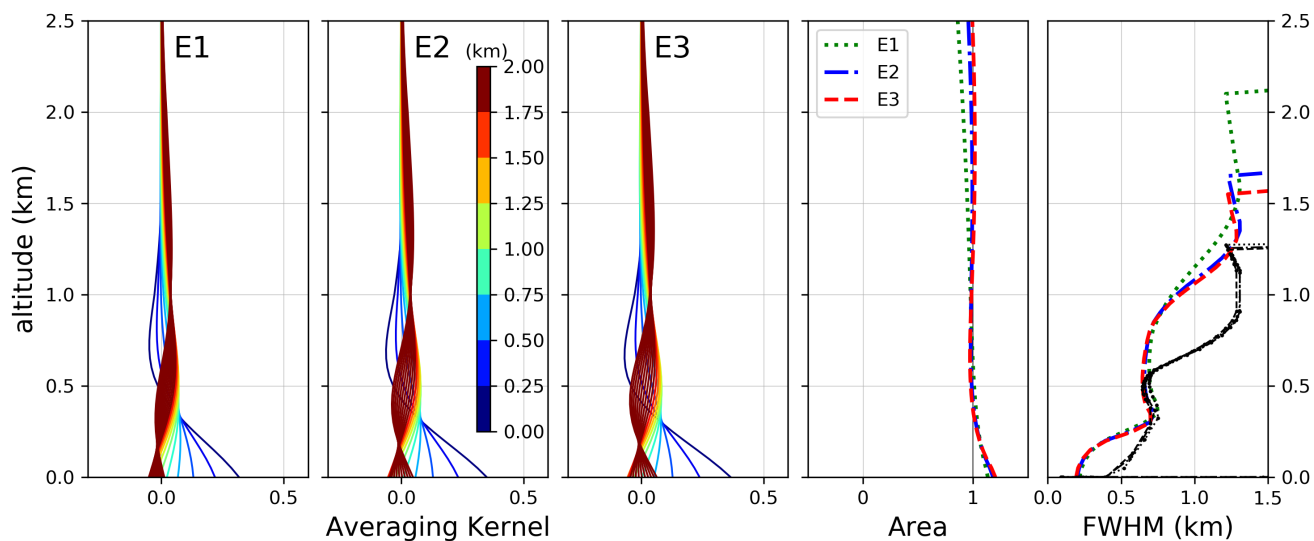
20

Figure 11. Averaging kernels of the NO_2 retrievals for scenarios E1-E3 (first three figures on the left side). Also shown are the area and FWHM of the AK on the right side. FWHM are depicted on their nominal heights (coloured) and on the height of their individual peaks (black).

The measurement site Cabauw is located in a rural region dominated by agriculture but is surrounded by four of the largest cities of the Netherlands (Rotterdam, Amsterdam, Den Haag and Utrecht). Thus, depending on the wind direction, long range transport from highly industrialized areas is likely which results in high pollution events. Here, three of the five investigated
5   days show a more or less steady wind from south-easterly directions with a change in wind direction in the evening of the 15th of September (see Fig. 12). On the 23rd, wind came from the west whereas one day later the wind came mostly from southerly directions.

   In this study, the instrumental set-up for the validation of aerosol and trace gas profiles consists of in situ and remote sensing instruments. Near-surface concentration/extinction values are provided by ceilometer, NO_2-LIDAR, long path DOAS (LP
10 DOAS) and in situ samplers (ICAD/CAPS, NAQMN). Integrated values are provided by Pandora and AERONET direct sun instruments. Besides the MAX-DOAS measurements, the only routinely retrieved profiling information comes from ceilometer and NO_2-LIDAR data. In addition, three NO_2-sondes were launched on one of the days investigated here (15.09.2016).
The profile validation is realized on two cloud free days (13. - 14.09.2016) and three days with broken clouds (15.09 and 23. -
24.09.2016). The operators of MAX-DOAS instruments were asked to perform elevation scans on the beginning of each hour
15 and at 11:15 and 11:45 UTC every day. The ancillary measurements introduced in the following subsections were resampled or averaged on this time interval to prevent discrepancies due to time lags between two observations. Each scan took around 8 minutes and consisted of the following elevation angles: $1°, 2°, 3°, 4°, 5°, 6°, 8°, 15°, 30°$. The telescope pointed into the western direction with a viewing azimuth angle of $107°$ from the south.
In this section, BOREAS retrievals were performed on data from the IUPB MAX-DOAS instrument on a $100\,\text{m}$ step width
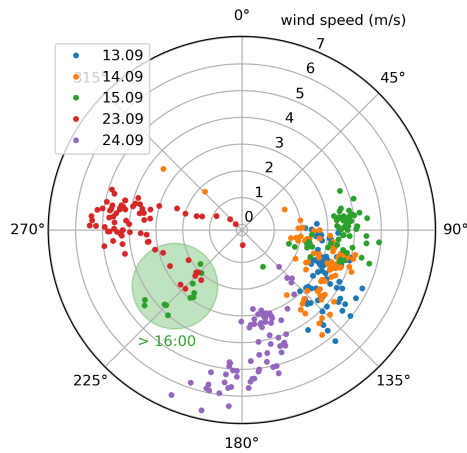
Figure 12. Wind speed and direction for the investigated days (CESAR, 2018) resampled to 5 minute values from 06:00 - 17:00 UTC.

vertical grid from the surface up to 4 km. The aerosol retrieval uses the a priori pre-scaling option with an exponential a priori profile described by a 1 km scale height and an aerosol optical thickness of 0.18. Asymmetry factor and single scattering albedo were chosen as 0.92 and 0.68, respectively. The SNR was set to 2500 with a Tikhonov-parameter of 2. The a priori variance was decreasing with altitude from 1.5 at the surface to 0.01 at 4 km. This definition was chosen to improve the profiling results for lower altitudes where the main aerosol load/concentration can be expected and in order to suppress instabilities at the upper grid boundary where the sensitivity is lowest. The trace gas retrieval uses again a priori pre-scaling with an exponentially decreasing profile with a scale height of 1 km and a vertical column density of $9x10^{15}$ molecules/cm^2. The a priori covariance matrix uses the same variances as the aerosol retrieval but includes Gaussian distributed side diagonal elements to account for correlations between individual layers (Barret et al., 2002). The measurement covariance matrix for NO_2 consists of the total differential slant column error on the diagonal elements only. Vertical profiles of pressure and temperature were created by taking the mean of 16 different sonde measurements taken during the years 2013-2015 in De Bilt (the Netherlands).

4.3.1 Validation of aerosol retrievals

Instrumentation for the aerosol validation

Aerosol profiles were validated using three different instruments. The retrieved AOT was compared with values from an AE-RONET station (AErosol RObotic NETwork, Dubovik et al. (2000); Holben et al. (1998)). The Level 2 AOT at 440 nm was scaled with the Angström Exponent from the ratio 440 nm/675 nm to calculate the AOT at 477 nm (see Fig. 13). Due to measurement intervals varying between 4 and 30 minutes, we decided to resample the AERONET signal. The errors from AERONET instruments are usually in the range of 0.01 (VIS, IR) to 0.02 (UV) (Sayer et al., 2013). Here, we used a constant error of 0.01. The bottom extinction coefficient of the retrieved aerosol profiles was compared with in situ PM10 concentrations from the

22

National Air Quality Monitoring Network (NAQMN) operated by the Dutch National Institute for Public Health and the Environment (RIVM). The NAQMN measurement site Wielsekade is located at a distance of around 900 m from the MAX-DOAS station. The site is listed as a regional background station and the PM10 measurement principle is beta attenuation (Thermo
5   Fisher Scientific FH62I-R). The instrument provides data on one minute intervals but only the hourly values are validated by RIVM. These hourly values were resampled on the MAX-DOAS times and the minute values were used to calculate the errors as standard deviation for the data points shown (see Fig. 14).

Furthermore, we used AERONET scaled ceilometer near surface extinction as a further validation dataset. The ceilometer (CHM15k Nimbus) was operated by the Royal Netherlands Meteorological Institute (KNMI) and sampled backscattering sig-
10   nals every hour at a wavelength of 1064 nm. The integrated backscattering signal was divided by the 1020 nm AERONET AOD to get a conversion factor which was applied to the backscattering signal for the conversion into extinction coefficients. This new ceilometer profile was again scaled with AERONETs AOT at 477 nm. The error is expressed as the standard deviation calculated from the temporal and vertical averaging.

15   *Comparison of aerosol retrieval parameters*
Figure 13 shows the time series and the scatter plot of AERONET and BOREAS derived AOT. The BOREAS data was filtered for profiles which reached the iteration limit during the retrieval. Grey areas indicate clouds within the specified time period.
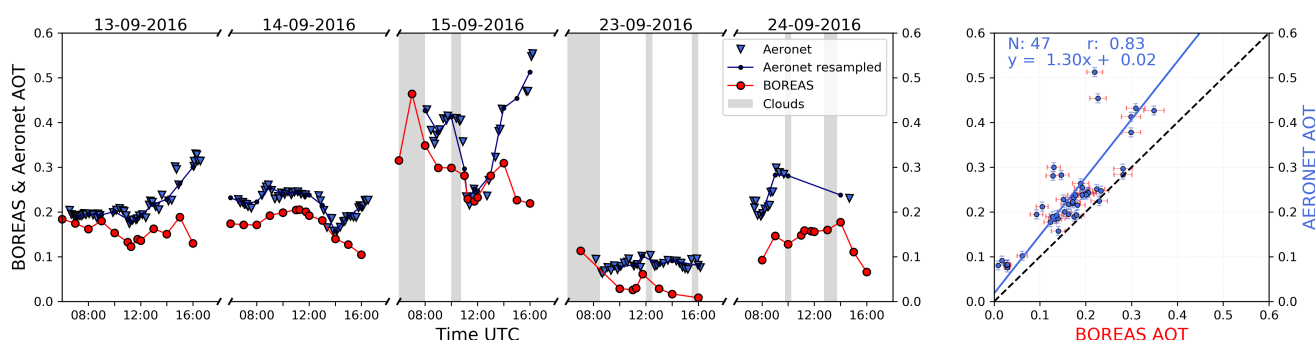
Figure 13. Left: time series of AERONET (blue) and BOREAS AOT (red). Small triangles show the original AERONET measurement, small dots with connecting lines depict the resampled data. Grey areas indicate clouds. Right: scatter plot of both datasets including parameters of the orthogonal regression and Pearsons correlation coefficient.

In the scatter plot, BOREAS errorbars were calculated by integrating the total error (Eq. (17)) vertically. On the first two cloud free days, the temporal variability shows a similar pattern with a slight offset between both instruments most likely introduced
20   by an underestimation of the AOT by BOREAS. Due to the limited sensitivity of MAX-DOAS profiling for higher altitudes (see Fig. 9), elevated aerosols do not contribute to BOREAS AOT but can be measured by direct sun instruments like AERONET sunphotometers.
In the evening, results of both instruments vary more. Different reasons for this finding are possible. First, a developing pla-

netary boundary layer (PBL) might exceed the vertical extension where BOREAS has sufficient sensitivity. Second, when pointing towards the sun, saturation of the CCD becomes a problem leading to low integration times which decrease SNR and fitting quality. In addition, RTM calculations might introduce uncertainties at high SZA, when the aerosol load is high and the light path is strongly increased. Furthermore, the aerosol phase function used leads to uncertainties as the forward scattering peak might be underestimated by the Henyey-Greenstein parametrization. The other days show a higher variability due to an increase in cloudy scenes. Note that especially in the morning and around noon, clouds may influence the instruments in various ways because of their different azimuthal viewing directions. BOREAS profile retrieval cannot be considered as reliable when one or several elevation angles pointed into clouds during the measurements, as intensity and light path vary in unpredictable ways. This might also lead to large iteration numbers or to no convergence at all. On the 15th of September, the temporal patterns of the two instruments differ strongly. Although the extinction values around noon agree well, AERONETs decrease before and the increase afterwards cannot be found this strongly by BOREAS. Especially in the evening, both curves deviate, indicating highly variable atmospheric conditions which might also be introduced by a change in wind direction (see Fig. 12). The aerosol load on the last two days is much lower because of rainfalls in the time between 16.09 and 22.09. In the morning of the 23rd, several profiles were discarded due to exceeded iteration limits.

The correlation coefficient of 0.83 is high and shows the general good agreement at three of five days. The regression line indicates the before mentioned small underestimation of the AOT by BOREAS.

Figure 14 shows the comparison of near-surface aerosol values. Extinction coefficients from BOREAS and ceilometer are depicted together with PM10 concentrations of the NAQMN in situ instrument. Note that the y-axis for PM10 concentrations was chosen to match the results of BOREAS on the 14th of September. The NAQMN in situ sampler and BOREAS show a good temporal agreement within the first three days. Only in the morning hours at the 13th and 15th, data from the two instruments show a larger spread. This deviation is most likely due to the insufficient vertical resolution of MAX-DOAS profile retrievals when the PBL has not yet evolved and near surface aerosol loads are dominant (see Fig. 9 and 15 for further details). On the 15th, early morning clouds might also have an impact on the deviation. Again, a larger variability for BOREAS results can be found for the last two days, when the retrieval was influenced by broken clouds. The in situ instruments show a smoother daily variation here. The ceilometer bottom extinction shows a good agreement with BOREAS and NAQMN on the first day and an underestimation on the second day. On the 15th of September, bottom values are influenced by thick clouds which might interfere with the backscattering signal of altitude ranges below the clouds (see Fig. 16). The 23rd shows more variability than the first two days but this can be found for the other instruments as well.

The correlation of BOREAS bottom extinctions with data from both validation instruments is high, indicating the good agreement on cloud free days. The correlation with ceilometer near-surface values is high as well but the regression line shows a general underestimation of ceilometer near surface values in comparison to BOREAS.

Figure 15 shows the aerosol layer height found by the ceilometer for all days. Especially during the first three days, an upward extending PBL can be identified from noon to the late afternoon. Only on the 15th, a more or less stable residual PBL seems to exist in the morning hours. The other days show a high variability in the morning with layer heights from 200 m to
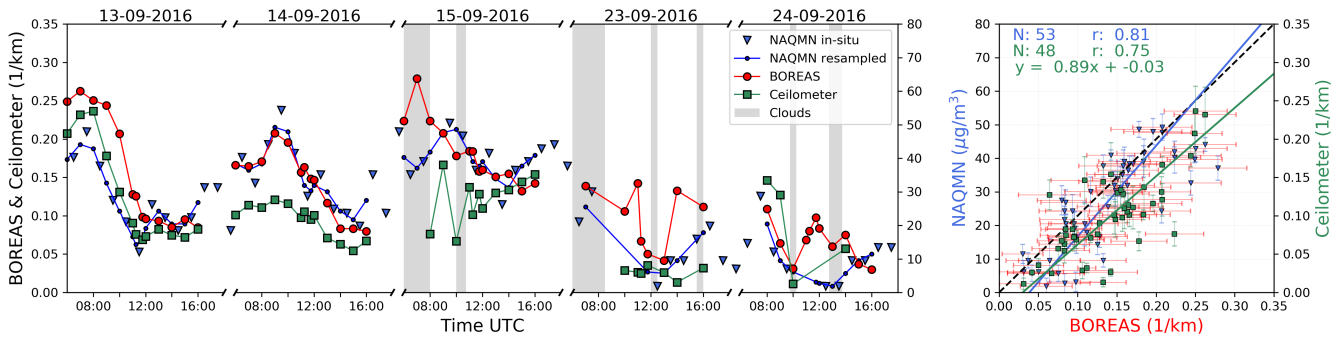
Figure 14. Left: time series of BOREAS (red), ceilometer (green) and NAQMN in situ (blue) and near surface aerosol parameters. Small triangles show the original hourly NAQMN measurements, small dots with connecting lines depict the resampled data. Green squares show ceilometer near-surface extinction values evaluated by averaging the 10 - 50 m coefficients. Grey areas indicate clouds. Right: scatter plot including parameters of the orthogonal regression and Pearsons correlation coefficients.

600 m with more or less individual high signals which might be produced by smaller clouds at higher altitudes. The 24th of September shows a stable layer around 200 m and a diffuse developing PBL in the afternoon.
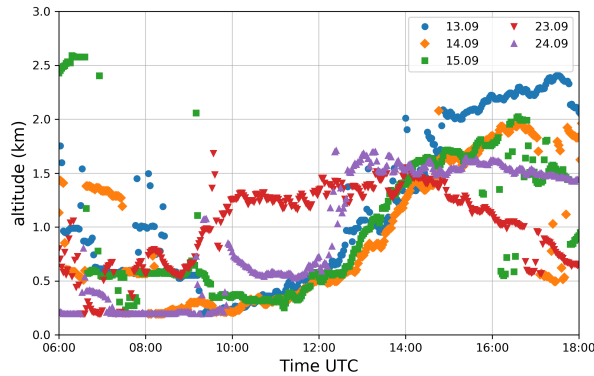
Figure 15. ceilometer aerosol layer height within the planetary boundary layer.

The underlying extinction coefficient profiles for the above discussed bottom extinction and AOT values can be seen in Figure 16. In the top row, temporal and vertically averaged ceilometer profiles are depicted. In the mid row, this data was smoothed to the MAX-DOAS vertical resolution by the application of BOREAS averaging kernels ($\mathbf{x}_{new} = \mathbf{x}_{apri} + \mathbf{A}(\mathbf{x}_{ceilo} - \mathbf{x}_{apri})$ see Rodgers and Connor (2003)). The first day shows a good agreement of BOREAS and ceilometer near surface extinction with a small offset between both curves. In the morning, both instruments find the aerosol load mainly located in the lowermost layers. Beginning around noon, the PBL starts developing with a maximum height of 2 km in the afternoon found by the ceilometer. BOREAS can not resolve this increasing PBL as well as the averaged ceilometer but the AK smoothed data

indicate that the reason might be a limited sensitivity for the top boundary of the PBL.

On the 15th of September, the averaged ceilometer data show high and thick clouds in the morning and a rising PBL in the afternoon. In the AK smoothed data, these clouds can not be identified anymore. BOREAS introduces elevated aerosol layers which can be understood as a retrieval artefact due to these cloudy scenes. In the afternoon, BOREAS finds an upward expansion in the PBL similar to the ceilometer with the exception of the last profile which was influenced by the telescope pointing towards the sun. BOREAS extinction values are smaller in the PBL which is a consequence of the already explained underestimation of BOREAS AOT to AERONETs AOT which was used for the backscatter signal scaling.

Figure 16. Comparison of aerosol extinction coefficient profiles from BOREAS and ceilometer for the 13.09.2016 (left) and 15.09.2016 (right).

4.3.2 Validation of nitrogen dioxide profiles

Instrumentation for the NO_2 *validation*

Several instruments were used for the validation of BOREAS nitrogen dioxide profiling results. The VCD results were validated with the help of a Pandora instrument (#128) operated by LuftBlick (Herman et al., 2009) and a NO_2 LIDAR from RIVM. In addition, three NO_2 sondes launched on the 15th of September by KNMI were also used.

The Pandora instrument was used with its direct sun capability to retrieve total nitrogen dioxide columns on hourly timesteps (see Fig. 17). Since the measurement time did not match to BOREAS scans, Pandora values were resampled. The stratospheric column was subtracted based on the approach of Knepp et al. (2015) by using OMI stratospheric columns during the Cabauw overpass (L2 OVP NASA (2018)). The data was quality filtered and the errors were provided by LuftBlick and are based on Herman et al. (2009).

26

The NO$_2$ LIDAR (Brinksma et al., 2008) measured not as frequently as Pandora and MAX-DOAS instruments but performed several measurements on the 15th of September. One LIDAR scan took approximately 30 minutes with the temporal midpoints of the scans on a non-regular temporal grid which necessitated resampling. The scan was done on different elevation angles which enabled the retrieval of vertical profiles with altitude points up to 2.5 km. For the VCD calculation, these profiles were vertically integrated. Errors were provided by the RIVM team and Gaussian error propagation was applied for the calculation of VCD errors. In addition to the remote sensing instrument, NO$_2$ sondes were launched on the 15th around 5:15, 8:04 and 10:25 UTC. The sondes provide NO$_2$ VMR as well as pressure, temperature and altitude data for the conversion to concentrations which were vertically integrated up to 4 km.

Near surface concentration validation was done with the help of in situ (NAQMN, ICAD, CAPS) and remote sensing instruments (LIDAR and LP DOAS). The in situ samplers NAQMN, CAPS and ICAD were operated by RIVM, the Royal Belgian Institute for Space Aeronomy (BIRA-IASB) and the institute for environmental physics in Heidelberg (IUPH), respectively. In addition to the aerosol bottom concentration, NAQMN provided also NO$_2$ concentrations (Teledyne API 200E, see Section 4.3.1 for details on data handling). IUPH and BIRA-IASB created a common NO$_2$ in situ dataset from IUPHs ICAD (Iterative CAvity DOAS, (Pöhler et al., 2017)) and BIRAs CAPS (Environment SA, AS32M- CAPS, Cavity Attenuated Phase Shift, (Kebabian et al., 2008)). This joint dataset filled gaps in the individual measurement series and fixed a scaling issue for CAPS. BIRA-IASB operated two different CAPS instruments which were installed at the 27 m and 200 m level of the Cabauw measurement tower. The joint ICAD/CAPS dataset as well as the 200 m CAPS data were averaged over 15 minutes time steps. For both instruments (ICAD/CAPS) an error of 1 ppb was assumed.

In addition to the in situ instruments, a long path DOAS (LP DOAS) provided by IUPH (Pöhler et al., 2010) was used for the validation. Four reflectors attached on different altitude levels of the measurement tower (12.7 m, 47 m, 107 m and 207 m) provided unique and well-defined light paths which enabled the calculation of concentration on several altitudes. The instruments elevation measurements lead to profiles every 30 minutes. Errors were calculated by the IUPH team.

Nitrogen dioxide profiles were provided only by the NO$_2$ LIDAR and sonde launches. The LP DOAS did not cover enough altitude levels for a comparison. The conversion from trace gas VMR to concentrations for all datasets was done with the meteorological data from the CESAR observatory (CESAR, 2018).

Comparison of NO$_2$ retrieval parameters

Figure 17 depicts the comparison of VCD for different instruments. The agreement with Pandora is good on all days with larger deviations in the morning and on the 15th of September in general with the exception around noon. Deviations in the morning might be (similar to the AERONET comparison) due to spatial differences in the NO$_2$ distribution, when Pandora points to the east and MAX-DOAS to the west. This argument is supported by the LIDAR measurement on the 15th that agreed well with BOREAS and shared the same azimuthal viewing direction. In the afternoon of that day, BOREAS VCD increase faster than Pandora and LIDAR with a strong overestimation for the last profile at 16:00 when the sun was low. Here, we can exclude horizontal gradients as a reason for differences, because of the same viewing direction of LIDAR and MAX-DOAS. On the same day, NO$_2$ sondes proved the BOREAS VCD only during the ascend (triangle with edge to the top) of the second

launch correct. The matching descend (triangle with edge to the bottom) for the first flight was approximately 38 km into the northwestern direction between Amsterdam and Rotterdam and agrees more with Pandora columns indicating differences due to azimuthal viewing directions. The strong differences in VCD for ascend and descend of the first and second sonde launches

5 show a high temporal and spatial variability of the NO_2 concentration which is supported by all remote sensing instruments. The correlation with Pandora is slightly better than with LIDAR but the regression parameter shows, that Pandora VCDs are higher than those from BOREAS whereas the LIDAR regression is closer to one.

In Figure 18, near surface NO_2 concentrations are depicted. Both in situ datasets (NAQMN and ICAD/CAPS) agree well with

Figure 17. Left: time series of Pandora, LIDAR and BOREAS NO_2-VCD. Blue diamonds show the original Pandora measurements, green squares the LIDAR datapoints. Small dots with connecting lines depict the resampled datasets of Pandora and LIDAR. BOREAS is shown as red circles. Grey areas indicate clouds. The plot includes orange triangles as the representation of the integrated NO_2 sondes measurements with the ascend and descend separated in different triangles with the edge to the top or to the bottom respectively. Right: scatter plot of the datasets including parameters of the orthogonal regression and Pearsons correlation coefficients.

each other and show larger differences only in the morning of the 14th of September. The LP DOAS profiles at 12.7 m and 47 m

10 show similar concentrations as the in situ instruments. Differences in the morning of the first two days between the lower and the higher LP DOAS values indicate a strong vertical inhomogeneity which was also found for the aerosols (see Section 4.3.1). BOREAS surface concentrations agree very well with all datasets except during the morning hours. On the 13th of September, in addition to the ICAD/CAPS data at the 27 m level (blue), the 200 m points are shown (green). The anti-correlated behaviour in the morning hours confirms the strong inhomogeneity and proves that nitrogen dioxide was mainly concentrated close to the

15 surface at that time. The mean values of both CAPS instruments (yellow line) show a better agreement with BOREAS than the 27 m and 200 m data.

It seems that BOREAS cannot fully resolve this thin near-surface layer and retrieves rather smooth profiles instead of sharp concentration peaks (see also the discussion about vertical sensitivity in subsection 4.2). This is again in agreement with LP DOAS results on the 24th of September, where the 200 m level LP DOAS finds similar concentrations as BOREAS. Note, that

20 the NO_2 LIDAR has a finer resolution within the lowest 100 m which might be the reason, why it depicts similar concentration numbers as the other instruments in the morning hours of the 15th of September. As a rough estimation of the thickness of the

individual thin layers in the morning, we divided BOREAS VCD by the ICAD/CAPS concentration and found, that the layer height lies around 200 m (06:00 - 08:00), 300 m (09:00) and 400 m (10:00) on the 13th of September. The mean AK FWHM for the surface layer on that day is 214 m indicating that the lowermost layer can be resolved only from around 09:00 UTC where the curves approach each other. A good agreement is found at 10:00 UTC when the concentration is focused in a layer twice as thick as BOREAS surface resolution.

The correlations are high for all instruments with the highest value for NAQMN and the NO_2 LIDAR. The in situ instruments show similar correlations but a slight underestimation of BOREAS can be found with slopes between 1.22 and 1.44.

Figure 19 depicts NO_2 profiles for BOREAS, LIDAR and sondes on the 15th of September. Similar to the aerosol profile

Figure 18. Left: time series of in situ and remote sensing NO_2 near surface concentrations. Triangles show in situ instruments for NAQMN (bright blue, triangles pointing upwards) and for ICAD/CAPS (dark blue, triangles pointing downwards). In addition, on the 13.09.2016, CAPS at the 200 m level is depicted as green triangles with the edge up and the mean values of both CAPS with the edge to the side (yellow). The NO_2 LIDAR is plotted as green squares and the LP DOAS as different sized circles in shades of magenta (lowest altitude as smallest circle). BOREAS is shown as large red circles. Right: scatter plot of the datasets including parameters of the orthogonal regression and Pearsons correlation coefficients.

comparison, averaging kernels were applied to LIDAR and sondes measurements. The vertical profiles of the unsmoothed LIDAR show the previously discussed high vertical inhomogeneity. We can clearly identify a high concentration close to the surface and another elevated NO_2 layer with altitudes varying between 100 m and 500 m. The unsmoothed sondes agree well with the LIDAR measurements only at the ascend of the second launch. After the application of averaging kernels, the two distinct layers with high concentrations are smoothed to one layer with NO_2 concentrated at the surface indicating again a lower vertical sensitivity of MAX-DOAS profiling. In addition, smoothed and unsmoothed LIDAR find larger concentrations for altitudes over 500 m before 8:00 UTC which was not found by BOREAS and the sonde profiles.
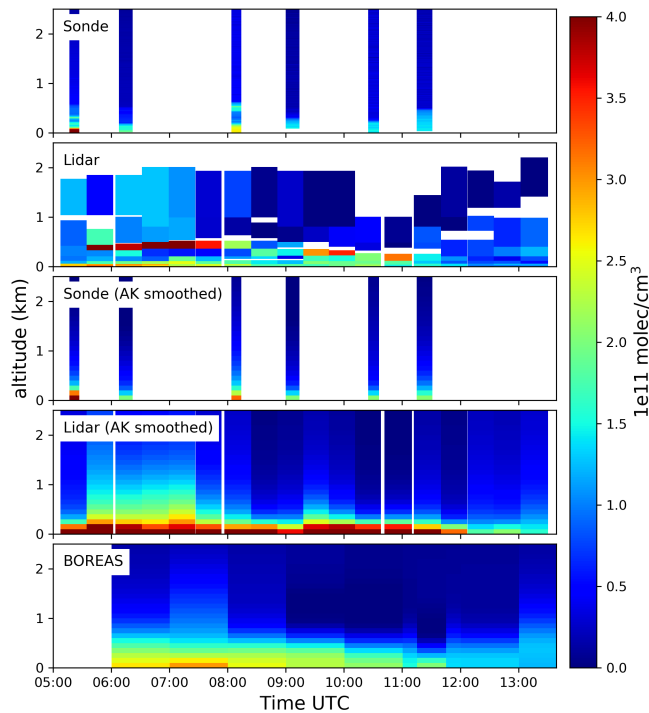
Figure 19. Comparison of NO$_2$ concentration profiles from BOREAS and LIDAR and sonde measurements for the 15.09.2016.

5 Conclusions

In this study, we introduced BOREAS, a new profiling algorithm for MAX-DOAS measurements. BOREAS retrieves aerosol extinction coefficient profiles around O$_4$ absorption bands from the oxygen dimers differential slant column densities. In contrast to existing inversion algorithms which are based on perturbation theory, BOREAS directly minimises the difference of modelled and measured optical depth by varying aerosol extinction coefficient profiles in an iterative Tikhonov regularization scheme. In addition, trace gas concentration profiles are retrieved via optimal estimation using the aerosol properties determined in the first step. For both retrieval parts, we introduced a priori pre-scaling as a simple method for improving results under variable atmospheric conditions.

The retrieval performance was demonstrated on the example of synthetic data calculated with SCIATRAN and with real measurements performed during the CINDI-2 campaign in Cabauw 2016. The synthetic scenarios were chosen to work as a stress test for BOREAS. One fix a priori profile was used for the retrieval of different large aerosol loads and NO$_2$ concentrations. The results are good when the scenario is relatively close to the a priori profile but fail for strong loads/concentrations. In a comprehensive variation of parameters we showed that, in non-ideal situations, either the shape/near-surface value or the integrated quantity can be optimized. The information content of a MAX-DOAS scan with degrees of freedom between ≈ 1

30

and ≈ 3.5 is not enough for a perfect retrieval. Furthermore, the frequently utilized assumption of using the trace gas errors from DOAS fits only as measurement variance was found to be insufficient since the regularisation ratio might be wrongly weighted. We suggest a manual change in measurement errors or an iterative approach for finding the best ratio.

5   In the second part of this study, BOREAS retrieval results from measurements of the IUPB MAX-DOAS instrument during the CINDI-2 campaign were validated with ancillary measurements. The agreement for all parameters was good with correlations equal or higher than 0.75. Systematic offsets or deviations depending on geometry, atmospheric condition and investigated air mass indicate limitations due to the specific measurement characteristics which were also found in earlier MAX-DOAS profiling studies. The correlation with AERONET AOT is 0.83 with an underestimation by BOREAS leading to a regression

10   slope of 1.30. The bottom value correlation is 0.75 for the ceilometer near surface extinction and 0.81 for NAQMN in situ measurements. The total column of NO_2 shows a good agreement with Pandora and LIDAR with correlations of 0.86 and 0.79 respectively. In contrast to the underestimation of BOREAS integrated aerosol, Pandora nitrogen dioxide columns are overestimated, especially in the morning hours. The correlations for near surface NO_2 concentrations are high with values larger than 0.84. Stronger deviations between BOREAS and in situ were found in the morning. This was explained by the limited vertical

15   resolution of BOREAS, while in the morning the highest concentrations are found close to the surface.

As a conclusion, BOREAS profiling capabilities are strong which was proven by high correlations with all validating instruments. Discrepancies were found due to different azimuthal viewing directions of the instruments and the limited vertical resolution of MAX-DOAS profiling when aerosol load or concentration is close to the surface in layers thinner than the BOREAS vertical resolution. Comparison of BOREAS results to the performance of other MAX-DOAS profiling algorithms will

20   be discussed in two upcoming papers (Frieß et al. (2018) and Tirpitz et al. (2018)).

25   **Appendix A: Additional plots and retrieval of box profiles**

A1   Additional aerosol scenarios and plots

The retrieval results for the box scenarios in Figure A1 are shown in Figure A2 for different Tikhonov parameters and SNR = 3000. A priori pre-scaling leads only for scenario B3 to a clear improvement since the bottom extinction is reached. For B2 and B3, the resulting profile shapes change slightly which indicates the before mentioned lack in improvements through

30   pre-scaling, when the a priori profile shape differs strongly from the true atmosphere. Nevertheless, since exponential profiles are improved a lot and box profiles show no degradation we highly recommend the usage of better and more flexible a priori profiles.
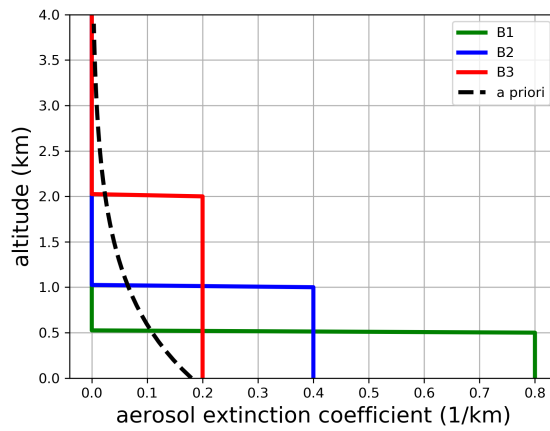
Figure A1. Box aerosol profiles for the synthetic sensitivity study. Also shown, the a priori profile for the aerosol retrieval (dashed line).

Figures A3 till A5 show the SNR and Tikhonov variation for the three aerosol box profiles. One can see, that for B2 the smallest γ values lead to the best bottom value, whereas for scenario B1 these values would result in an overestimation. Also the optimal SNR/γ range for the AOT differs strongly for all box profiles which show again, that regularization should be considered as a flexible choice of parameters, depending on the specific atmospheric conditions.

Figure A2. Retrieval results with a fix (left) and a pre-scaled a priori profile (right) with varying Tikhonov parameters γ for SNR = 3000. Small γ values mean less smoothing of the resulting profiles.
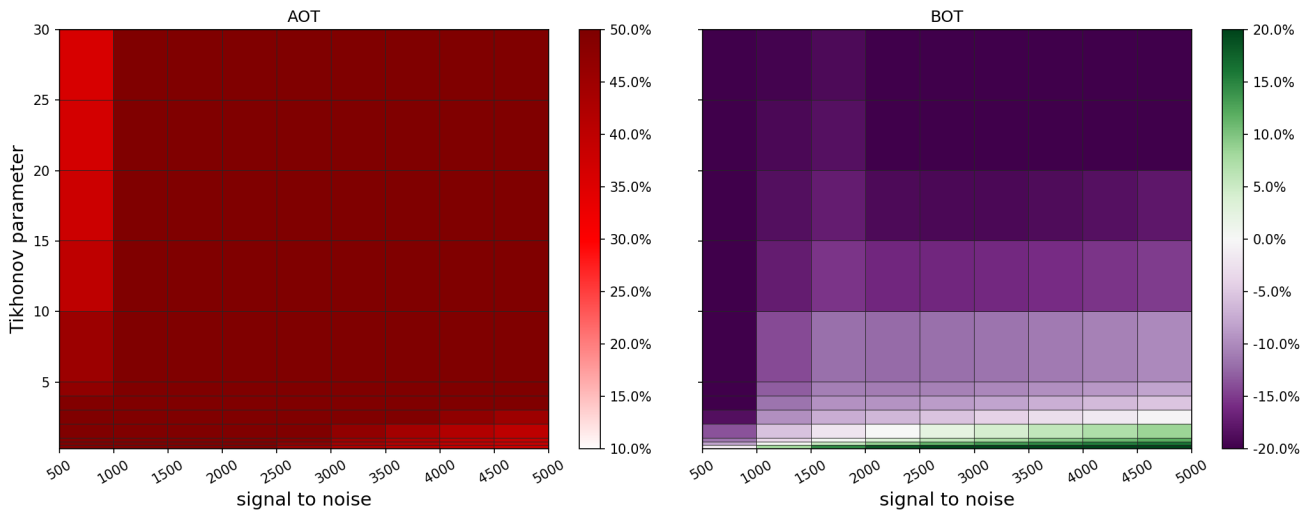
Figure A3. Variation of signal to noise and Tikhonov parameter with the relative difference of AOT and bottom extinction to the true value, colour coded for scenario B1 with a priori pre-scaling.
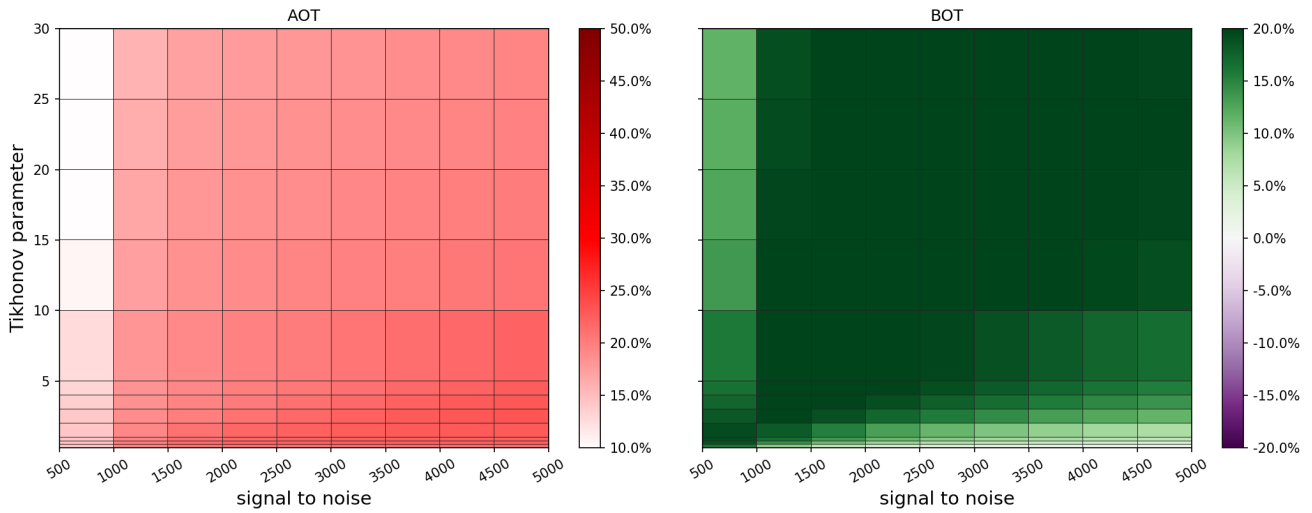

Figure A4. Same as figure A3 but for scenario B2.

Figures A6 and A7 show the SNR/Tikhonov variation for the exponential profiles E1 and E2. Note that for E1 all parameter combinations lead to good profiling results because the a priori profile is close to the true atmosphere. In comparison to E3, E2 shows a better adaptation of AOT with a coincidently similar performance for the bottom extinction.
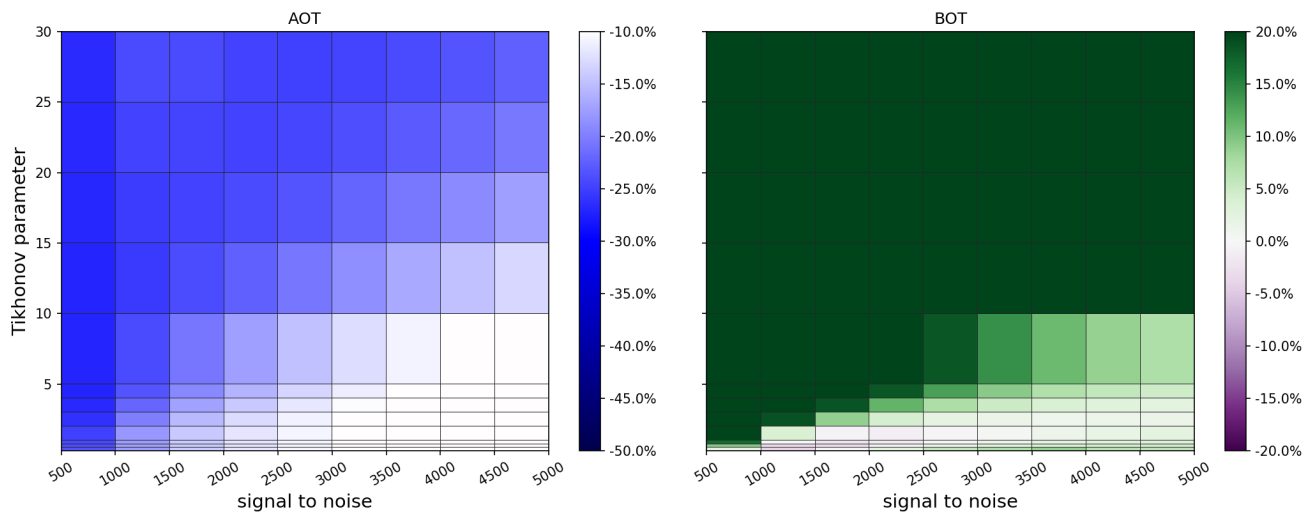
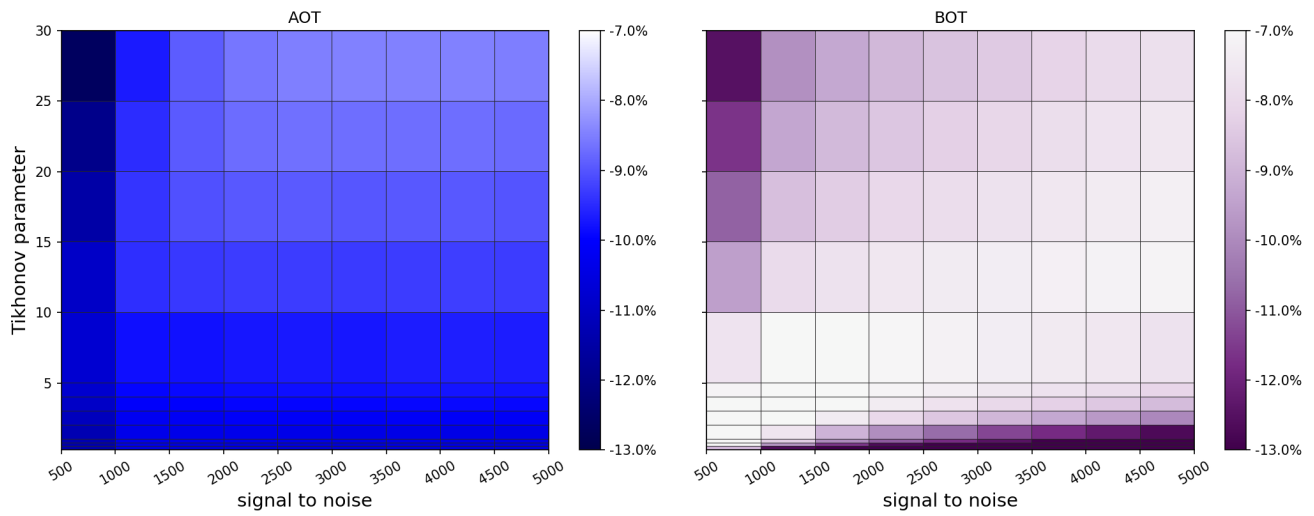**Figure A5.** Same as Figure A3 but for scenario B3.
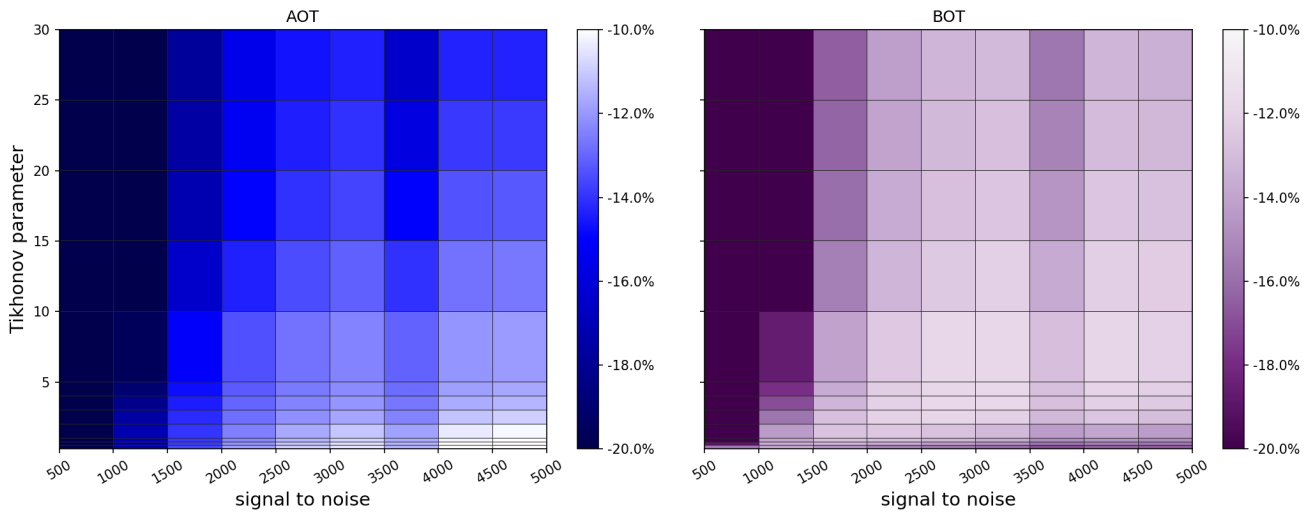

Figure A6. Same as Figure 5 but for scenario E1.

Figure A7. Same as Figure 5 but for scenario E2.

A2 Additional NO$_2$ scenarios and plots

Figure A8 shows the box NO$_2$ scenarios which are retrieved for different g values in Figure A9. The standard regularisation ratio for $g = 1$ is again found to be oscillating without reaching the proper bottom concentrations for E2 and E3. Higher g factors show an improvement for both, fix a priori and pre-scaled initial guess.
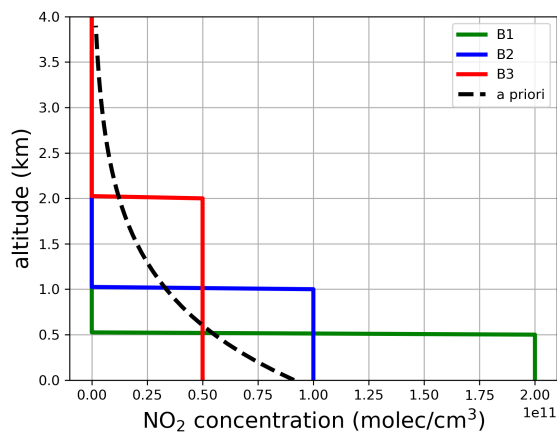

Figure A8. Box NO$_2$ profiles for the synthetic sensitivity study. Also shown, the a priori profile for the aerosol retrieval (dashed line).
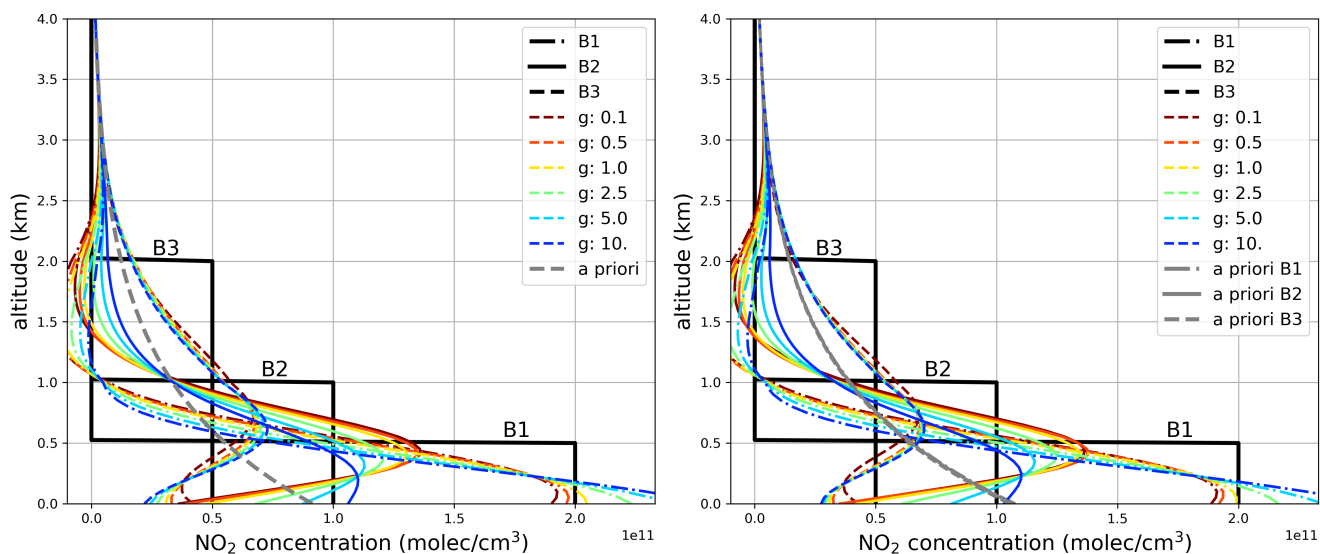
Figure A9. Retrieval results with a fix (left) and a pre-scaled a priori profile (right) with g factors. Small g values mean less measurement weighting for the resulting profiles.

References

Barret, B., De Mazière, M., and Demoulin, P.: Retrieval and Characterization of Ozone Profiles from Solar Infrared Spectra at the Jungfrau-joch, Journal of Geophysical Research: Atmospheres, 107, 4788, doi:10.1029/2001JD001298, 2002.

5 Bobrowski, N., Hönninger, G., Galle, B., and Platt, U.: Detection of Bromine Monoxide in a Volcanic Plume, Nature, 423, 273–276, doi:10/bv8hq8, 2003.

Brinksma, E. J., Pinardi, G., Volten, H., Braak, R., Richter, A., Schönhardt, A., van Roozendael, M., Fayt, C., Hermans, C., Dirksen, R. J., Vlemmix, T., Berkhout, A. J. C., Swart, D. P. J., Oetjen, H., Wittrock, F., Wagner, T., Ibrahim, O. W., de Leeuw, G., Moerman, M., Curier, R. L., Celarier, E. A., Cede, A., Knap, W. H., Veefkind, J. P., Eskes, H. J., Allaart, M., Rothe, R., Piters, A. J. M., and Le-

10 velt, P. F.: The 2005 and 2006 DANDELIONS NO$_2$ and Aerosol Intercomparison Campaigns, Journal of Geophysical Research, 113, doi:10.1029/2007JD008808, 2008.

CESAR: Cesar Observatory, http://www.cesar-observatory.nl/index.php, 2018.

Clémer, K., Van Roozendael, M., Fayt, C., Hendrick, F., Hermans, C., Pinardi, G., Spurr, R., Wang, P., and De Mazière, M.: Multiple Wavelength Retrieval of Tropospheric Aerosol Optical Properties from MAXDOAS Measurements in Beijing, Atmospheric Measurement

15 Techniques, 3, 863–878, doi:10.5194/amt-3-863-2010, 2010.

Dubovik, O., Smirnov, A., Holben, B. N., King, M. D., Kaufman, Y. J., Eck, T. F., and Slutsker, I.: Accuracy Assessments of Aerosol Optical Properties Retrieved from Aerosol Robotic Network (AERONET) Sun and Sky Radiance Measurements, Journal of Geophysical Research: Atmospheres, 105, 9791–9806, doi:10.1029/2000JD900040, 2000.

Dubovik, O., Holben, B., Eck, T. F., Smirnov, A., Kaufman, Y. J., King, M. D., Tanré, D., and Slutsker, I.: Variability of Absorption and Optical Properties of Key Aerosol Types Observed in Worldwide Locations, Journal of the Atmospheric Sciences, 59, 590–608, doi:10/cdvdp3, 2002.

5   Engl, H. W. and Grever, W.: Using the L–Curve for Determining Optimal Regularization Parameters, Numerische Mathematik, 69, 25–31, doi:10/bdzkp4, 1994.

Eriksson, P.: Analysis and Comparison of Two Linear Regularization Methods for Passive Atmospheric Observations, Journal of Geophysical Research: Atmospheres, 105, 18 157–18 167, doi:10.1029/2000JD900172, 2000.

Frieß, U., Monks, P. S., Remedios, J. J., Rozanov, A., Sinreich, R., Wagner, T., and Platt, U.: MAX-DOAS O_4 Measurements:
10   A New Technique to Derive Information on Atmospheric Aerosols: 2. Modeling Studies, Journal of Geophysical Research, 111, doi:10.1029/2005JD006618, 2006.

Frieß, U., Klein Baltink, H., Beirle, S., Clémer, K., Hendrick, F., Henzing, B., Irie, H., de Leeuw, G., Li, A., Moerman, M. M., van Roozendael, M., Shaiganfar, R., Wagner, T., Wang, Y., Xie, P., Yilmaz, S., and Zieger, P.: Intercomparison of Aerosol Extinction Profiles Retrieved from MAX-DOAS Measurements, Atmospheric Measurement Techniques, 9, 3205–3222, doi:10.5194/amt-9-3205-2016, 2016.

15   Hansen, P.: Analysis of Discrete Ill-Posed Problems by Means of the L-Curve, SIAM Review, 34, 561–580, doi:10/c2dntc, 1992.

Hartl, A. and Wenig, M. O.: Regularisation Model Study for the Least-Squares Retrieval of Aerosol Extinction Time Series from UV/VIS MAX-DOAS Observations for a Ground Layer Profile Parameterisation, Atmospheric Measurement Techniques, 6, 1959–1980, doi:10.5194/amt-6-1959-2013, 2013.

Hendrick, F., Barret, B., van Roozendael, M., Boesch, H., Butz, A., De Mazière, M., Goutail, F., Hermans, C., Lambert, J.-C., Pfeilsticker,
20   K., and Pommereau, J.-P.: Retrieval of Nitrogen Dioxide Stratospheric Profiles from Ground-Based Zenith-Sky UV-Visible Observations: Validation of the Technique through Correlative Comparisons, Atmospheric Chemistry and Physics, 4, 2091–2106, 2004.

Hendrick, F., Müller, J.-F., Clémer, K., Wang, P., De Mazière, M., Fayt, C., Gielen, C., Hermans, C., Ma, J. Z., Pinardi, G., Stavrakou, T., Vlemmix, T., and Van Roozendael, M.: Four Years of Ground-Based MAX-DOAS Observations of HONO and NO_2 in the Beijing Area, Atmospheric Chemistry and Physics, 14, 765–781, doi:10.5194/acp-14-765-2014, 2014.

25   Henyey, L. G. and Greenstein, J. L.: Diffuse Radiation in the Galaxy, The Astrophysical Journal, 93, 70–83, doi:10.1086/144246, 1941.

Herman, J., Cede, A., Spinei, E., Mount, G., Tzortziou, M., and Abuhassan, N.: NO_2 Column Amounts from Ground-Based Pandora and MFDOAS Spectrometers Using the Direct-Sun DOAS Technique: Intercomparisons and Application to OMI Validation, Journal of Geophysical Research: Atmospheres, 114, D13 307, doi:10.1029/2009JD011848, 2009.

Holben, B. N., Eck, T. F., Slutsker, I., Tanré, D., Buis, J. P., Setzer, A., Vermote, E., Reagan, J. A., Kaufman, Y. J., Nakajima, T., Lavenu, F.,
30   Jankowiak, I., and Smirnov, A.: AERONET—A Federated Instrument Network and Data Archive for Aerosol Characterization, Remote Sensing of Environment, 66, 1–16, doi:10.1016/S0034-4257(98)00031-5, 1998.

Hönninger, G. and Platt, U.: Observations of BrO and Its Vertical Distribution during Surface Ozone Depletion at Alert, Atmospheric Environment, 36, 2481–2489, doi:10/bkjbwh, 2002.

Hönninger, G., von Friedeburg, C., and Platt, U.: Multi Axis Differential Optical Absorption Spectroscopy (MAX-DOAS), Atmospheric
35   Chemistry and Physics, 4, 231–254, 2004.

Irie, H., Takashima, H., Kanaya, Y., Boersma, K. F., Gast, L., Wittrock, F., Brunner, D., Zhou, Y., and Van Roozendael, M.: Eight-Component Retrievals from Ground-Based MAX-DOAS Observations, Atmospheric Measurement Techniques, 4, 1027–1044, doi:10.5194/amt-4-1027-2011, 2011.

37

Kebabian, P. L., Wood, E. C., Herndon, S. C., and Freedman, A.: A Practical Alternative to Chemiluminescence-Based Detection of Nitrogen Dioxide: Cavity Attenuated Phase Shift Spectroscopy, Environmental Science & Technology, 42, 6040–6045, doi:10/fs8pg7, 2008.

Knepp, T., Pippin, M., Crawford, J., Chen, G., Szykman, J., Long, R., Cowen, L., Cede, A., Abuhassan, N., Herman, J., Delgado, R., Compton, J., Berkoff, T., Fishman, J., Martins, D., Stauffer, R., Thompson, A. M., Weinheimer, A., Knapp, D., Montzka, D., Lenschow, D., and Neil, D.: Estimating Surface NO_2 and SO_2 Mixing Ratios from Fast-Response Total Column Observations and Potential Application to Geostationary Missions, Journal of Atmospheric Chemistry, 72, 261–286, doi:10.1007/s10874-013-9257-6, 2015.

Lee, H., Irie, H., Kim, Y. J., Noh, Y., Lee, C., Kim, Y., and Chun, K. J.: Retrieval of Aerosol Extinction in the Lower Troposphere Based on UV MAX-DOAS Measurements, Aerosol Science and Technology, 43, 502–509, doi:10.1080/02786820902769691, 2009.

Lelieveld, J., Berresheim, H., Borrmann, S., Crutzen, P. J., Dentener, F. J., Fischer, H., Feichter, J., Flatau, P. J., Heland, J., Holzinger, R., Korrmann, R., Lawrence, M. G., Levin, Z., Markowicz, K. M., Mihalopoulos, N., Minikin, A., Ramanathan, V., de Reus, M., Roelofs, G. J., Scheeren, H. A., Sciare, J., Schlager, H., Schultz, M., Siegmund, P., Steil, B., Stephanou, E. G., Stier, P., Traub, M., Warneke, C., Williams, J., and Ziereis, H.: Global Air Pollution Crossroads over the Mediterranean, Science, 298, 794–799, doi:10/fntp6v, 2002.

Leser H., Hönninger G., and Platt U.: MAX-DOAS Measurements of BrO and NO_2 in the Marine Boundary Layer, Geophysical Research Letters, 30, doi:10/fjm8bv, 2003.

Li, X., Brauers, T., Shao, M., Garland, R. M., Wagner, T., Deutschmann, T., and Wahner, A.: MAX-DOAS Measurements in Southern China: Retrieval of Aerosol Extinctions and Validation Using Ground-Based in-Situ Data, Atmospheric Chemistry and Physics, 10, 2079–2089, doi:10.5194/acp-10-2079-2010, 2010.

NASA: U.S. Standard Atmosphere, 1976, Office, U.S. Government Printing, Washington, D.C., 1976.

NASA: AVDC | DATA - AURA - NASA EOS -Aura Validation Data Center - Correlative Data, Field of View Predictions, Data Subsets, https://avdc.gsfc.nasa.gov/index.php?site=2045907950, 2018.

Pinardi, G., Van Roozendael, M., Abuhassan, N., Adams, C., Cede, A., Clémer, K., Fayt, C., Frieß, U., Gil, M., Herman, J., Hermans, C., Hendrick, F., Irie, H., Merlaud, A., Navarro Comas, M., Peters, E., Piters, A. J. M., Puentedura, O., Richter, A., Schönhardt, A., Shaiganfar, R., Spinei, E., Strong, K., Takashima, H., Vrekoussis, M., Wagner, T., Wittrock, F., and Yilmaz, S.: MAX-DOAS Formaldehyde Slant Column Measurements during CINDI: Intercomparison and Analysis Improvement, Atmospheric Measurement Techniques, 6, 167–185, doi:10.5194/amt-6-167-2013, 2013.

Piters, A. J. M., Boersma, K. F., Kroon, M., Hains, J. C., Van Roozendael, M., Wittrock, F., Abuhassan, N., Adams, C., Akrami, M., Allaart, M. A. F., Apituley, A., Beirle, S., Bergwerff, J. B., Berkhout, A. J. C., Brunner, D., Cede, A., Chong, J., Clémer, K., Fayt, C., Frieß, U., Gast, L. F. L., Gil-Ojeda, M., Goutail, F., Graves, R., Griesfeller, A., Großmann, K., Hemerijckx, G., Hendrick, F., Henzing, B., Herman, J., Hermans, C., Hoexum, M., van der Hoff, G. R., Irie, H., Johnston, P. V., Kanaya, Y., Kim, Y. J., Klein Baltink, H., Kreher, K., de Leeuw, G., Leigh, R., Merlaud, A., Moerman, M. M., Monks, P. S., Mount, G. H., Navarro-Comas, M., Oetjen, H., Pazmino, A., Perez-Camacho, M., Peters, E., du Piesanie, A., Pinardi, G., Puentedura, O., Richter, A., Roscoe, H. K., Schönhardt, A., Schwarzenbach, B., Shaiganfar, R., Sluis, W., Spinei, E., Stolk, A. P., Strong, K., Swart, D. P. J., Takashima, H., Vlemmix, T., Vrekoussis, M., Wagner, T., Whyte, C., Wilson, K. M., Yela, M., Yilmaz, S., Zieger, P., and Zhou, Y.: The Cabauw Intercomparison Campaign for Nitrogen Dioxide Measuring Instruments (CINDI): Design, Execution, and Early Results, Atmospheric Measurement Techniques, 5, 457–485, doi:10.5194/amt-5-457-2012, 2012.

Platt, U. and Stutz, J.: Differential Optical Absorption Spectroscopy: Principles and Applications, Physics of Earth and space environments, Springer, Berlin, 2008.

Pöhler, D., Vogel, L., Frieß, U., and Platt, U.: Observation of Halogen Species in the Amundsen Gulf, Arctic, by Active Long-Path Differential Optical Absorption Spectroscopy, Proceedings of the National Academy of Sciences, 107, 6582–6587, doi:10/cqnpj4, 2010.

Pöhler, D., Lutz, E., Horbanski, M., Lampel, J., and Platt, U.: High Precision NO_2 and NO Measurements with the ICAD Instrument during S-b-s Campaign Hohenpeißenberg 2016, vol. 19, p. 14336, 2017.

Rodgers, C. D.: Inverse Methods for Atmospheric Sounding: Theory and Practice, no. 2 in Series on atmospheric oceanic and planetary physics, World Scientific, Singapore, reprinted edn., oCLC: 254137862, 2004.

Rodgers, C. D. and Connor, B. J.: Intercomparison of Remote Sounding Instruments, Journal of Geophysical Research: Atmospheres, 108, 4116, doi:10.1029/2002JD002299, 2003.

Rozanov, V. V. and Rozanov, A. V.: Differential Optical Absorption Spectroscopy (DOAS) and Air Mass Factor Concept for a Multiply Scattering Vertically Inhomogeneous Medium: Theoretical Consideration, Atmospheric Measurement Techniques, 3, 751–780, doi:10.5194/amt-3-751-2010, 2010.

Rozanov, V. V., Rozanov, A. V., Kokhanovsky, A. A., and Burrows, J. P.: Radiative Transfer through Terrestrial Atmosphere and Ocean: Software Package SCIATRAN, Journal of Quantitative Spectroscopy and Radiative Transfer, 133, 13–71, doi:10.1016/j.jqsrt.2013.07.004, 2014.

Sayer, A. M., Hsu, N. C., Bettenhausen, C., and Jeong, M.-J.: Validation and Uncertainty Estimates for MODIS Collection 6 "Deep Blue" Aerosol Data, Journal of Geophysical Research: Atmospheres, 118, 7864–7872, doi:10.1002/jgrd.50600, 2013.

Sinreich, R., Frieß, U., Wagner, T., and Platt, U.: Multi Axis Differential Optical Absorption Spectroscopy (MAX-DOAS) of Gas and Aerosol Distributions, Faraday Discussions, 130, 153, doi:10.1039/b419274p, 2005.

Sinreich, R., Merten, A., Molina, L., and Volkamer, R.: Parameterizing Radiative Transfer to Convert MAX-DOAS dSCDs into near-Surface Box-Averaged Mixing Ratios, Atmospheric Measurement Techniques, 6, 1521–1532, doi:10.5194/amt-6-1521-2013, 2013.

Stocker, T., ed.: Climate Change 2013: The Physical Science Basis: Working Group I Contribution to the Fifth Assessment Report of the Intergovernmental Panel on Climate Change, Cambridge University Press, New York, 2014.

van Roozendael, M., Fayt, C., Post, P., Hermans, C., and Lambert, J. C.: Retrieval of Tropospheric BrO and NO2</Subscript> from UV-Visible Observations, in: Sounding the Troposphere from Space, pp. 155–165, Springer, Berlin, Heidelberg, doi:10.1007/978-3-642-18875-6_19, 2004.

Vlemmix, T., Piters, A. J. M., Berkhout, A. J. C., Gast, L. F. L., Wang, P., and Levelt, P. F.: Ability of the MAX-DOAS Method to Derive Profile Information for NO_2: Can the Boundary Layer and Free Troposphere Be Separated?, Atmospheric Measurement Techniques, 4, 2659–2684, doi:10.5194/amt-4-2659-2011, 2011.

Vlemmix, T., Hendrick, F., Pinardi, G., De Smedt, I., Fayt, C., Hermans, C., Piters, A., Wang, P., Levelt, P., and Van Roozendael, M.: MAX-DOAS Observations of Aerosols, Formaldehyde and Nitrogen Dioxide in the Beijing Area: Comparison of Two Profile Retrieval Approaches, Atmospheric Measurement Techniques, 8, 941–963, doi:10.5194/amt-8-941-2015, 2015.

Wagner, T., Dix, B., v. Friedeburg, C., Frieß, U., Sanghavi, S., Sinreich, R., and Platt, U.: MAX-DOAS O_4 Measurements: A New Technique to Derive Information on Atmospheric Aerosols-Principles and Information Content: MAX-DOAS O_4 MEASUREMENTS OF AERO-SOLS, Journal of Geophysical Research: Atmospheres, 109, n/a–n/a, doi:10.1029/2004JD004904, 2004.

Wagner, T., Beirle, S., Brauers, T., Deutschmann, T., Frieß, U., Hak, C., Halla, J. D., Heue, K. P., Junkermann, W., Li, X., Platt, U., and Pundt-Gruber, I.: Inversion of Tropospheric Profiles of Aerosol Extinction and HCHO and NO_2 Mixing Ratios from MAX-DOAS Observations in Milano during the Summer of 2003 and Comparison with Independent Data Sets, Atmospheric Measurement Techniques, 4, 2685–2715, doi:10.5194/amt-4-2685-2011, 2011.

Wang, Y., Lampel, J., Xie, P., Beirle, S., Li, A., Wu, D., and Wagner, T.: Ground-Based MAX-DOAS Observations of Tropospheric Aerosols, NO_2, SO_2 and HCHO in Wuxi, China, from 2011 to 2014, Atmos. Chem. Phys., 17, 2189–2215, doi:10.5194/acp-17-2189-2017, 2017.

Wittrock, F.: The Retrieval of Oxygenated Volatile Organic Compounds by Remote Sensing Techniques, Dissertation, University of Bremen, Bremen, 2006.

Wittrock, F., Oetjen, H., Richter, A., Fietkau, S., Medeke, T., Rozanov, A., and Burrows, J. P.: MAX-DOAS Measurements of Atmospheric Trace Gases in Ny-Ålesund - Radiative Transfer Studies and Their Application, Atmospheric Chemistry and Physics, 4, 955–966, doi:10.5194/acp-4-955-2004, 2004.

Zieger, P., Weingartner, E., Henzing, J., Moerman, M., de Leeuw, G., Mikkilä, J., Ehn, M., Petäjä, T., Clémer, K., van Roozendael, M., Yilmaz, S., Frieß, U., Irie, H., Wagner, T., Shaiganfar, R., Beirle, S., Apituley, A., Wilson, K., and Baltensperger, U.: Comparison of Ambient Aerosol Extinction Coefficients Obtained from In-Situ, MAX-DOAS and LIDAR Measurements at Cabauw, Atmospheric Chemistry and Physics, 11, 2603–2624, doi:10.5194/acp-11-2603-2011, 2011.